THE UNIVERSITY OF OKLAHOMA

GRADUATE COLLEGE

CONSTRUCTION AND LOAD TESTING OF TWO FIELD-SCALE MODEL GRS BRIDGE ABUTMENTS

A THESIS

SUBMITTED TO THE GRADUATE FACULTY

in partial fulfillment of the requirements for the

Degree of

MASTER OF SCIENCE

By

KIRBY FALCON

Norman, Oklahoma

2021

CONSTRUCTION AND LOAD TESTING OF TWO FIELD-SCALE MODEL GRS BRIDGE ABUTMENTS

A THESIS APPROVED FOR THE

SCHOOL OF CIVIL ENGINEERING AND ENVIRONMENTAL SCIENCE

BY THE COMMITTEE CONSISTING OF

Dr. Kianoosh Hatami, Chair

Dr. Gerald Miller

Dr. K.K. Muraleetharan

ACKNOWLEDGEMENTS

There are many people who, directly or indirectly, contributed to the completion of this study. First, none of this would have been possible without the support, mentorship, and friendship from Dr. Kianoosh Hatami. Whether in the classroom or out, he has continued to push me to be the best version of myself. His demand for excellence is contagious and admirable. Dr, Hatami, I cannot thank you enough for the impact you have had on me throughout my time at The University of Oklahoma. I hope we get the opportunity to work together again in the future.

I would like to thank John Bullock for his contributions to this project. Though this study would not have been possible without his hard work, I am most thankful for his advice, guidance, and friendship. John, thank you for everything you have done for me during our short time together. You made work enjoyable. It's a beautiful day.

Thank you to my committee members, Dr. Gerald Miller and Dr. K.K. Muraleetharan, for not only contributing to the quality of this thesis but also for the quality of my education. I would also like to extend my deepest gratitude to Dr. Christopher Ramseyer for all the work he contributed to towards the completion of this research. Additionally, I would like to thank all my professors and instructors at The University of Oklahoma for their impact on my education.

I am also very appreciative of the students, past and present, who helped me with this study. I want to thank Ridvan Doger and Jerome Boutin for showing me the ropes. They have continued to help and support me throughout this project, despite the distance. To Javier Chaves Camargo, Daniel

Graumann, Tate Hammersley, Ryan Lindsey, Joseph Pitzer, Justin Reynolds, Stephen Roswurm, and Stephen Schnabel, thank you for helping me complete this research. Without a doubt, one of the best things to come out of this project is your friendships.

To the rest of my friends and family, thank you for everything.

Table of Contents

List of Tables

List of Figures

ABSTRACT

Geosynthetic Reinforced Soil-Integrated Bridge System (GRS-IBS) is an alternative bridge construction technique to conventional, deep-foundation bridge abutments. GRS-IBS has shown signs of expedited construction speeds and can be constructed with locally sourced materials, leading to a cost-effective solution. Most suitable for small county roads, the integrated approach may reduce the magnitude of the "bump-at-the-end-of-the-road" by eliminating differential settlement between the superstructure and existing roadway. Factors effecting the performance of these bridge systems have been previously studied through field-scale models located at The University of Oklahoma. As an extension of those studies, this paper aims to further explore various combinations of factors and their effects on the structural performance of GRS-IBS. The findings of this research will be compared with those from previous studies.

Two models were constructed, tested and compared to previously tested models. Constructed with large facing blocks, dense-graded aggregate and three compaction passes, GRS Abutment Model #7 was anticipated to produce the stiffest response of all models. Though still in accordance with FHWA guidelines, the model did not produce the anticipated stiffness as it responded similarly to other models constructed with large facing blocks, regardless of the backfill type, compaction effort, and spacing of reinforcement. The second model, GRS Abutment Model #8, aimed to produce results that most realistically reflected the performance of in-service GRS-IBS structures by implementing a beam seat width that satisfies the FHWA guidelines. Results show that the increased beam seat width (24 vs 8 inches) permitted larger loads for similar settlement magnitudes. The facing deformations and reinforcement strains increased largely relative to

previously tested GRS abutment models, though this is likely closely associated with the decreased setback distance.

Chapter 1 – INTRODUCTION

1.1 GRS Background

Geosynthetic Reinforced Soil (GRS) is a widely used construction alternative for earthwork applications dating back to the 1970's (Adams et al., 2011a). The technology incorporates alternating layers of compacted aggregate and geosynthetic reinforcement. Though there are a variety of applications incorporating GRS, this research focuses on the performance of GRS bridge abutments. Roughly 14% of the bridges in the National Bridge Inventory are functionally obsolete, failing to provide serviceability (Akhnoukh, 2019). The adoption of accelerated bridge construction techniques can help increase the number of serviceable bridges throughout the United States. Geosynthetic Reinforced Soil-Integrated Bridge System (GRS-IBS) is a practical alternative to traditional, deep-foundation bridge abutments. These structures can reduce construction time, minimize traffic disruption, and can be built using locally sourced materials leading to cost-savings of up to 65% (Hatami et al., 2018). Additionally, the geotextile helps integrate the superstructure and roadway, essentially creating a composite material. The resulting effect can help alleviate the magnitude of the "bump at the end of the road". With the support and promotion from the Federal Highway Administration (FHWA), the number of servicing GRS-IBS structures has increased nationwide over the last decade (Adams et al., 2011a).

1.2 Purpose of Study

Performance tests over field-scale GRS abutment models are needed in order to help promote these structures and help integrate them into current practice. This study is an extension of research completed by previous students at the University of Oklahoma. Doger (2020) and Boutin (2020)

studied the influence of facing types and compaction efforts over a series of six, full-scale (8 ft × 8 ft × 15.5 ft) GRS bridge abutment models. This study included performance tests over two additional models, GRS Abutment models #7 and #8. The results of these two GRS Abutment Models are compared with the data from the previously constructed models. Further information over the GRS Abutment Models is summarized in Table 1.

Table 1 – Summary of GRS abutment models constructed at The University of Oklahoma

GRS Abutment Model	Facing Type	Spacing (in.)	Compaction Passes	Aggregate Type	Beam Seat Width (in.)
1	CMU	8	1	3/8" #2 Cover	8
2	Large Block	8	1	3/8" #2 Cover	8
3	Large Block	12	1	3/8" #2 Cover	8
4	CMU	8	3	3/8" #2 Cover	8
5	CMU	8	3	3/8" #2 Cover	8
6	CMU	8	3	ODOT Type A	8
7*	Large Block	8	3	ODOT Type A	8
8*	CMU	8	3	3/8" #2 Cover	24

*Models constructed and tested in this study

1.3 Study Hypotheses and Objectives

The hypotheses of this study were:

1) Large-block (2 ft × 2 ft × 4 ft) facing could facilitate the construction of GRS abutments with well-graded backfill. Boutin (2020) cited well-graded backfill to be difficult to work with due to a greater percent of fines present relative to an open-graded fill (i.e., a maximum of 12% vs. 5% fines allowed). For instance, approximately one inch of uneven settlement has been reported to occur due to compaction, making it difficult to precisely meet the reinforcement spacing requirement and backfill unit weight measurements for a

given model. In comparison to open-graded aggregate, the well-graded material exhibits low workability which creates challenges when leveling each lift of aggregate. The use of large block facing should counter some of the issues related to the well-graded backfill in relation to construction time and facing movements.

2) Combining well-graded backfill and large block facing elements could improve the load bearing performance of GRS abutments in relation to abutments constructed with CMU (concrete masonry unit) blocks and open-graded backfill.
3) Loading of GRS Abutment Models using a field-scale beam width could lead to larger backfill and facing deformations, especially at greater depths, relative to the data obtained using a narrower spreader beam used in previous studies. Results obtained using the wider beam are understood to yield more accurate predictions of abutment load-deformation performance relative to bridge settlements and facing deformations.

The primary objectives of the study based on the hypotheses outlined above were to investigate the following:

1) Possible advantages of large block facing in expediting the construction of GRS Abutment Models with well-graded backfills.
2) Possible differences in load-bearing performance of GRS abutments built with well-graded backfill and large block facing elements relative to abutments that are more commonly constructed using CMU blocks and open-graded backfill.
3) Load-bearing performance of GRS Abutment Models using a field-scale beam seat relative to those of otherwise identical abutment models using a reduced-width loading beam in earlier OU studies by Doger (2020) and Boutin (2020).

Chapter 2 – LITERATURE REVIEW

This extended study focuses on the effect of various design factors while following design requirement and recommendations set by the FHWA guidelines. Section 2.1 outlines design-related factors discussed in FHWA publications and by previous contributors of this study, Doger (2020) and Boutin (2020). Various case studies related to GRS-IBS are discussed in Section 2.2.

2.1 GRS-IBS Design Factors

2.1.1 Facing Element

Any structural contributions of the facing are conservatively ignored in the stability calculations of GRS abutments. Therefore, FHWA guidelines accommodate different choices of facing without any structural consequences to the stability and performance of GRS abutments (Adams and Nicks, 2018). However, Doger (2020), Doger and Hatami (2020) and Hatami and Doger (2021), studied the influence of facing on the construction and performance of field-scale GRS abutments and observed that models with large-block facing outperformed the control model that had been built with a standard CMU facing, relative to footing settlements and facing deformations. They also found that the use of large concrete blocks could reduce the time of construction by more than 50% compared to CMU's. In relation to CMU's, the significantly heavier large blocks reduced the lateral deformation during construction, which allowed the use of compaction equipment directly behind the facing. This is not the case with CMU facings (this is discussed further in section 2.4). Even with a fewer number of reinforcement layers (12-inch reinforcement spacing vs. 8 inches), large blocks proved to increase the performance of GRS-IBS structures with respect to facing deformations and load-bearing capacity compared to CMU facings (Hatami and Doger, 2021).

2.1.2 Reinforcement

The purpose of geosynthetic reinforcement is to aid in resistance of tensile forces and restrain lateral deformation of the backfill soil (Adams et al., 2011b). Though geogrids are permitted for GRS-IBS construction by the FHWA, the reinforcement used throughout these models is geotextiles. The FHWA requires a minimum tensile strength of 4,800 lb/ft, which is met by the selected reinforcement (FHWA, 2012). Reinforcement spacing influences the ultimate capacity of GRS abutments greater than the strength of the reinforcement itself. Adams et al. (2011a) recommends a maximum reinforcement spacing of 12 inches. Nicks et al. (2013) concluded that reinforcement spacing greater than 12 inches does not utilize the full strength of the reinforcement. With a spacing larger than 12 inches, failure occurred from the soil between the reinforcement rather than through the reinforcement (Nicks et al., 2013). Hatami and Doger (2021) confirmed that decreasing the spacing from 0.3 to 0.2 meters can improve the load bearing performance of GRS abutments.

2.1.3 Backfill

Locally sourced backfill is an ideal constituent for GRS-IBS as it provides benefits related to construction costs. FHWA permits the use of both open-graded and well-graded aggregate if it conforms to the guidelines listed in Table 2 (Adams and Nicks, 2018). Both gradations may provide benefits to the GRS structure. Open-graded aggregate is low-weight, drainable, and easier to construct with when spreading, leveling, and compacting the backfill. Well-graded aggregate provides increased stiffness to the GRS mass (Hatami and Boutin, 2021). Boutin (2020) had cited

difficulty when working with well-graded aggregate. Due to the poor workability, an uneven settlement of 1 inch occurred when compacting well-graded aggregate (Boutin, 2020).

Table 2 – FHWA backfill requirements for GRS abutments (Adams and Nicks, 2018); (left) for open-graded aggregate, (right) for well-graded aggregate

Parameter	**Requirement**
Minimum aggregate size	≥ 0.5 in.
Maximum aggregate size	≤ 2 in.
Percent passing No. 50 sieve	≤ 5%
Friction angle	≥ 38°
Soundness	Backfill must be substantially free of shale or other low durability particles. Sodium sulfate loss of less than 15% after 5 cycles

Parameter	**Requirement**
Minimum aggregate size	≥ 0.5 in.
Maximum aggregate size	≤ 2 in.
Percent passing No. 200 sieve	≤ 12%
Friction angle	≥ 38°
Coefficient of uniformity	≥ 4
Coefficient of curvature	1-3
Plasticity Index	≤ 6
Soundness	Backfill must be substantially free of shale or other low durability particles. Sodium sulfate loss of less than 15% after 5 cycles

2.1.4 Compaction

FHWA requires the backfill material to be compacted to a minimum of 95 percent of the maximum dry density for well-graded aggregate and three passes of compaction equipment for open-graded aggregate (Adams and Nicks, 2018). Boutin (2020) studied the influence of compaction on full-scale GRS-IBS models. During this study, Boutin (2020) implemented three passes of compaction equipment per lift and concluded that the increased compaction effort contributed to increased

stability of the GRS mass. Boutin (2020) was able to achieve a minimum factor of safety of 11 for all three of the tested models, meeting the FHWA settlement requirements.

2.1.5 Beam Seat Width and Setback Distance

FHWA guidelines require a minimum beam seat width of 2 and 2.5 feet for bridge spans less than and greater than 25 feet, respectively. Setback distance must be at least eight inches (Adams and Nicks, 2018).

2.2 Case Studies

Saghebfar et al. (2016) investigated the performance of the Maree Michel bridge, a GRS-IBS in Louisiana, based on deformations, settlements, and reinforcement strains, vertical and horizontal stress with the GRS abutment, and pore water pressures. This study found that the maximum total settlements were less than that of the design value. Settlement within the abutment and reinforced soil foundation (RSF) contributed to less than 30% of the total settlement; the rest of the settlement was associated with the foundation soil. Majority of the lateral deformation transpired after the placement of the steel girders. Though the reinforcement strains fell within the range of the FHWA guidelines, the magnitude and locations of strain within the reinforcement layers were observed to vary with depth.

Xie and Leshchinsky (2015) ran a series of numerical simulations using Limit Analysis to investigate the critical collapse state of Mechanically Stabilized Earth (MSE) walls based on two different reinforcement configurations. The first configuration, “top-down”, consists of a higher reinforcement spacing density at the top of the wall. The second, “bottom-up”, configuration does

the opposite. The “top-down” approach provided increased stability when subjected to a constant surcharge. Benefits of the “top-down” approach levelled off when the known as the reinforcement density ratio (this is the ratio of the height-of-wall-with-dense-reinforcement to height-of-wall or RDR) fell between 0.4 and 0.8. As the RDR increased for the “bottom-up” approach, the failure mechanism moved upward above the dense reinforcement zone until the densely reinforced zone fell within the range of bearing capacity failure. Because lateral earth pressure is greatest near the toe of the wall, the “bottom-up” configuration can provide more stability for walls not subjected to surcharge loading.

Through numerical modeling, Zheng et al. (2018) investigated the effects of geogrid reinforcement spacing, backfill friction angle, and abutment geometry on reinforcement tensile forces at service load and failure condition. This study concluded that maximum tensile forces in the geogrid increases as reinforcement spacing increases and backfill friction angle decreases. The location of maximum reinforcement tensile forces at the failure condition produces a y-shape starting at the toe and heel of the beam seat. This shape converges with depth and migrates toward the toe of the wall.

Using Plaxis 2D, Gebremariam et al. (2020) investigated the effects of reinforcement spacing, reinforcement stiffness, presence of bearing bed and RSF, and compressibility of subgrade on lateral facing deformation, maximum tension in reinforcement, connection strength, and the settlement difference between the superstructure and integrated approach zones in reinforced soil structures. This study concluded the following. Though the bearing bed provided no settlement difference within reinforcement spacings of 0.2 meters, it increased the stiffness of the abutment

and reduced the settlement difference between the layers within the abutment and the integrated approach zones. Variations in the reinforcement spacing and stiffness, bearing bed, and RSF showed no effects on the magnitude of settlement experienced by the foundation. The presence of the bearing bed and RSF proved to reduce lateral deformations, maximum tension in the reinforcement, connection strength, settlement of the foundation, and settlement difference with the GRS mass.

Ardah et al. (2020) developed a 2D finite element model to investigate the effects of backfill friction angle, width of RSF, secondary reinforcement within bearing bed, setback distance, bearing width and length of reinforcement on the performance of GRS-IBS. Performance was based on lateral facing displacement, strain distribution along reinforcement, and location of failure zone. This study concluded that reinforcement strain and lateral deformation increased as backfill friction angle decreased. The addition of secondary reinforcement decreased the maximum magnitude of strain throughout the abutment; greater effects were cited in the upper portions of the abutment while minor effects were found in abutment's lower portions. Additionally, this investigation demonstrated that the width of the RSF and length of reinforcement did not affect strain distribution nor lateral deformation of the facing.

Shen et al. (2020) used 2D finite difference numerical software to investigate GRS abutments under working stress conditions to analyze the effects of combinations of reinforcement spacing and reinforcement stiffness, beam seat width, and setback distance on the responses of additional vertical stresses under the beam centerline, additional horizontal stresses under the beam centerline and behind the facing, and maximum tension in the reinforcement. A field monitored GRS-IBS in

Virginia was modeled and verified using FLAC2D in order to carry out the investigation. This study found that various combinations of reinforcement spacings and stiffnesses (given the same reinforcement stiffness-to-reinforcement spacing ratio) produces similar distributions of vertical and horizontal stresses. Maximum tensile forces in the reinforcement were found to decrease in a nearly proportional manner with decreasing reinforcement spacing. This study concluded larger beam seat widths and setback distances resulted in lower additional vertical and horizontal stresses under the centerline of the beam seat, horizontal stresses behind the facing, and maximum tension in reinforcements in the upper reinforcement layers.

Chapter 3 – METHODS

In this section, construction of GRS abutment models and data acquisition techniques are discussed. It is worth mentioning that methods discussed below are not necessarily applicable to both abutment models. Methods and materials used for only one of the models will be specified throughout this section. For additional information over the test station and materials used, refer to Doger (2020) and Boutin (2020).

3.1 Test Station

GRS Abutment Models #7 and #8 were constructed and tested in an 8 ft × 8 ft × 15.5 ft test station located at Fears Structural Laboratory in Norman, Oklahoma. The test station is equipped with hydraulic cylinders attached to the steel frame atop of the structure. Data acquisition systems are housed in a shed next to the test station. In the spring of 2021, between the constructions of GRS Abutment Models #7 and #8, the test station received a small renovation. A 30 ft × 16 ft surface was paved in front of the test station. This provides space to hold the aggregate, minimizing the risk of contaminating the material from underlying clay during construction. Additionally, the pavement provides easy access to the test station for larger equipment, such as the front-loading tractor and forklift. In order to compare test data from GRS Abutment Model #8 with previously constructed models, the model will need to experience a much greater load due to the increased footprint of the beam seat. To ensure the test will be carried out safely, bracings were created to prevent any bending of the frame. The newly paved test station and bracings can be seen in Figure 1.

Figure 1 – Improvements to test station for GRS Abutment Model #8; (Top) paved test station, (Bottom) frame bracings

A series of holes at various elevations are drilled through the backside of the test station to permit the connection between the reinforcements and WPs. The WP cables travel through holes in the

shed to feed information to the data acquisition systems. Figure 2 provides a visual of the instrumented layout for GRS Abutment Model #8. Further information regarding the test station and data acquisition systems are detailed in the paper by Doger (2020).

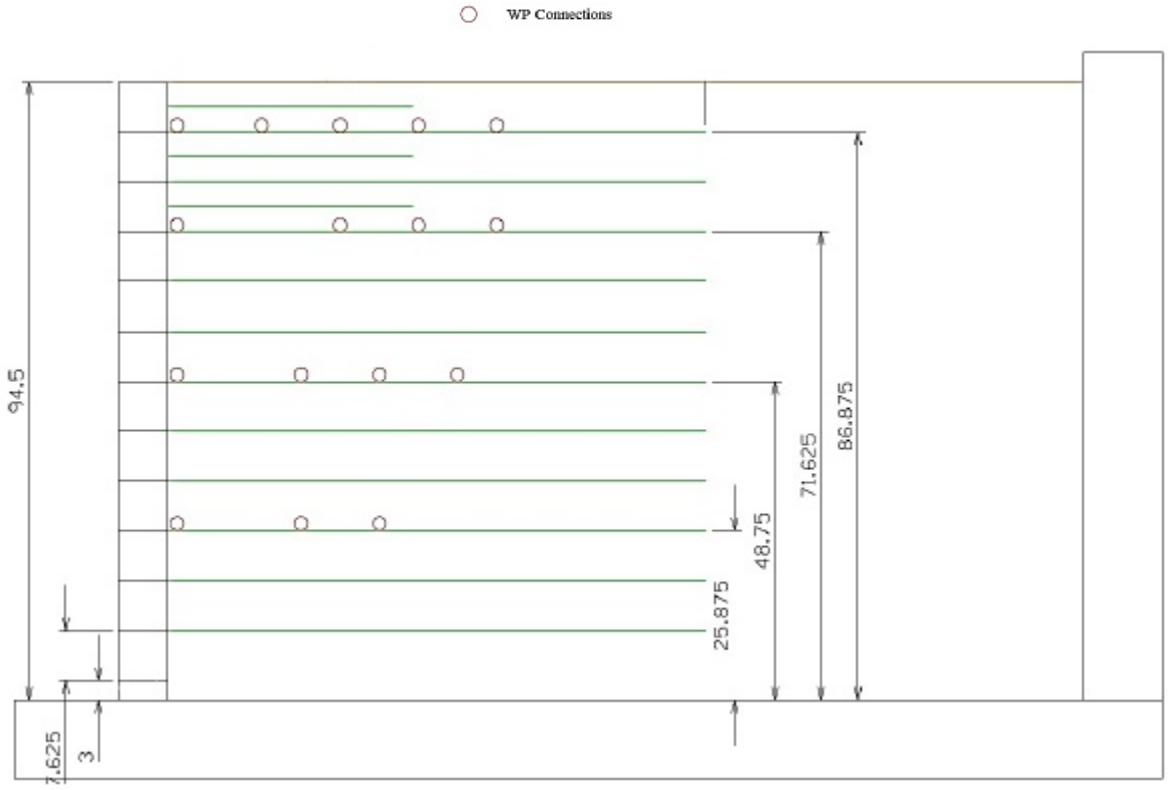

Figure 2 – Schematic layout of GRS abutment models (image provided by Doger, 2020)

As mentioned earlier, GRS Abutment Models #1 through #7 were tested using an 8-ft-long, 8-inch-wide loading beam. To conform to FHWA guidelines, the original loading beam was cut and mounted on a 7.5-ft-long, 2-ft-wide reinforced concrete slab. Additionally, the 2-foot-wide beam will provide enough setback (12 inches) to correspond to FHWA guidelines. The new loading beam used in GRS Abutment Model #8 is shown in Figure 3.

Figure 3 – Loading beam used in GRS Abutment Model #8

3.2 Materials

This section provides an overview of the constituent materials used throughout this study. Table 3 outlines the materials used in relation to GRS Abutment Models #7 and #8.

Table 3 – Abutment constituents

GRS Abutment Model	Facing Element	Instrumented Reinforcement	Aggregate Type
7	Large Block	No	ODOT Type A
8	CMU	Yes	3/8” #2 Cover

3.2.1 Geosynthetic Reinforcement

GRS Abutment Models #7 and #8 were both built with 8-inch reinforcement spacing. Geotextiles were cut from a 15 ft × 300 ft roll of Mirafi HP 570 polypropylene woven geotextile by TenCate Geosynthetics. The ultimate tensile strength of this product is 4,800 lb/ft (70 kN/m), satisfying

FHWA requirements for geotextile. Table 4 outlines the dimensions of geotextiles needed for each model.

Table 4 – Geotextile used in abutment models

Dimension	Quantity	Reinforcement Location
48” × 90”	11	Throughout the full height of the abutment’s observation section
24” × 90”	22	Throughout the full height of the abutment, outside of observation section
48” × 45”	3	Throughout the top quarter of the abutment’s observation section
24” × 45”	6	Throughout the top quarter of the abutment, outside of observation section

The shorter reinforcements were placed in between the top three main layers to form an embedded footing in the abutment (Adams and Nicks, 2018). The instrumented, observation section of each model abutment was its central 4-foot-wide central section of the model (Figure 4). This region is of particular interest as it is subjected to reduced frictional effects from the east and west walls of the test station. For this reason, the WPs are connected only to reinforcements within the observation section. Instrumented geotextiles were placed above the 3rd, 6th, 9th, and 11th layers. Steel wires protected by plastic tubing were attached to the reinforcement using a series of nuts, bolts, washers, 2” × 2” patches of geotextiles and glue. The wires ran through the backfill and out of the holes in the back wall of the test station to connect to the WPs. Figure 5 displays an instrumented geotextile and the WP connections behind the test station. Plastic bags were taped around the WPs to prevent any potential for water damage.

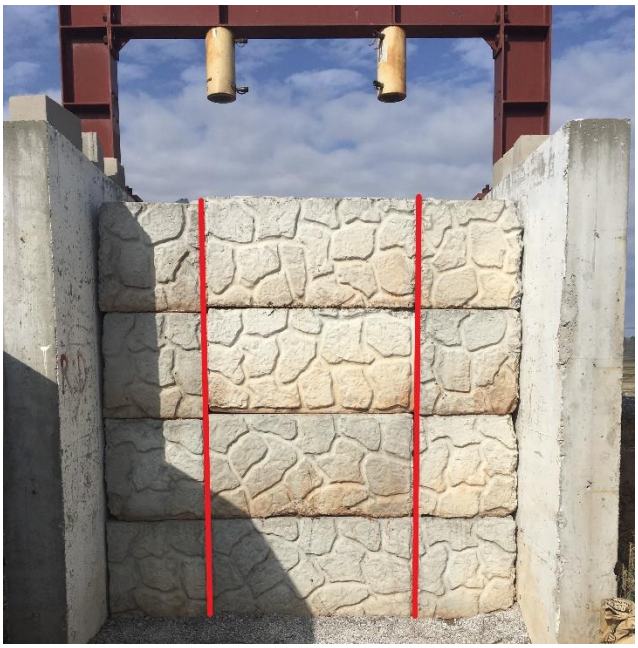

Figure 4 – Observation section (between the red lines)

Figure 5 – Geotextile instrumentation; (Left) instrumented geotextile, (Right) WP connections to geotextiles

3.2.2 Facing Elements

GRS Abutment Models #7 and #8 were constructing using large blocks (2 ft × 2 ft × 4 ft) and CMUs (7.625 in. × 7.625 in. × 15.625 in.), respectively, as facing elements. The large blocks can be observed on the right edge of Figure 1. While CMUs could be placed by hand, the significantly heavier large blocks (2,400 lbs) required a forklift to placed. The large blocks have a key located on top of the block that interlocks with a void space with the overlying block. This allows the forklift to easily place overlying blocks by sliding them over the key. Both the large blocks and CMUs were stored next to the test station for easy access.

3.2.3 Backfill

GRS Abutment Model #7 and #8 used ODOT Type A (dense-graded) and 3/8" #2 Cover gravel (open-graded), respectively. Pictures of the aggregate can be seen in Figure 6. Discussed further in the following section, both aggregates produced unwanted settlements during the compaction process. ODOT Type A proved to exhibit low workability when attempting to level any given layer. Additional information over these aggregates can be found in Chapter 4.

Figure 6 – Aggregate used for construction of GRS Abutment Models #7 and #8; (Left) ODOT Type A, (Right) 3/8" #2 Cover

3.3 Construction Process

To begin, a 3-inch sand bed was placed directly under the first row of blocks. The sand bed width was dependent on the size of the overlying facing elements (large blocks or CMUs). For previous models, the sand bed served the purpose of protecting embedded earth pressure cells (EPCs). Unfortunately, the EPCs failed to respond for GRS Abutment Model #7 and was therefore dismissed from the construction process for GRS Abutment Model #8. Nevertheless, a sand bed was created for both constructed models to maintain dimensional consistency with GRS Abutment Models #1 through #6. It is important the sand be completely level before continuing the construction process to prevent any chance of batter. Because the sand bed has potential to wash out due to rain, aggregate was placed in front of the facing. Both the sand bed and protection of can be observed in Figure 7.

Figure 7 – Sand bed installation and protection; (Top) sand bed installation for GRS Abutment Model #7, (Bottom) aggregate placement for bed protection for GRS Abutment Model #8

After the sand bed is placed and prior to placing aggregate in front of the model, the first row of facing is placed directly above the sand bed. For each lift during construction of GRS Abutment Model #8, CMUs were placed 0.5 inches back from the target facing line to account for outward movement due to compaction (Adams and Nicks, 2018). The blocks must be free of any attached soil or aggregate to ensure the individual rows of blocks maintain the same elevation across the facing. Compared to CMUs, the large blocks will extrude further outward in order to provide the

same abutment fill geometry (i.e., the back of the blocks will be at the same location). A layout of the facing placements can be seen in Figure 8.

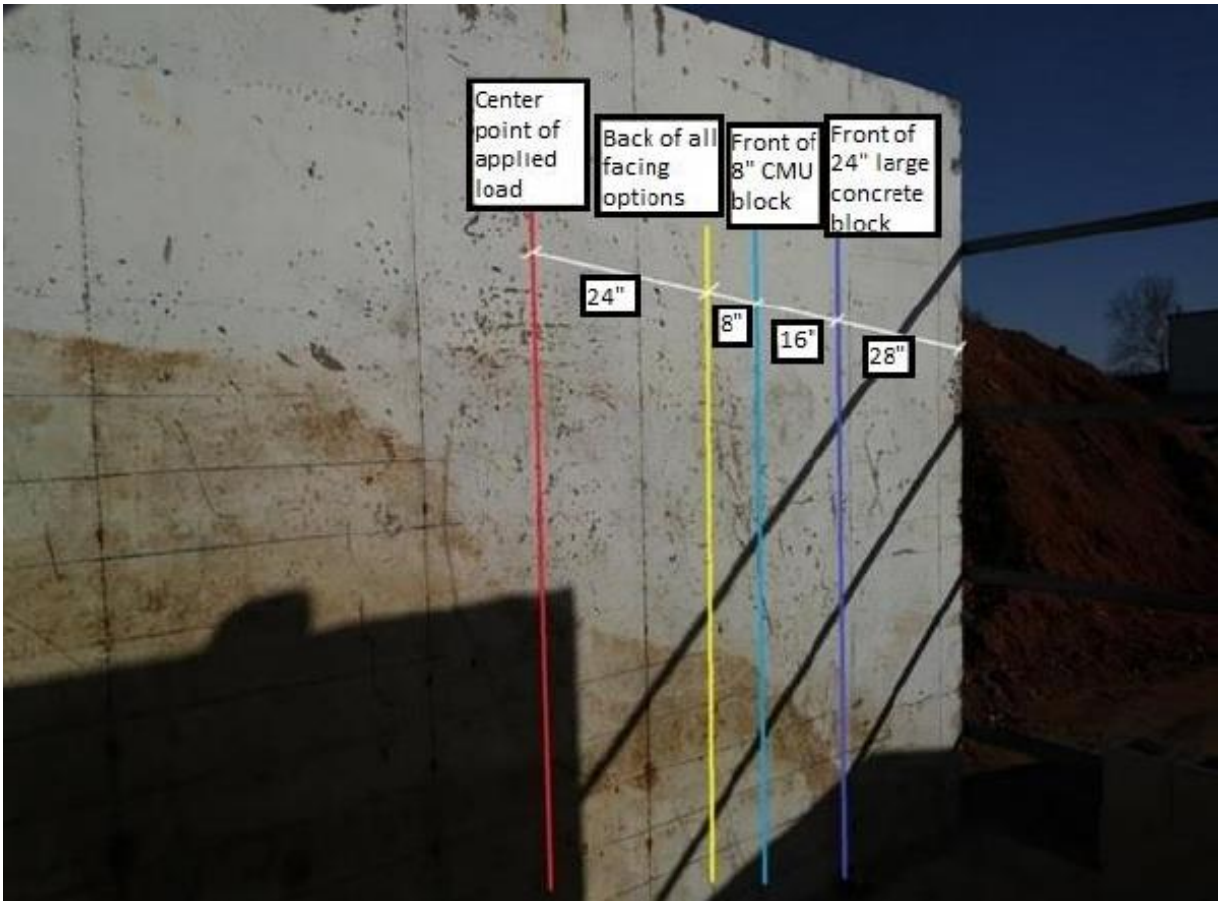

Figure 8 – Locations of facing elements projected on the sidewalls of the test station (image provided by Doger, 2020)

After the initial row of blocks has been placed, aggregate is dumped into the test station using a front-loading tractor as seen in Figure 9. The aggregate is then shoveled and raked level slightly above the desired height of the lift. Once level, three-passes of compaction equipment is carried out by a spiraling-pattern from the outside-in (Figure 9). Noted in Section 2.1, the large block facing elements permitted the use of heavy compaction equipment directly behind the facing. As for construction of GRS Abutment Model #8, hand tamping was used within 1.5 feet of the facing to prevent too much outward movement from the facing.

Figure 9 – Filling and compacting the abutment model; (Left) dumping aggregate via front-loading tractor; (Right) compaction pattern

Boutin (2020) had cited that compaction of the dense-graded, ODOT Type A aggregate produced differential settlement of roughly 1 inch and compaction of 3/8" #2 Cover aggregate had not presented any issues. In this study, using the same aggregate types, ODOT Type A aggregate has been observed to experience settlements of more than 1 inch and occasionally settlements of 2 inches upon compaction. Additionally, 3/8" #2 Cover had experienced settlements between 0.5 and 1 inch. To combat the effects of compaction, as previously mentioned, aggregate has been leveled above the desired lift height prior to compaction. Both aggregates presented compaction-related issues for GRS Abutment Models #7 and #8.

Once compacted, geotextile is installed in the model by wedging the reinforcements between the recently compacted layer and the overlying row of blocks. Mentioned in Section 3.2.1, instrumented geotextiles are placed at nominal heights of 27, 51, 75, and 91 inches and connected to the WPs behind the test station. Sand is placed around the connecting wires to prevent any potential damage from aggregate. The construction process is repeated upon completion of reinforcement installation. Additional half-sized reinforcements are installed at nominal heights of

79, 87, and 95 inches. In order to replicate previous abutment models, compaction of the top layer occurs on the day of testing. Both abutment models can be seen in Figure 10.

Figure 10 – GRS abutment models prior to surcharge loading; (Left) #7, (Right) #8

Adams and Nicks (2018) suggests filling the top 3 rows of CMU blocks with concrete and 20-inch-long rebar to prevent unwanted movement. The upper portion of the facing is more susceptible to displacement because of the absence of weight provided by overlying layers. Using a knife, the reinforcement is cutout of the CMU voids to create room for the concrete and rebar to penetrate all 3 rows. In previously constructed models with CMUs, 6 rebars were placed in alternating voids. Concrete was poured and allowed to cure for at least 7 days. For GRS Abutment Model #8, the top three rows of CMU facing were filled with concrete and reinforced with rebars in all 12 CMU voids. Additional rebar was used for GRS Abutment Model #8 due to the new leading beam's width, leading to a closer proximity to the facing. Because of the addition of the

wider and taller loading beam, the height of GRS Abutment Model #8 had to be modified to accommodate necessary swivels prior to testing. Four inches of aggregate, and the corresponding half-sized reinforcement were removed from the layer. The excavation resulted in a facing height of 94.5 inches and backfill elevation of nearly 91 inches. In the previous abutment models, it had been possible to manually shift the loading beam if it was not perfectly level. With the added weight of the wider loading beam, it was not possible to make these on-site adjustments for GRS Abutment Model #8. Instead, a levelled one-inch sand bed was created to help combat this issue.

3.4 Manual Surveying

Manual surveys to acquire facing and reinforcement deformations were conducted throughout the construction and deconstruction of the abutment models. Facing deformations were not recorded during the construction of GRS Abutment Model #7 due to the negligible outward movement imposed on the large facing blocks. Surveys were conducted over the elevations of reinforcement layers during the deconstruction of both abutment models. GRS Abutment Model #8 adopted the same elevation acquisition system during construction to visualize reinforcement movement due to surcharge loading.

3.4.1 Facing Deformation Survey

Measurements were obtained upon the compaction of each layer to analyze facing deformations induced by compaction. Additionally, the measurements helped gauge how far the subsequent layer of CMUs needed to be setback in order to achieve a vertical facing. Depending on the number of crew members available, the survey was conducted by holding or taping a piece of string to the

east and west walls of the test station at a reference line. A measuring tape was used to determine the horizontal distance from the string to the facing at each layer as seen in Figure 11.

Figure 11 – Facing deformation survey measurement

3.4.2 Reinforcement Elevation Survey

The elevations of reinforcement layers were determined by using a steel bar, a level, and a measuring tape. The steel bar was placed on top of the facing element one layer above the reinforcement of interest, providing a reference height for each measurement. Once the steel bar was confirmed to be level, the elevation was determined by measuring the distance from the steel bar to the reinforcement at a given point, as seen in Figure 12. Elevation readings were recorded

every 5 inches from the back of the facing to the tail end of the reinforcement. Additionally, measurements were taken 8, 24, and 40 inches from the west side of the reinforcement.

Figure 12 – Elevation survey measurement

Chapter 4 – MATERIALS TESTING

GRS Abutment Model #7 was constructed with the same ODOT Type A used in GRS Abutment Model #8. Because this material had been previously used, additional tests needed to be run to confirm its properties conform with FHWA guidelines. Additionally, the new 3/8" #2 Cover gravel for GRS Abutment Model #8 required testing to ensure it met the criteria required by FHWA guidelines. Aggregate was obtained from various locations of the aggregate piles to ensure the tests were conducted on representative samples.

4.1 Sieve Analyses

In accordance with ASTM C136, sieve analyses were conducted on both aggregates. The samples were dried for at least 24 hours at 230 ± 10 °F. Table 5 reiterates the gradation requirements from the FHWA guidelines previously mentioned in section 2.3. Both aggregates have maximum grain sizes between 0.5 and 2 inches. 0.6% of the 3/8" #2 Cover gravel passes the No. 50 sieve and 1.2% of the ODOT Type A aggregate passes the #200 sieve, confirming that both aggregates used in the construction of GRS Abutment Model #7 and #8 meet the requirements set by the FHWA guidelines (Adams and Nicks, 2018). Though not used for this study, the FHWA suggests the use of AASHTO No. 89 and VDOT 21-A as GRS abutment fill. These aggregate types are compared to 3/8" #2 Cover and ODOT Type A in Figure 13. The granular backfill requirements by ODOT are compared with the aggregates used throughout this research in Figure 14 ("Oklahoma Department of Transportation Standard Specifications", 2009). Both aggregates are accepted by ODOT.

Table 5 – FHWA backfill gradation requirements (Adams and Nicks, 2018)

	Open-graded Aggregate	**Well-graded Aggregate**
Max. Aggregate Size (x)	$0.5 \leq x \leq 2$ inches	$0.5 \leq x \leq 2$ inches
% Passing No. 50 Sieve	$\leq 5\%$	-
% Passing No. 200 Sieve	-	$\leq 12\%$

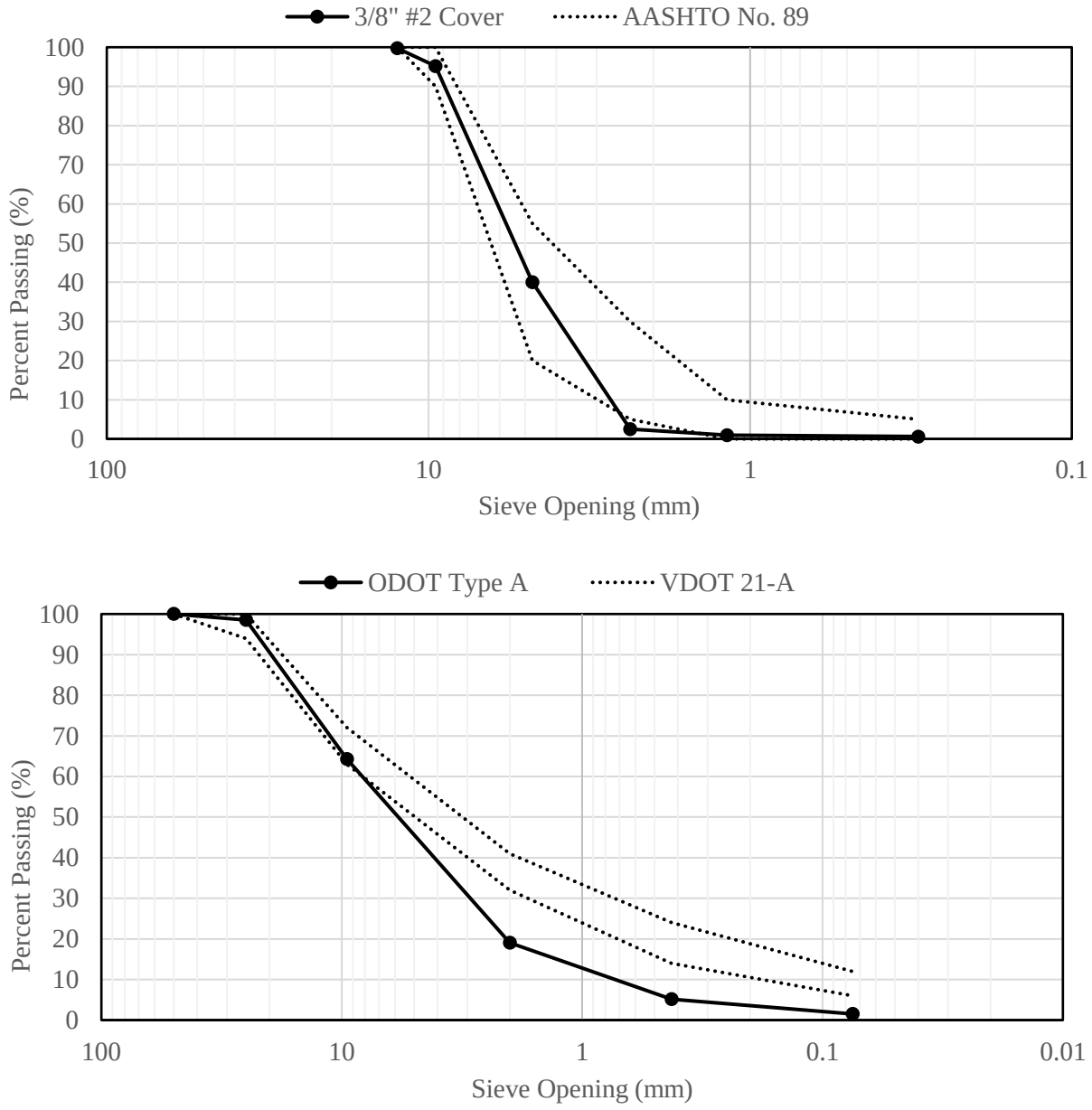

Figure 13 – Aggregate used in study compared to FHWA suggested backfills; (Top) open-graded, (Bottom) well-graded

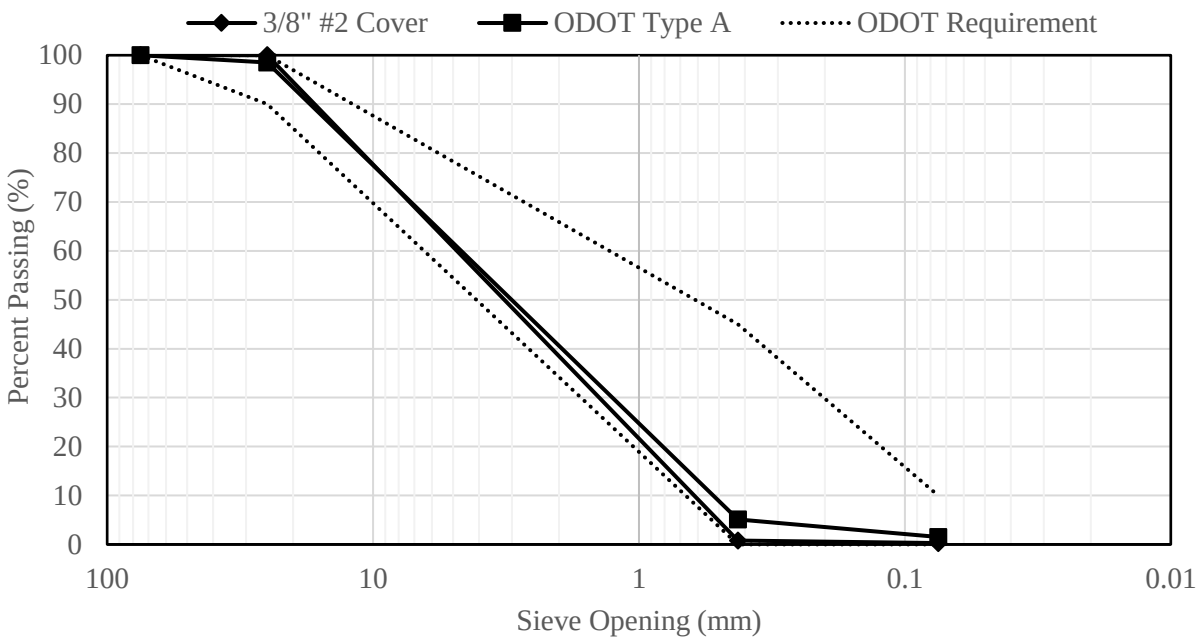

Figure 14 – Aggregate used in this study compared to ODOT backfill requirements

It is important to compare gradation results of the aggregate used in previous models to determine if its properties are consistent with those of current and future GRS abutment models. Figure 15 compares the 3/8" #2 Cover aggregates used for construction GRS Abutment Models #1, #4, and #8. While GRS Abutment Models #1 and #4 were constructed using the same batch of aggregate, GRS Abutment Model #8 was constructed using a new batch of aggregate. Results show that the batch of 3/8" #2 Cover aggregate used for GRS Abutment Model #8 was more well-graded in comparison to the previously mentioned models.

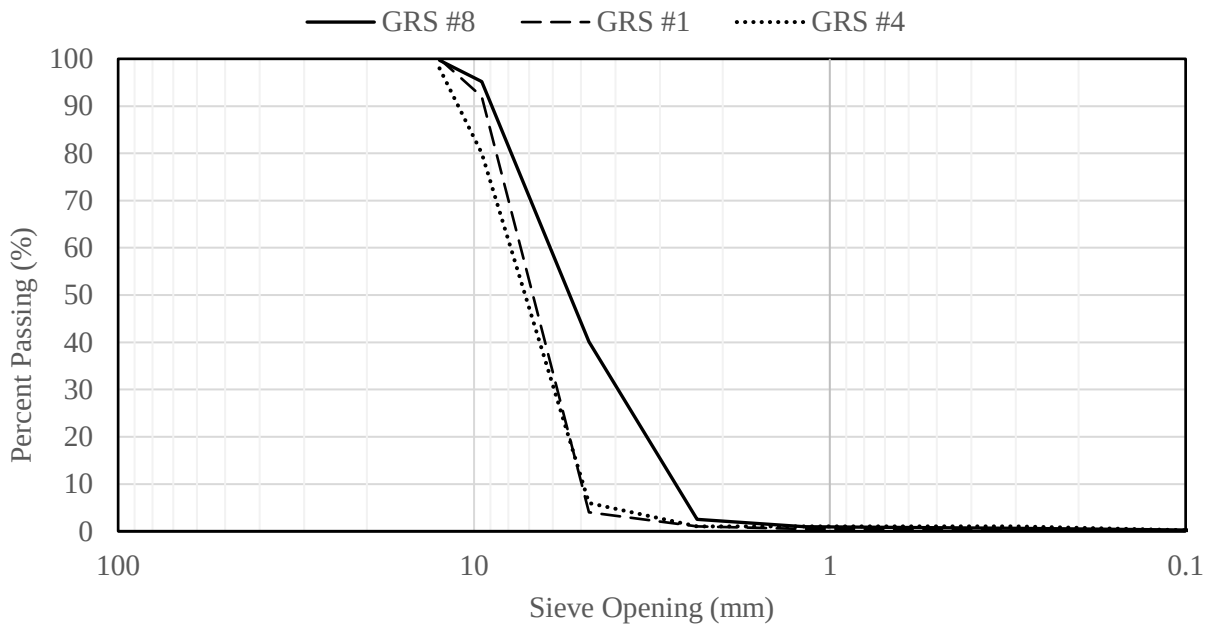

Figure 15 – Grain size distributions of 3/8" #2 Cover aggregate used for construction of GRS Abutment Models #1, #4, and #8

Because the aggregate used in GRS Abutment Model #7 had previously been used in GRS Abutment Model #6, one could expect the percent of fines to increase between uses. Though Figure 16 shows the percent of fines to be slightly greater in GRS Abutment Model #6, it can be concluded that the gradations of the backfills were consistent and within the sample-to-sample variations that would be expected for aggregate reuse. The agreement between the two gradation curves in Figure 16 also indicates that the well-graded aggregate used in GRS Abutment Model #7 had a satisfactory degree of durability.

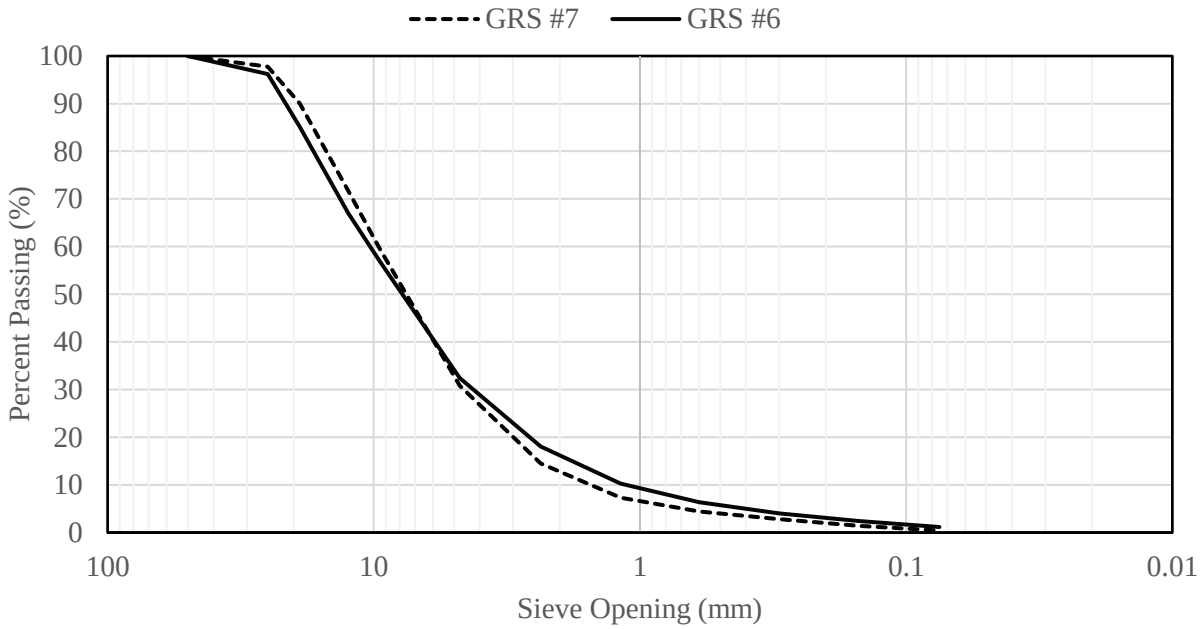

Figure 16 – Grain size distributions of ODOT Type A aggregate used for construction of GRS Abutment Models #6 and #7

4.2 Direct Shear Tests

Direct Shear Tests (DSTs) were conducted on the recycled ODOT Type A aggregate to ensure its friction angle conforms with FHWA guidelines. ASTM D3080 states that the gap size should be approximately equal to the diameter of the maximum sized particle. Based on the sieve analysis results (Figure 13), the largest particle size of 25 mm in the ODOT Type A aggregate represents a very small portion of the entire sample (1.4%). Because of this, a gap size of 12 mm was used throughout this test. Tests were performed with a shear rate of 0.04 in/m The resulting friction angle was found to be 56°, well above the required 38°. Figure 17 displays the results of the DST performed. Doger (2020) and Boutin (2020) found friction angles of both aggregates to be above 38°. Due to the consistency of data previously obtained, it was decided that DSTs would not be conducted for the 3/8” #2 Cover aggregate used in GRS Abutment Model #8.

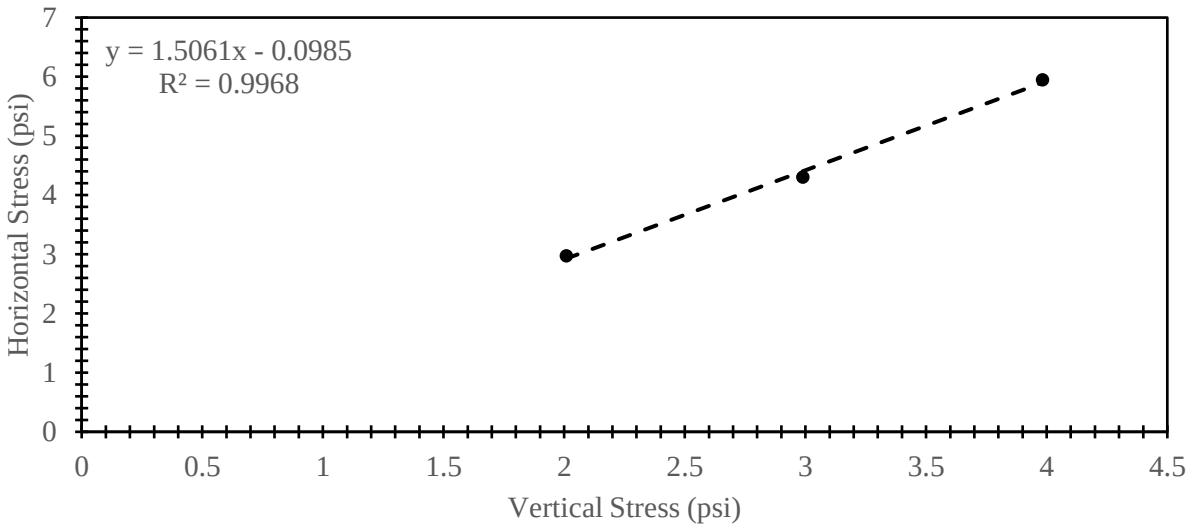

Figure 17 – DST results using recycled ODOT Type A aggregate

4.3 Unit Weight Tests

Because the compaction effort is difficult to replicate in the lab, a series of large-scale tests have been conducted to determine the unit weight of the backfill. The testing procedures will be discussed in this chapter while the results of these tests will be discussed in the following chapters.

4.3.1 Constructed Density Test Cube

Prior to the construction of GRS Abutment Model #7, the large blocks were arranged to create a 4 ft × 4 ft × 4 ft cube. The test cube was filled by shoveling ODOT Type A aggregate into plastic bins, weighing the bins, and dumping aggregate inside. The aggregate was compacted with three passes of compaction equipment every 8 inches until the cube reached its maximum height. The large blocks were not perfectly placed so measurements were taken to accurately obtain the volume. Images of the test cube can be seen in Figure 18. Two days were needed to construct the cube, with rainfall occurring between the two days.

Figure 18 – Constructed Test Cube

4.3.2 Sand-Cone Method

During the deconstruction of GRS Abutment Model #7, unit weights were obtained by the Sand-Cone Method in accordance with ASTM D1556. The tests were conducted at elevations of the 2nd, 5th, 8th, and 11th reinforcement layers. Unit weights were obtained near the facing, directly under the beam, approximately 57 inches from the back of the facing (distance between loading location and tail end of reinforcement), and approximately half the distance from the tail of the reinforcement to the back wall of the test station, as seen in Figure 19.

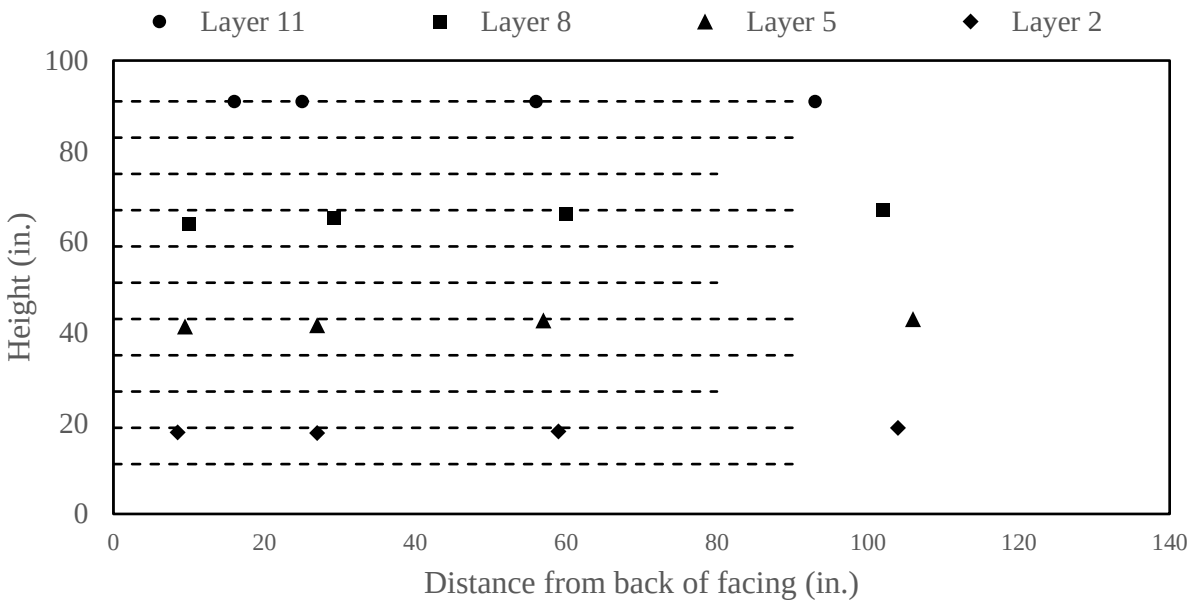

Figure 19 – Sand-Cone Method test locations

4.3.3 Deconstructed Density Test Cubes

In the final stages of deconstructing GRS Abutment Models #7 and #8, the aggregate was carved using a pickaxe and demolition hammer to obtain two cube-like shapes in the northwest (NW) and northeast (NE) corners of the test station. Once the shapes were carved, length measurements were obtained for the exposed sides of the cubes every 5 inches. Figure 20 displays the deconstructed cubes from GRS Abutment Models #7 and #8; the yellow lines provide a visual of the measurements taken. For the sides touching the walls of the test station, length measurements were taken at the top and bottom of the cubes and interpolated for every 5 inches. One at a time, the test cubes were deconstructed. The aggregate was shoveled into plastic bins and placed on a scale to obtain the weight of the cubes. Representative aggregate samples were collected to retrieve the water contents of each cube.

Figure 20 – Deconstructed test cubes; (Top) GRS Abutment Model #7 (yellow lines represent the measurement pattern), (Bottom) GRS Abutment Model #8

4.4 Concrete Testing

As mentioned in Section 3.3, the top three layers of CMUs were filled with concrete and rebar in all 12 facing voids. Because there are no successive layers to provide overburden pressure, the reinforced facing serves the purpose of eliminating the potential of unwanted facing deformations (Adams and Nicks, 2018). FHWA guidelines (2012) and Adams and Nicks (2018) suggest using class A concrete with a compressive strength of 4 ksi.

Other than the use of ready-mix concrete, there is no cited evidence of any specified mix ratios, cure times, and testing of concrete for GRS Abutment Models #1, #4, #5, and #6 by Doger (2020) and Boutin (2020). It is important to note that even without any mix design, the previous abutment models did not show signs of cracking in the top three rows of facing after surcharge loading. For the purpose of establishing a standard for future abutment models, two batches of a mix using 40 pounds water, 69 pounds of Type I/II Portland Cement, and 227 pounds of both sand and 3/8" aggregate were used to reinforce the CMU facing. Excess concrete was used to create nine 4" × 8" cylinders. Three cylinders were tested for compressive strength after 7 days, 14 days, and the day of the surcharge loading test. Table 6 presents the results of the compressive strength testing done in accordance with ASTM C39.

Table 6 – Compressive strength of concrete used in facing

Cure Time (days)	Average Compressive Strength (psi)
7	3,075
14	3,781
18 (test date)	4,011

Chapter 5 – RESULTS AND ANALYSES

This section presents and discusses the results related to facing deformations, load-settlement performance, reinforcement strain, elevation surveys and unit weights of GRS Abutment Models #7 and #8. For safety reasons, the loading of GRS Abutment Model #7 was kept below 250 kips. With the additional support of the frame provided by the bracings, GRS Abutment Model #8 was permitted to experience higher loads. Following, the construction and labor requirements of this study's abutment models will be presented and compared to those from GRS Abutment Models #1 through #6.

5.1 GRS Abutment Model #7

5.1.1 Facing Deformations

WPs at the 2nd, 3rd, and 4th rows of blocks measured the lateral deformation of the abutment model throughout the loading test. Figure 21 displays the displacement results with respect to surcharge load. The maximum displacement was found to be 0.47 inches which is within the allowable lateral deformation limit of 1% of the facing height under service load (Adams et al., 2011b). The facing appears to deform exponentially with increasing load. Figure 22 shows lateral deformation along the height of the facing at various loads. Data was not received for any load less than 190 kips during the unloading phase of the test. Therefore, the EOT (end of testing) line in Figure 22 represents the lowest load recorded by the DAS. Doger (2020) measured facing deformations throughout construction of two models with large facing blocks. Both models experienced less than 0.6 inches deformations upon completion of construction. Because of the minimal movement

experienced by Doger (2020), facing deformation readings were not recording during the construction process for GRS Abutment Model #7.

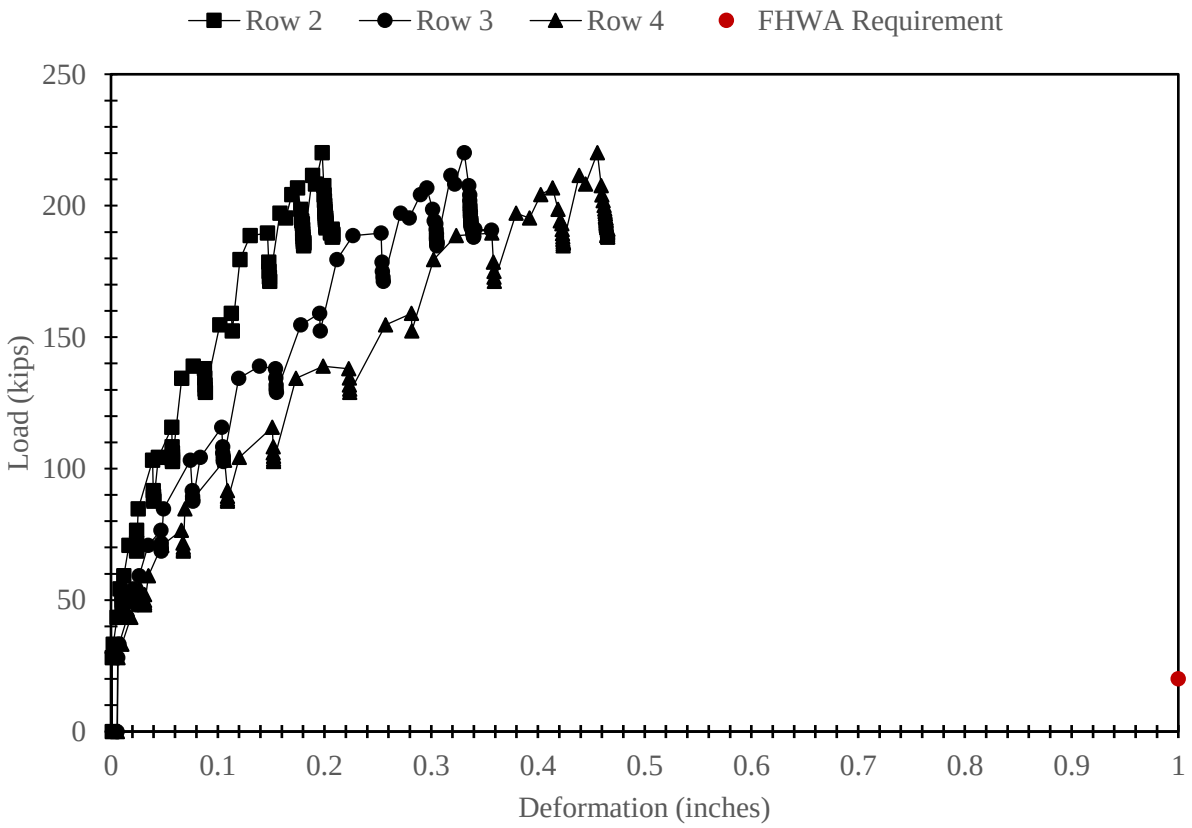

Figure 21 – Load-deformation response of GRS Abutment Model #7

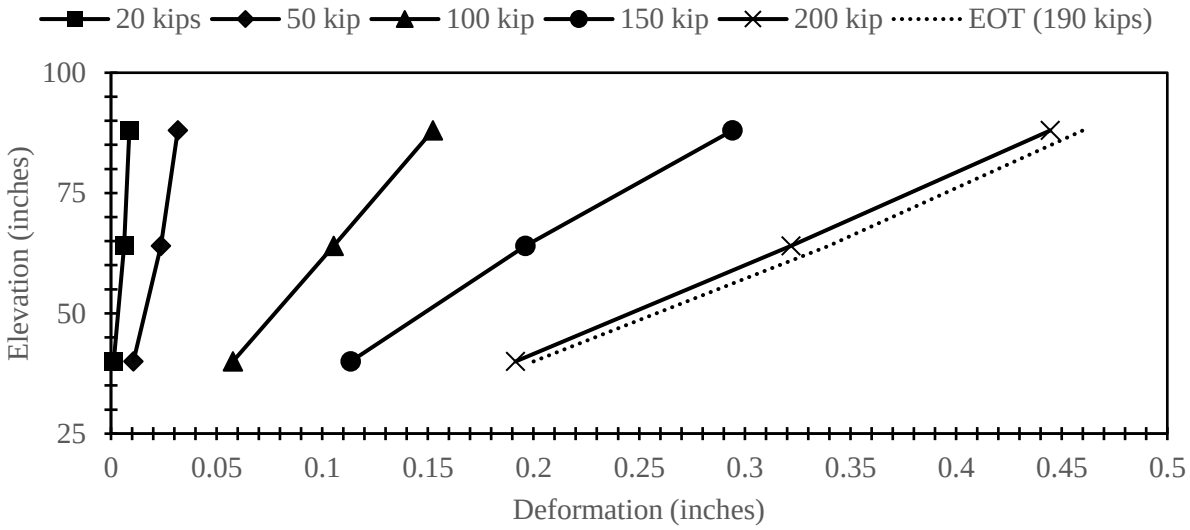

Figure 22 – Lateral deformation with respect to elevation of GRS Abutment Model #7

5.1.2 Load-Settlement Performance

Figure 23 displays the load settlement response of the abutment model with respect to the FHWA guideline's requirement. During the initial loading sequence, it was noticed that one of the LCs was not responding properly (later, it was discovered the LC wires had been torn within the cable). During efforts to fix the problem, the LC was periodically loaded to in hopes of restoring the connection. These efforts resulted in roughly 6 mm of settlement and can be observed in Figure 21 at the beginning of the loading test. FHWA guidelines state the allowable bearing pressure on a GRS Abutment is 4 ksf and the vertical strain is limited to 0.5% of the height of the abutment (Xiao et al., 2016). By this standard, a 20-kip load must not result in more than 0.5 inches of settlement for this model. The abutment model did not experience 0.5 inches of settlement until nearly 15 ksf were applied, providing a factor of safety (FS) of 3.75.

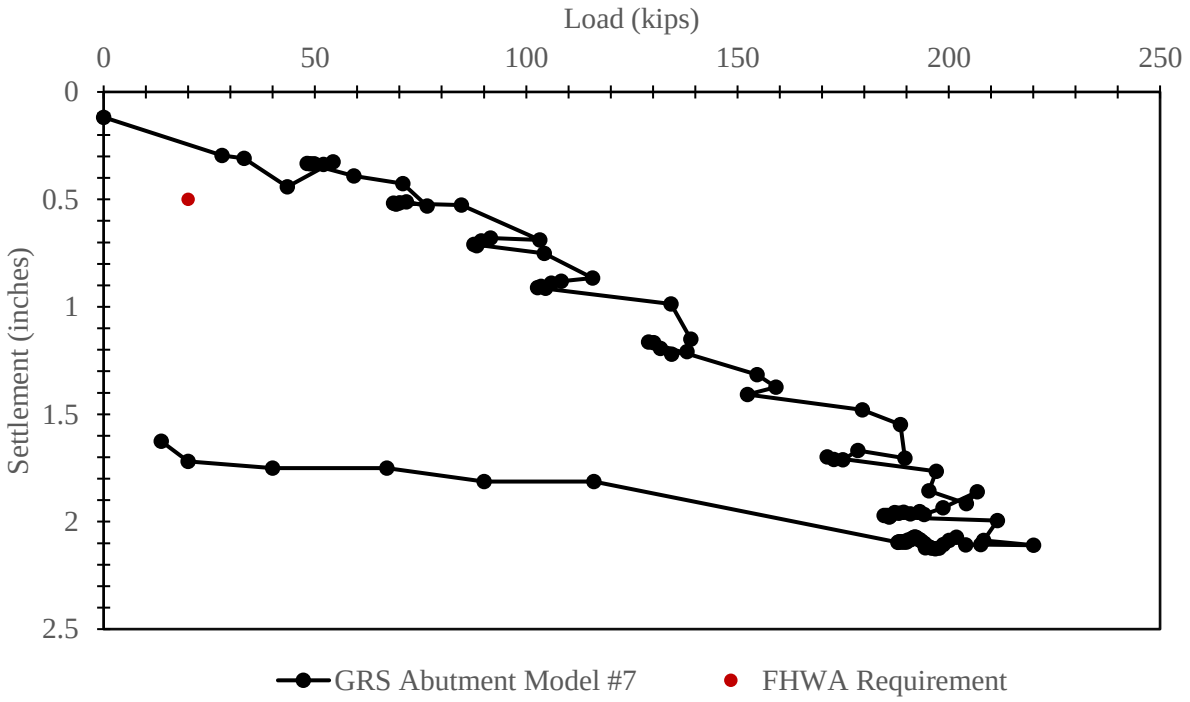

Figure 23 – Load-settlement performance of GRS Abutment Model #7

5.1.3 Elevation Survey

As shown in Figure 24, elevation measurements began at the top of the 9th layer when it became visibly clear that the reinforcements were no longer spaced at 8 inches. The reinforcement at this height was severely depressed close to the facing as shown in Figure 25. Figure 24 also includes the potential slip plane (outlined in red) based on the maximum theoretical depression of each reinforcement layer. Upon construction of the model, the geotextiles were placed up to the edge of the large blocks' keys. Measurements were not taken during construction, so it is possible that layers were not perfectly spaced to begin with. The poor workability and high level of compressibility of the well graded aggregate made it extremely difficult to ensure the reinforcement layers were level upon compaction.

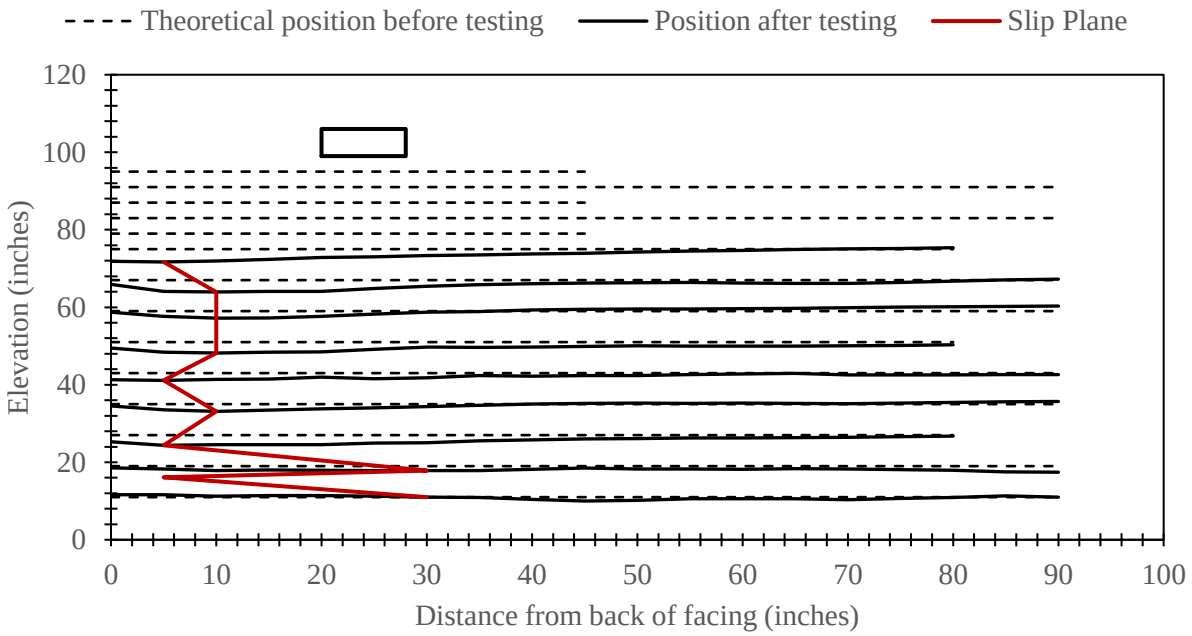

Figure 24 – Elevation survey of GRS Abutment Model #7

Figure 25 – Reinforcement at 75-inch elevation of GRS Abutment Model #7

5.1.4 Backfill Unit Weight

Figure 26 displays the resulting unit weights and dry unit weights using the Sand-Cone method. Based on the maximum particle size, the minimum volume of the test hole must be 0.075 ft^3. Secondary reinforcements were located 4 inches beneath the 11^{th} layer. This made it extremely difficult to excavate test holes to the required volume. This may explain why the unit weights recorded for the 11^{th} layer are less than those of the 8^{th} layer. Figure 27 shows the difference in water contents between the samples. One can see that the water contents are generally higher for the lower layers due to drainage.

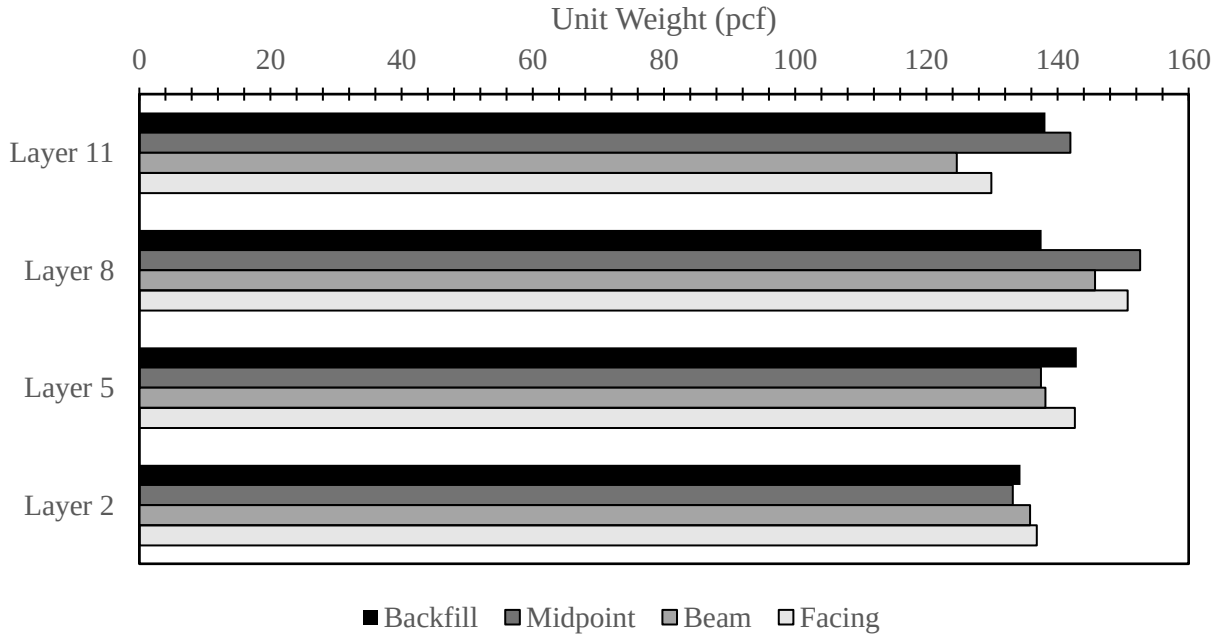

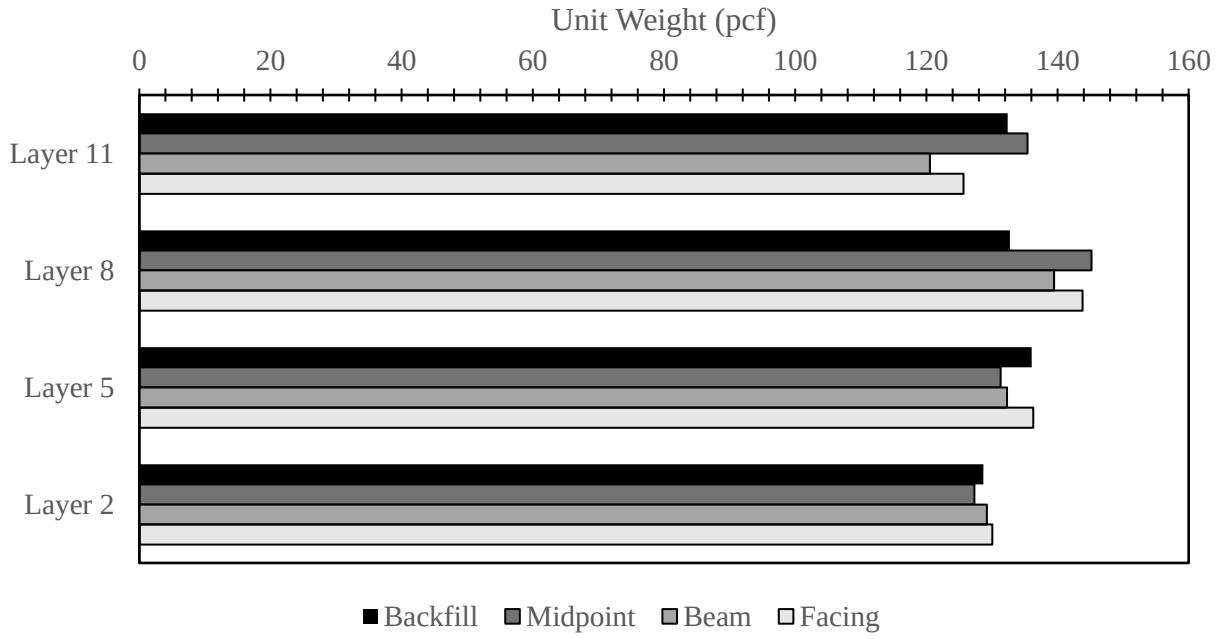

Figure 26 – Unit weight of backfill after surcharge loading of GRS Abutment Model #7; (Top) in-place unit weight, (Bottom) dry unit weight

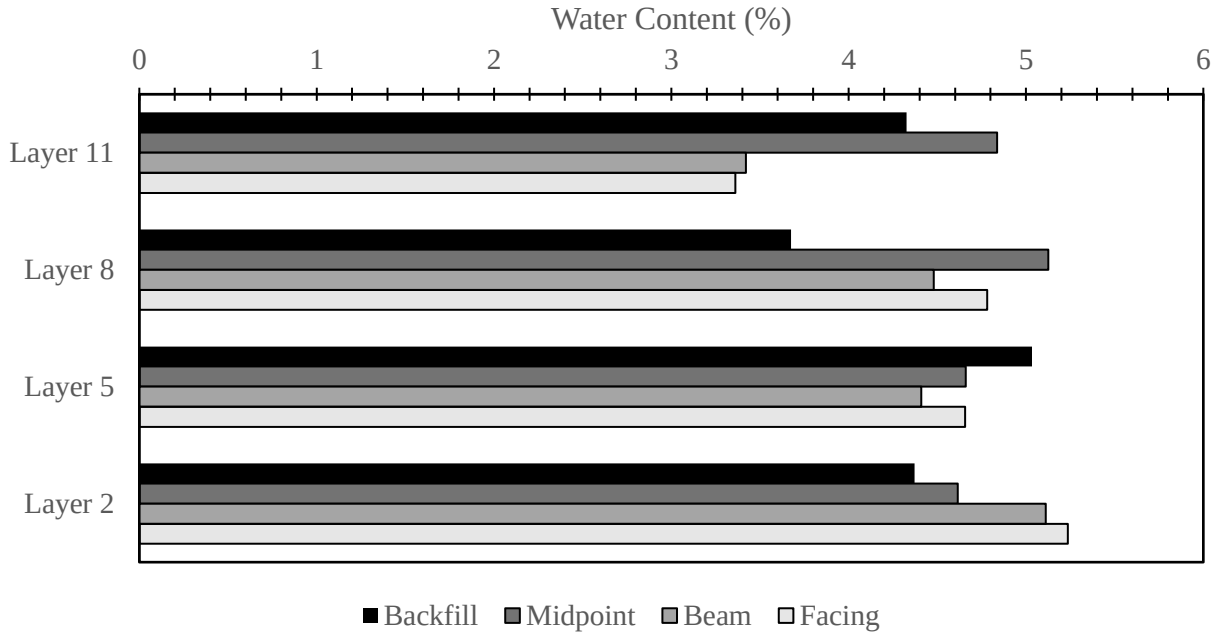

Figure 27 – Water contents of backfill after surcharge loading of GRS Abutment Model #7

5.1.5 Density Test Cubes

To accurately calculate the volume, the deconstructed test cubes were modelled in AutoCad Civil 3D using the measurements obtained (Figure 28). Table 7 presents the data acquired from both the constructed and deconstructed test cubes associated with GRS Abutment Model #7.

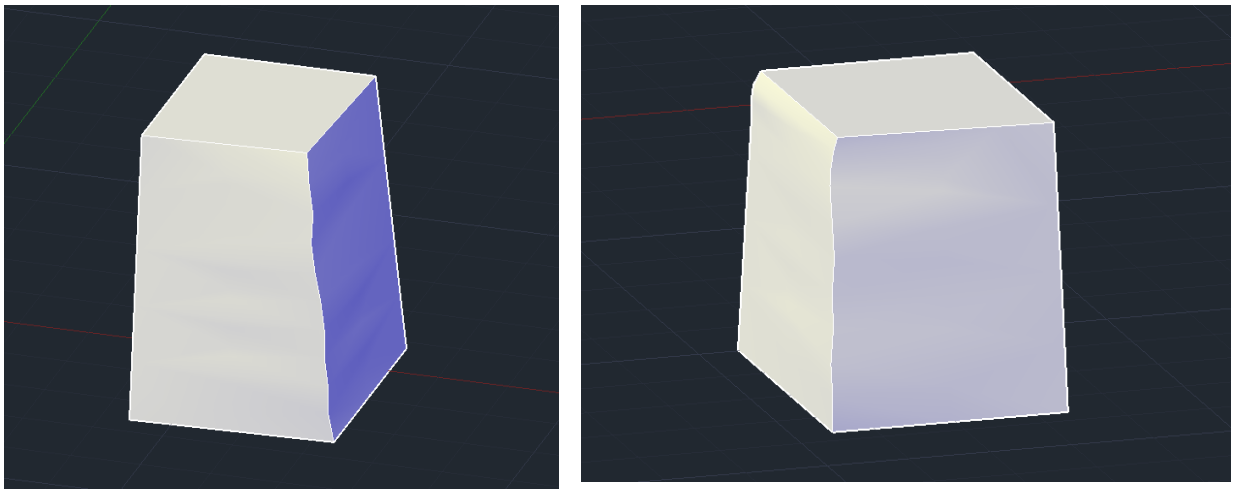

Figure 28 – Deconstructed test cubes modelled in AutoCad Civil 3D

Table 7 – Properties obtained from density test cubes related to GRS Abutment Model #7; (W) water content, (γ) unit weight, (γ_d) dry unit weight

Test Cube	W (%)	γ (pcf)	γ_d (pcf)
Constructed	5.79	135.87	128.22
Deconstructed - NW	4.68	131.68	125.79
Deconstructed - NE	4.89	134.61	128.33

The results are within an acceptable range of variation. It is important to note that the exposed sides of the deconstructed cubes were not flat. Because of this, it was extremely difficult to obtain measurements with extreme precision.

5.2 GRS Abutment Model #8

5.2.1 Facing Deformations

During abutment construction, the facing showed signs of negative batter. Like previous models built with CMUs, a half-inch setback of overlying CMUs was implemented to prevent any negative batter that may be induced by compaction. The CMUs did not experience any uncommon outward movement from compaction. It was later noticed that the negative batter was a product of a slightly angled facing. This could be caused by several reasons such as, an imperfectly leveled sand bed or small pieces of aggregate wedged in between facing units. The negative batter was most significant on the west side (1.4-inch difference between crest and toe of abutment) and less significant on the east side (0.6 inches). The control zone experienced an overall average batter angle of 0.53°. Adams and Nicks (2018) state that "any deviations greater than 0.5 inches [relative to a vertical facing] should be corrected". The negative batter in the control zone ranged from 0.6 to 1 inch. Though this deformation is greater than that permitted by the FHWA, there are cited GRS abutments that have been built with poor facing alignments while exhibiting satisfactory stability (Adams and Nicks, 2018). Figure 29 shows the facing movements due to the compaction of overlying layers and lateral earth pressure of the backfill at the end of construction (EOC). Because the top few rows did not experience many overlying compactions, and because the top row was compacted 18 days after concrete was poured, minimal lateral deformation occurred. Figure 30 displays the abutment facing prior to testing relative to the target vertical plane.

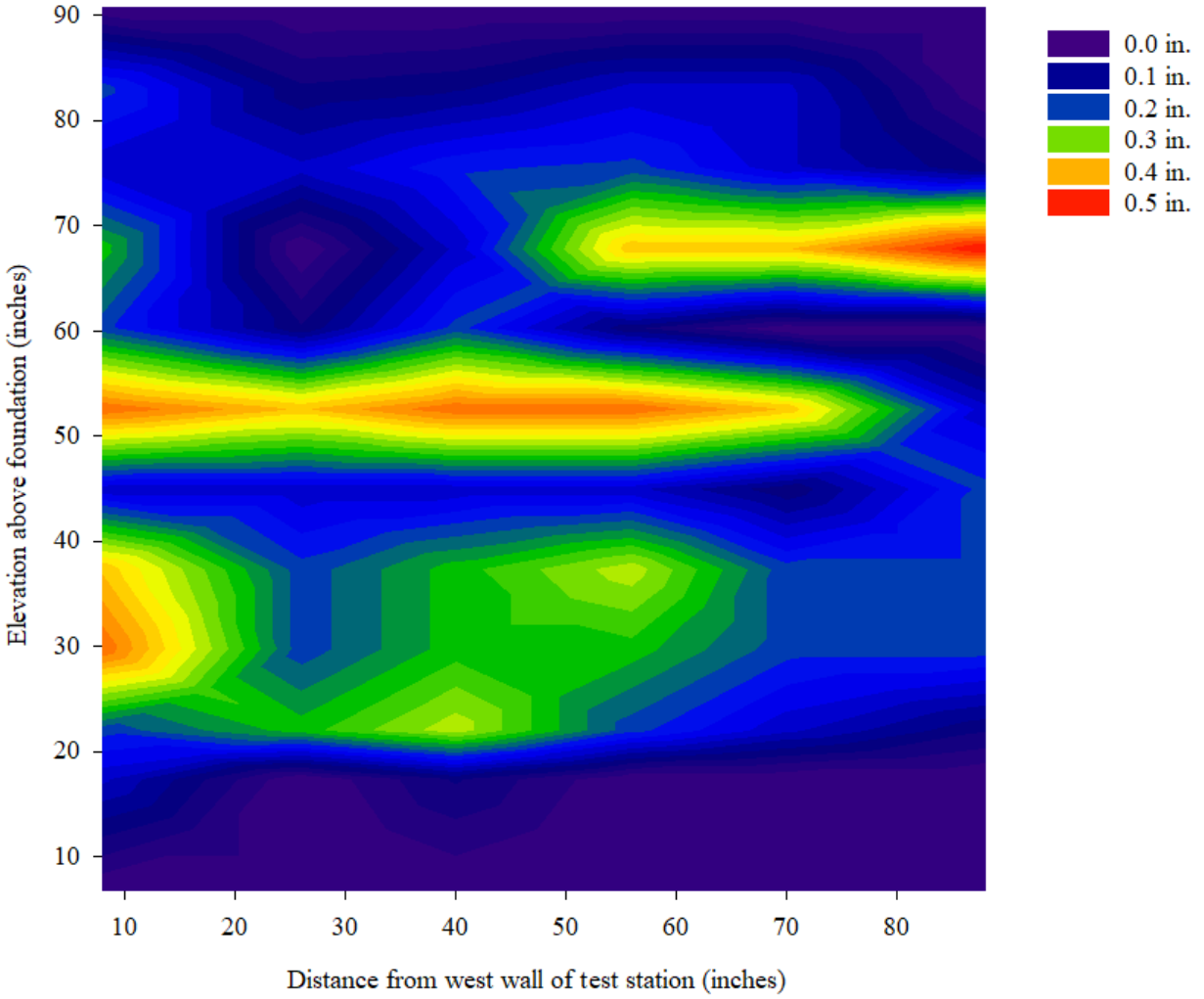

Figure 29 – EOC lateral deformation of GRS Abutment Model #8

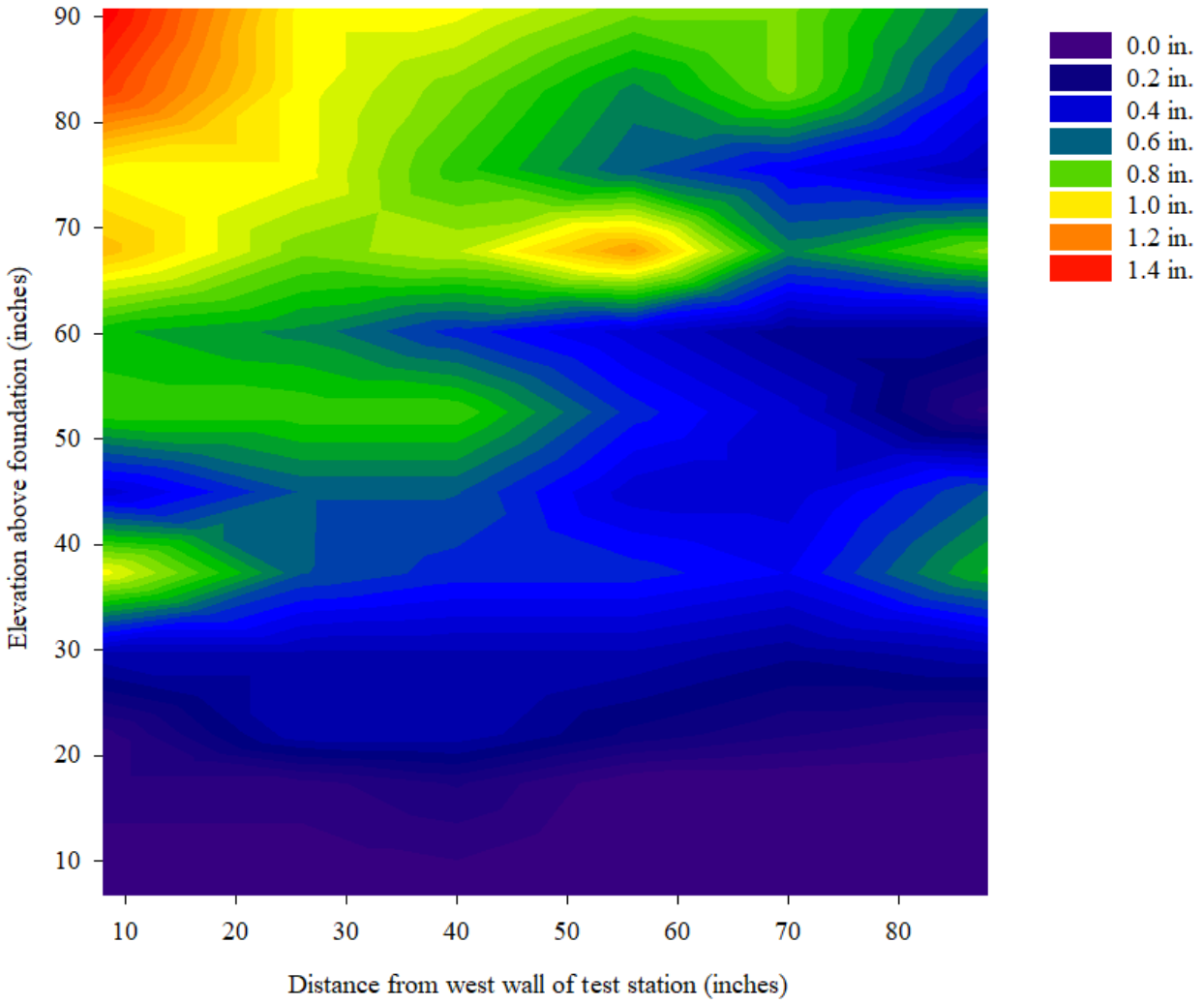

Figure 30 – Outward position of abutment facing at EOC relative to target vertical plane of GRS Abutment Model #8

Figures 31 and 32 show the deformation of the facing throughout the performance test. The deformation does not exceed the FHWA requirements until over 21 ksf were loaded on the abutment, which is over four times greater than the maximum service load for GRS abutments. Contrary to GRS Abutment Model #7, this model displayed a bulge-like movement as the belly of the facing experienced the greatest deformations.

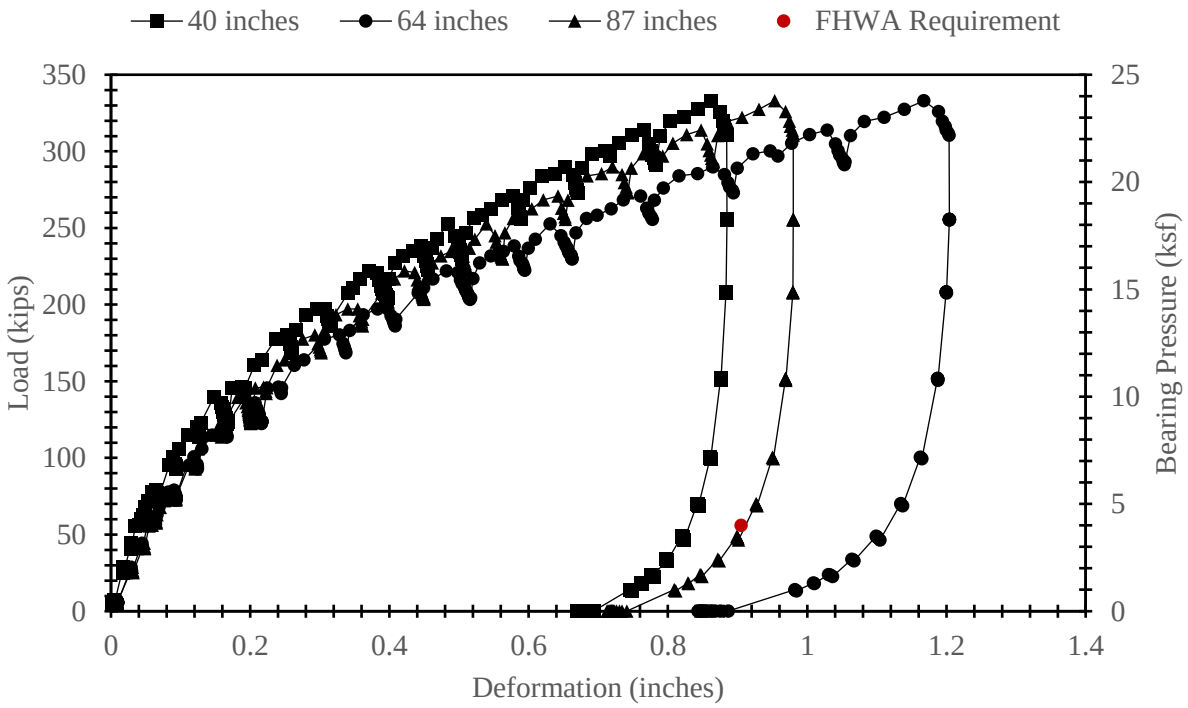

Figure 31 – Load-deformation response of GRS Abutment #8

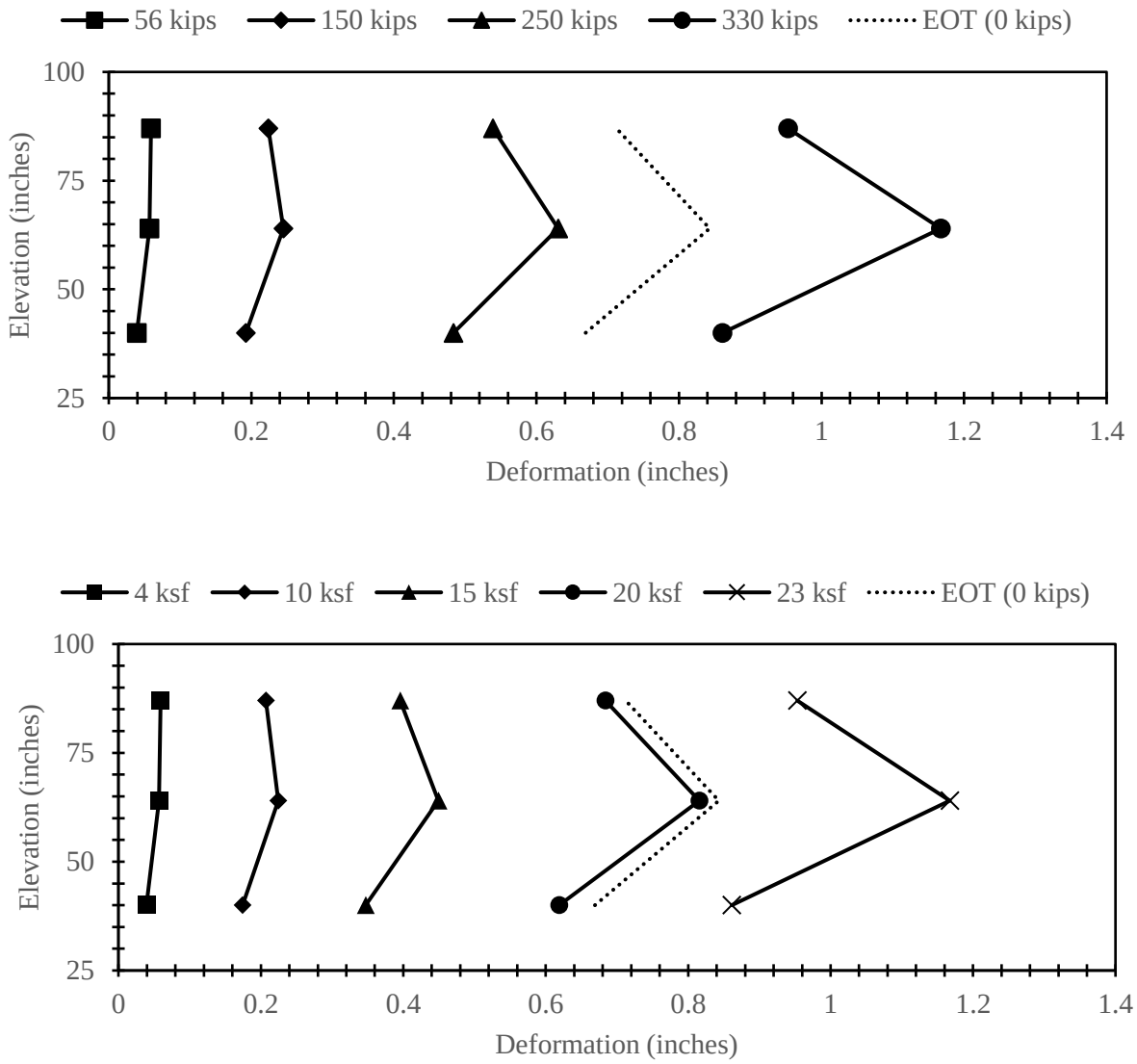

Figure 32 – Lateral deformation with respect to elevation of GRS Abutment Model #8; in terms of (Top) kips, and (Bottom) ksf

Figure 33 displays a contour map of lateral deformation experienced after performance testing. It can be observed that the contour map does not display the same degree of deformation when compared to Figure 32. GRS structures are assumed to be of constant volume. Facing deformations and settlements were permitted to rebound following the performance test and prior to the facing deformation survey, which provides explanation as to why Figures 32 and 33 display different results. Nonetheless, both figures show representation of a bulge-like movement where the peak

deformations occur in the 60 to 70-inch elevation range. CMU fractures were observed in the 9th layer during the later phases of the performance test; Figure 34 outlines the cracks. Though not visible, an additional crack of the eastmost CMU in layer 5 was discovered upon deconstruction.

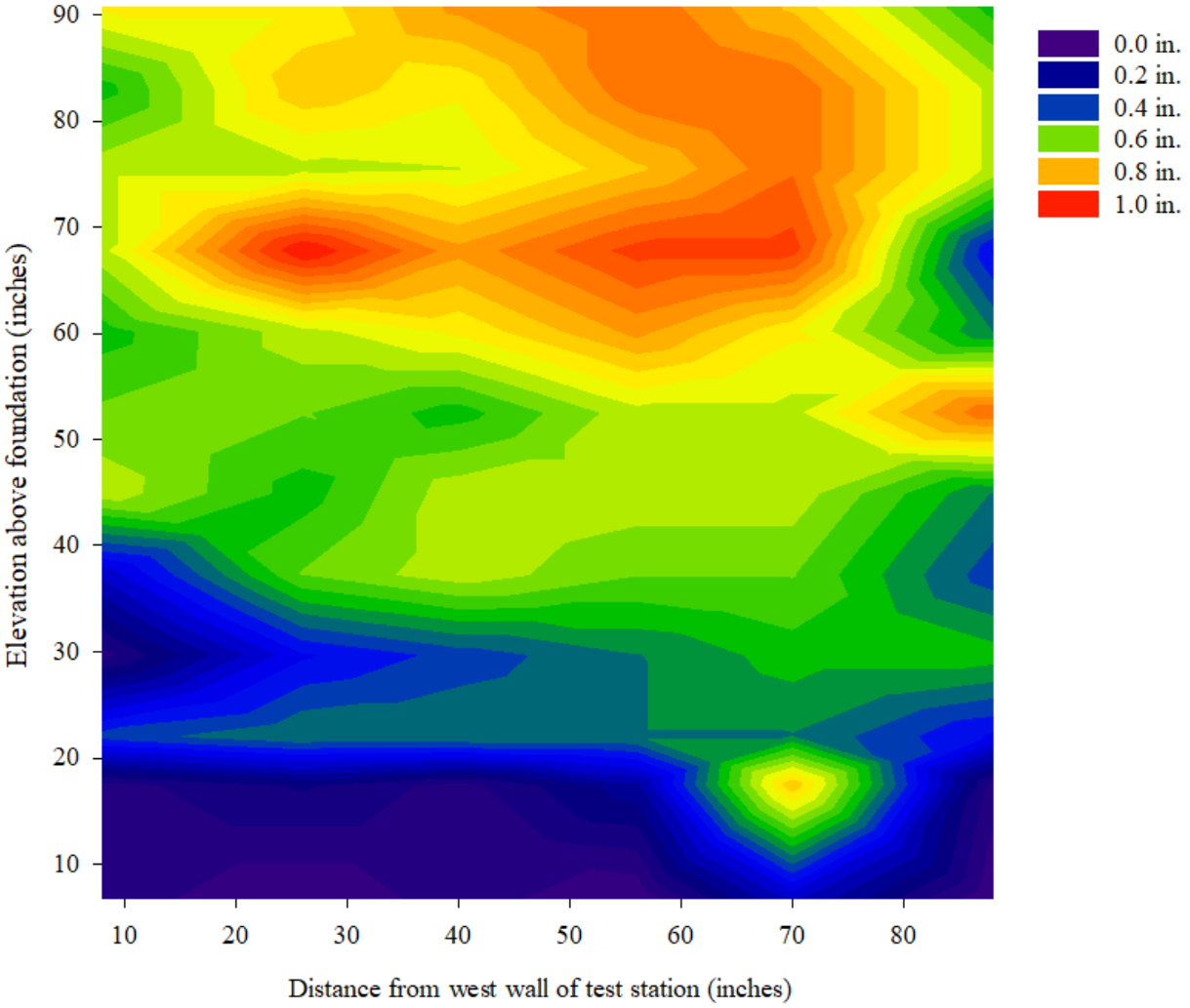

Figure 33 – Lateral deformation due to 23.8 ksf applied load on GRS Abutment Model #8

Figure 34 – CMU fractures from GRS Abutment Model #8 performance test (outlined in yellow)

The cracks in the 9th layer extended from 60.5 to 68.125 inches above the foundation slab. Figure 35 presents a cut section of the abutment superimposed with a chart of Boussinesq's pressure distribution for an infinitely long footing (Bowles, 1982). The vertical red line and horizontal black line represent the abutment facing and foundation slab, respectively. The largest magnitude of pressure experienced behind the abutment facing occurs at roughly 67 inches above the foundation slab, which correlates to the 9th layer and provides explanation for the cracks propagated at this location.

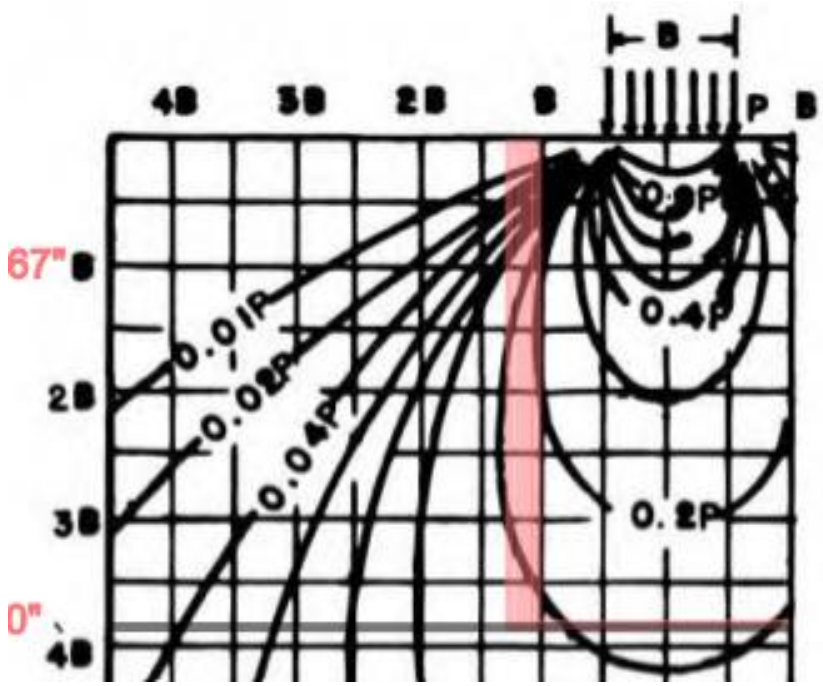

Figure 35 – Abutment cut section superimposed with Boussinesq's pressure distribution (the red line represents the facing column, black line represents floor slab; initial image provided by Bowles, 1982)

5.2.2 Load-Settlement Performance

Figure 36 displays the load-settlement response of the abutment model. The abutment experienced roughly 0.35 inches of settlement shortly after loading began due to compression of the sand bed created for this model. The data showing the early settlement had been removed from this plot to focus on the performance of the model. The model experienced a maximum load of 330 kips (24 ksf) and a maximum settlement of 1.6 inches. Because the abutment height was reduced to provide room for the LCs, the FHWA requirements limit settlement to 0.45 inches at the service load of 4 ksf. GRS Abutment Model #8 provided a factor of safety of 3 against settlement at service load.

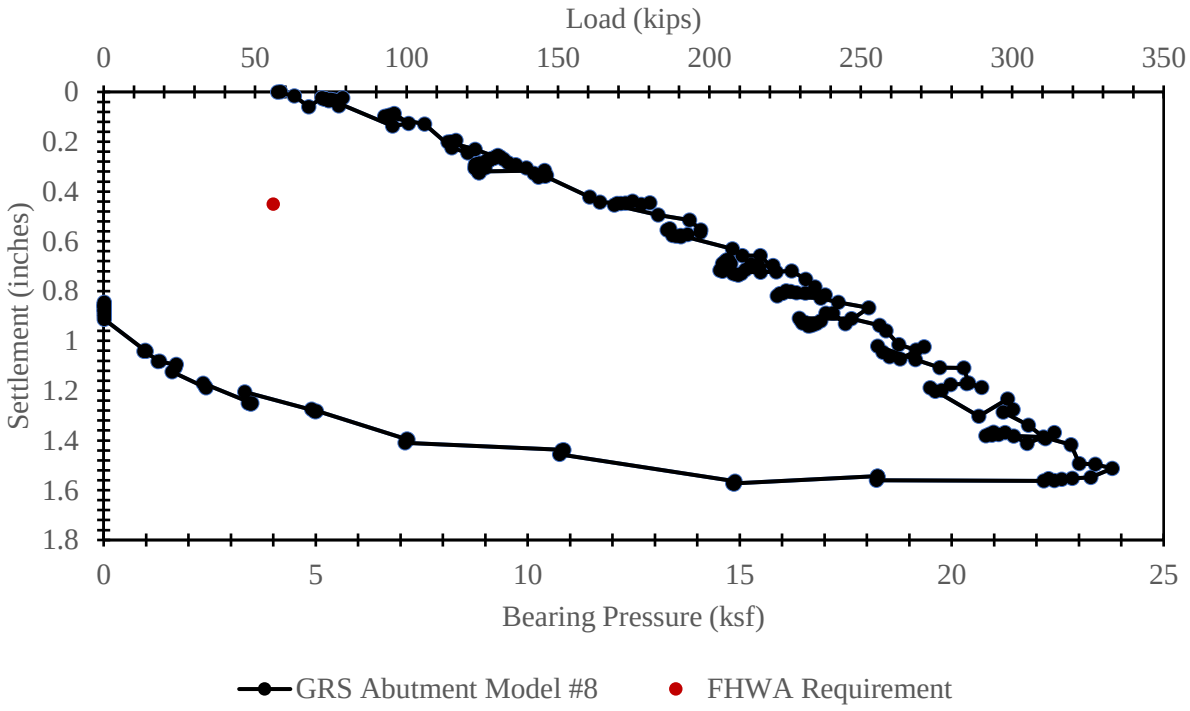

Figure 36 – Load-settlement performance of GRS Abutment Model #8; graph is modified due to roughly 0.35 inches of settlement from sand bed

5.2.3 Reinforcement Strains

Figure 37 displays the strains of the reinforcement encountered throughout testing of the model. Manual measurements of the internal WPs were recorded for layers at elevations of 51, 75, and 91 inches, nominally. It was noticed that the manual measurements and data collected from the DAS did not matchup at the end of construction (EOC). Because the DAS is turned off between construction sessions, any WP movement occurring on non-construction days would not be recorded. Therefore, the EOC data acquired was deemed invalid and reinforcement strains presented in the following figures displays strains recorded during testing.

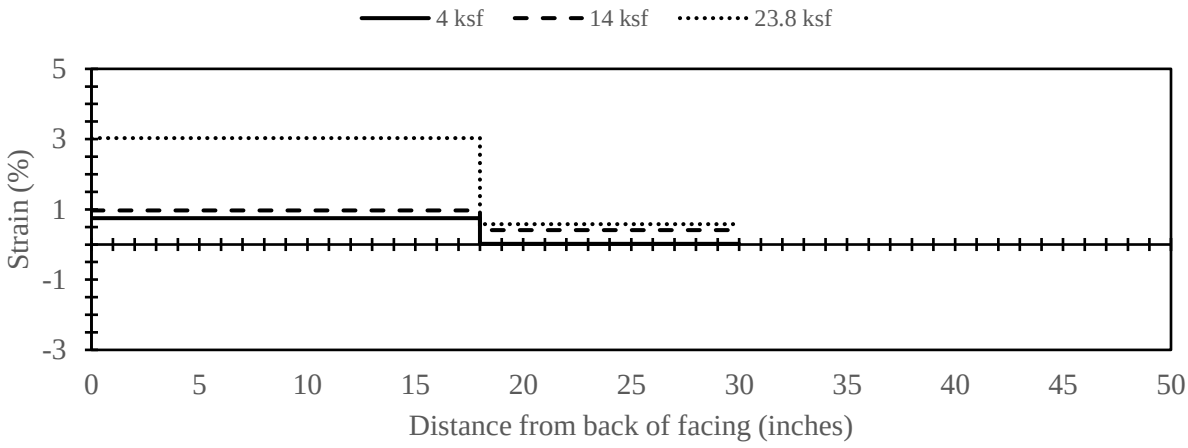
4 ksf
14 ksf
23.8 ksf
Strain (%)
5
3
1
-1
-3
0
5
10
15
20
25
30
35
40
45
50
Distance from back of facing (inches)

(a)

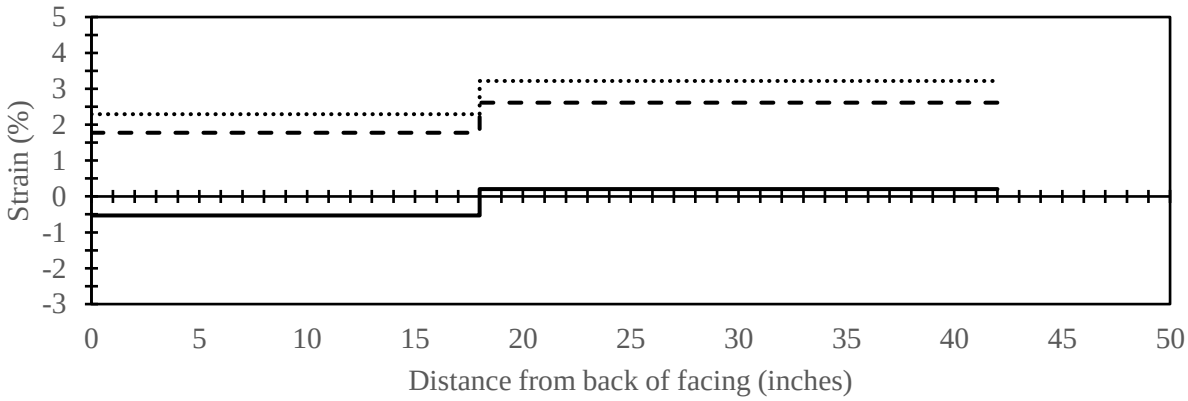
Strain (%)
5
4
3
2
1
0
-1
-2
-3
0
5
10
15
20
25
30
35
40
45
50
Distance from back of facing (inches)

(b)

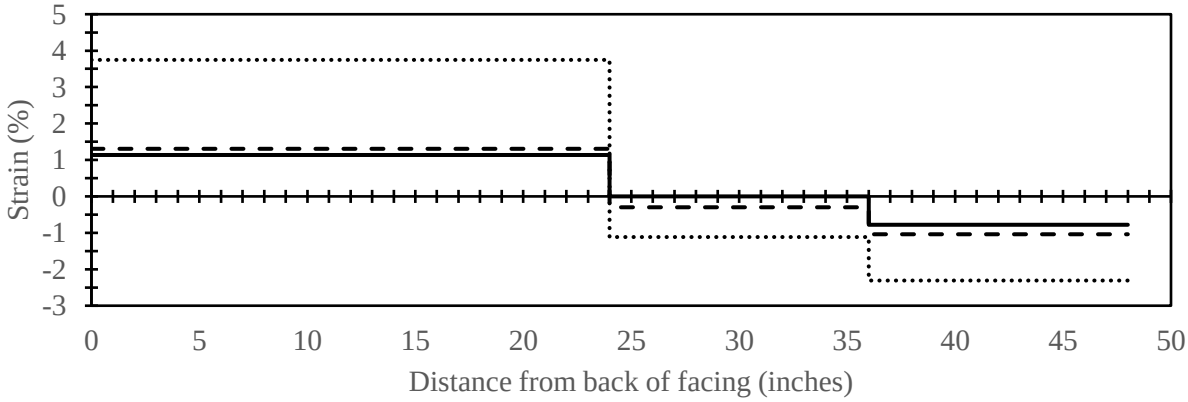
Strain (%)
5
4
3
2
1
0
-1
-2
-3
0
5
10
15
20
25
30
35
40
45
50
Distance from back of facing (inches)

(c)

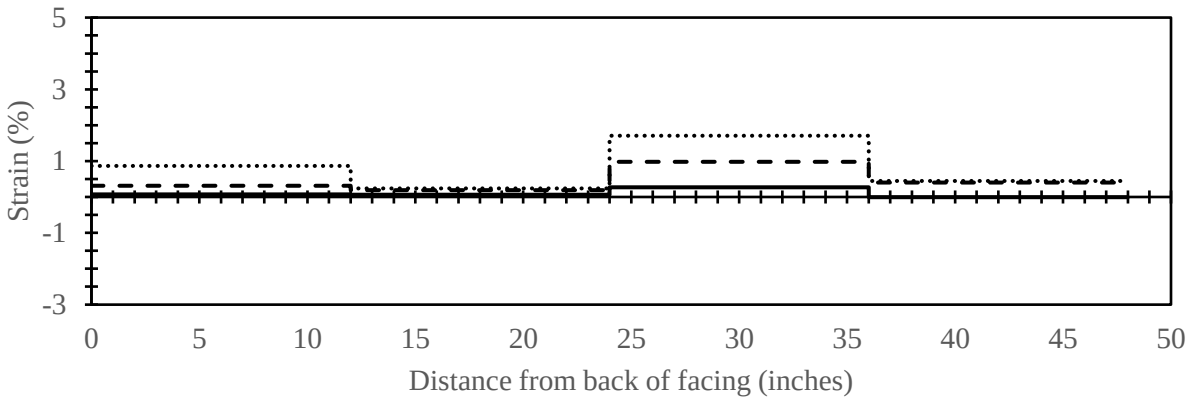

(d)

Figure 37 – Reinforcement strains at EOC, 4 ksf, 14 ksf, and 23.8 ksf; (a) at 27 inches, (b) at 51 inches, (c) at 75 inches, (d) at 91 inches above foundation slab

The reinforcement data shows that much of the strain endured throughout loading occurred near the facing, with strains ranging from -0.5 to 4% for all instrumented layers. As mentioned earlier, the facing experienced bulging at 75 inches above the foundation slab. The strain data reiterates the bulging effect as the largest near-facing strain occurred at the same elevation. In general, the strains presented are relatively large. This may be attributed to the fact that the setback distance was shorter relative to other models (12 inches instead of 20 inches). The increased pressure near the facing contributed to the large strains endured by the frictionally connected reinforcements.

5.2.4 Elevation Survey

Previously mentioned, measurements were taken every five inches behind the back of the facing at three different locations, 8, 24, and 40 inches from the west side of the reinforcement. Figure 38 and Table 8 present the average elevations before and after testing and the water contents upon deconstruction, respectively. Additionally, Figure 38 displays the potential slip plane of GRS Abutment Model #8 based on the location of maximums reinforcement strains. Presented in

Figures 39, 40, 41, 42, and 43 are contour maps of the deformation experienced by the reinforcements located in the upper reinforcement zone.

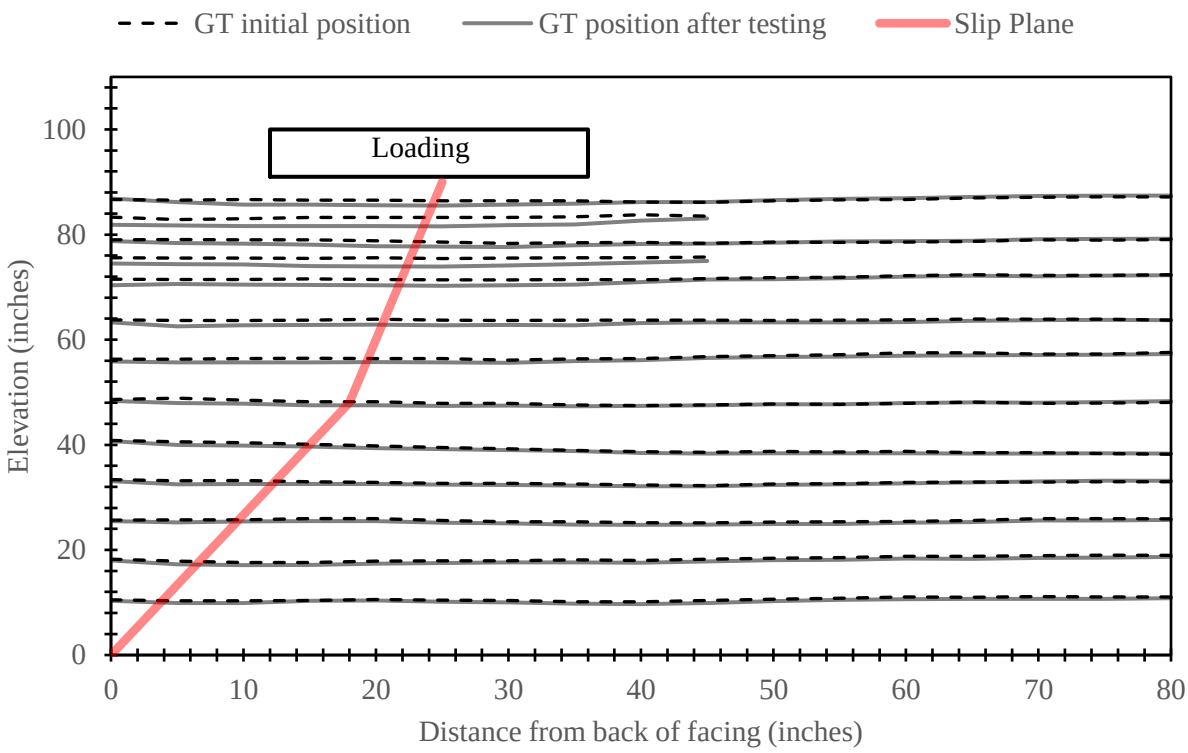

Figure 38 – Elevation survey of GRS Abutment Model #8; GT, geotextile

Table 8 – Water contents from GRS Abutment Model #8

Layer	2	4	6	8	10	11
Water Content (%)	1.87	1.71	1.60	2.25	1.68	1.18

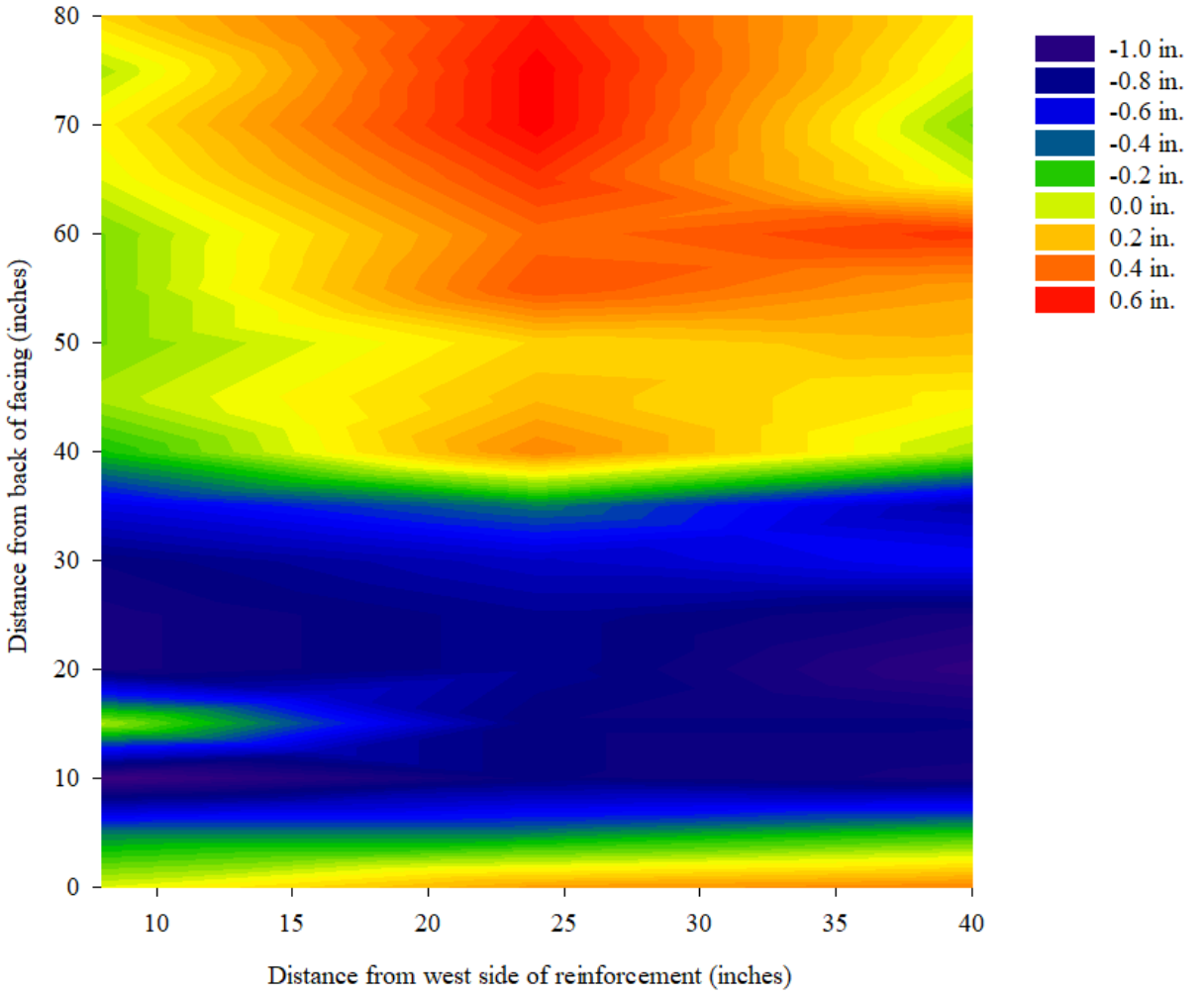

Figure 39 – Plan view of backfill settlement at reinforcement layer 11

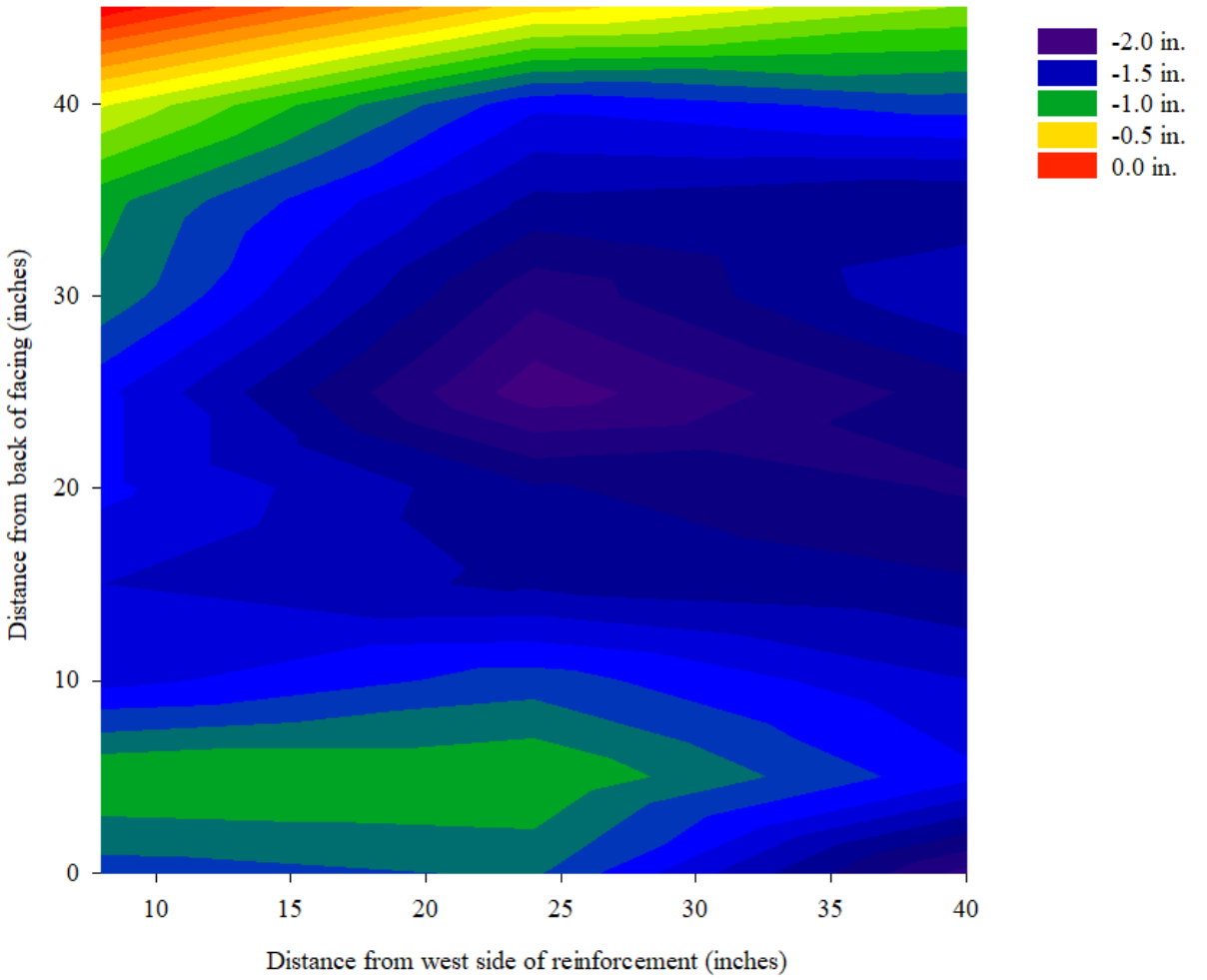

Figure 40 – Plan view of backfill settlement at secondary reinforcement layer 10

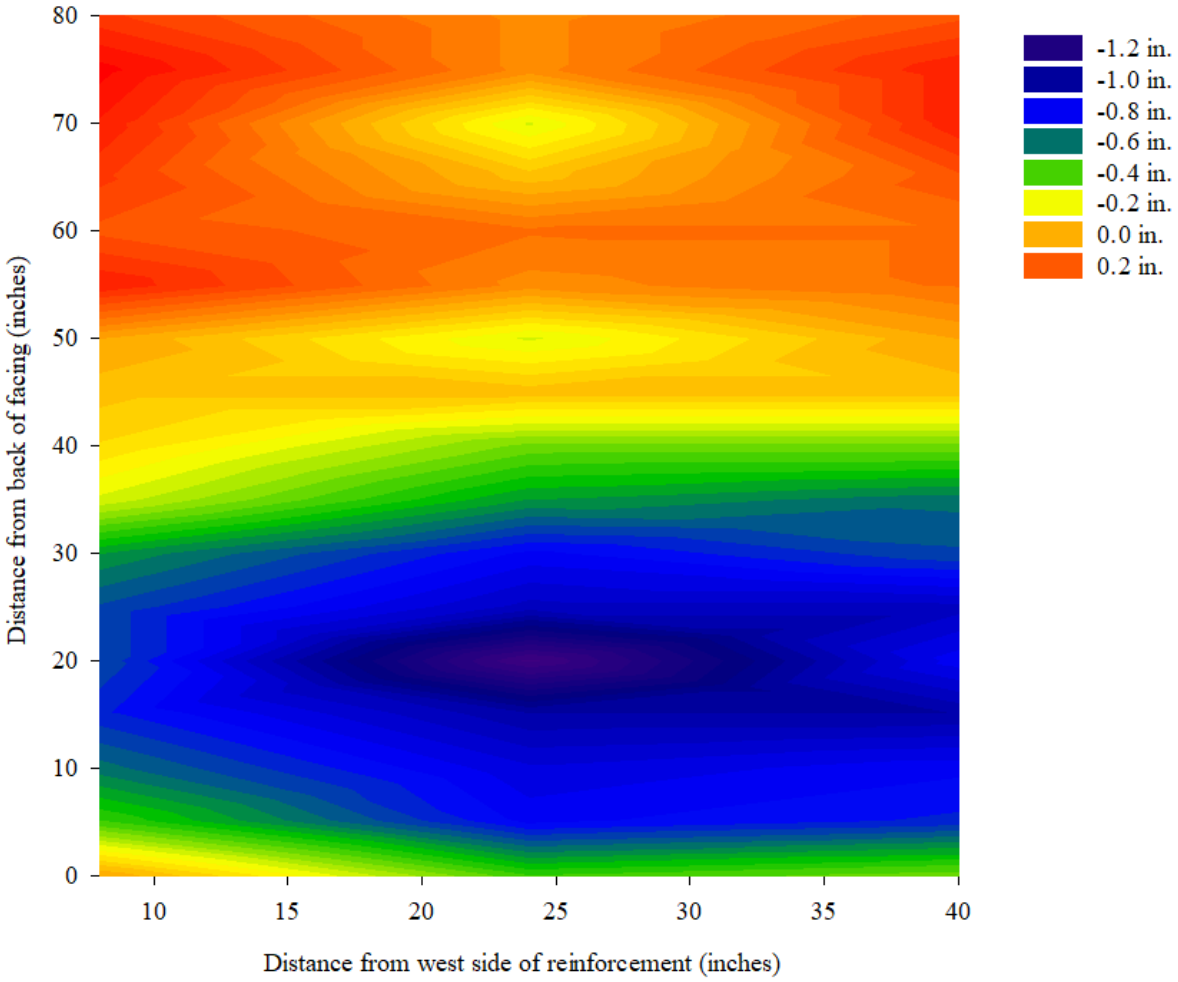

Figure 41 – Plan view of backfill settlement at reinforcement layer 10

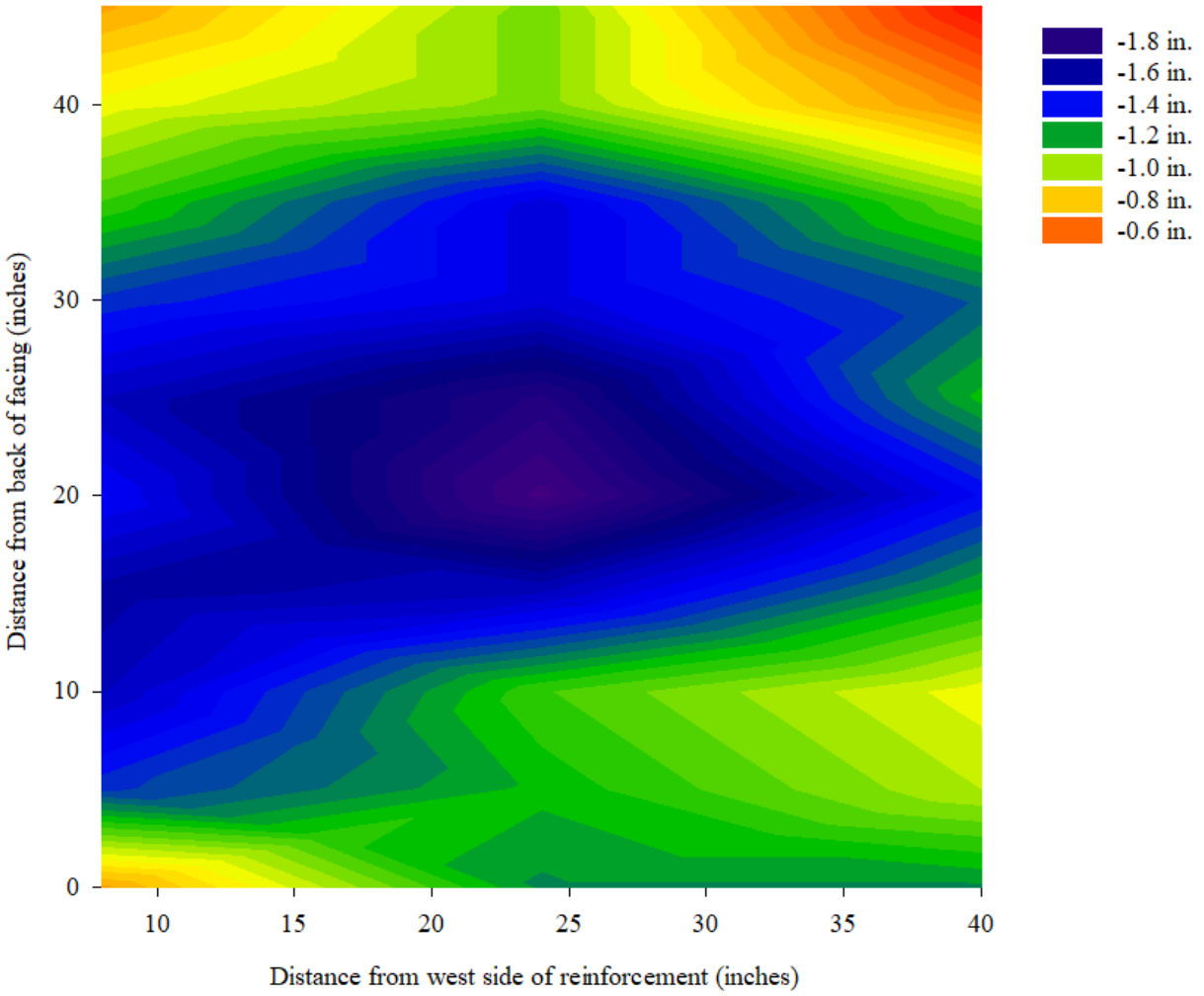

Figure 42 – Plan view of backfill settlement at secondary reinforcement layer 9

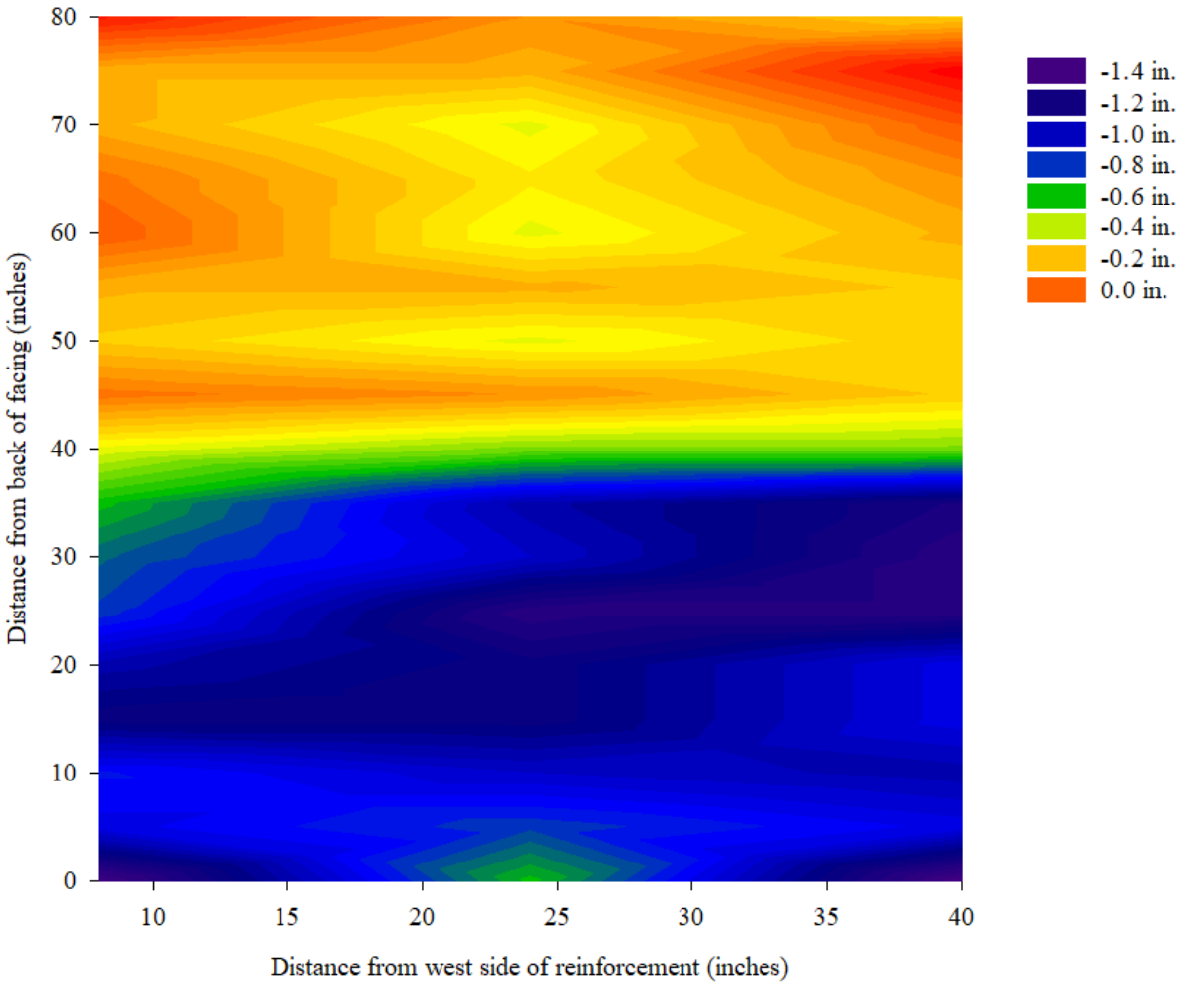

Figure 43 – Plan view of backfill settlement at reinforcement layer 9

The uppermost reinforcement (Figure 39) exhibited bulged effects in areas surrounding the loading beam, whereas the reinforcement above layer 10 (Figure 41) experienced bulging almost strictly behind the loading beam. The reinforcement above the 9th layer deformed greater than the two full-sized reinforcements above it. This can be related to the higher degree of lateral deformation of the facing near this elevation. The secondary reinforcements experienced the most deformation. Because the fill is not compacted in between layers, it is likely that much of this deformation occurred from compaction of overlying layers. It is important to note that the measurements in the upper reinforcement zone were obtained relative to the top of the 12th layer (94.5 inches) because

the concrete-filled facing could not be moved. Because of the extended measurements, there is a higher risk of inaccurate measurements.

5.2.5 Deconstructed Density Test Cubes

Table 9 highlights the data obtained from the deconstructed test cubes obtained from GRS Abutment Model #8. Though the results show a degree of variation, Boutin (2020) conducted a similar test setup using 3/8" #2 Cover aggregate and found the unit weight to be roughly 105 pcf.

Table 9 – Properties obtained from deconstructed test cubes related to GRS Abutment Model #8; (W) water content, (γ) unit weight, (γ_d) dry unit weight

Test Cube	W (%)	γ (pcf)	γ_d (pcf)
Deconstructed - NW	2.30	104.29	101.95
Deconstructed - NE	2.85	113.57	110.42

5.3 Labor Requirements

Figure 44 compares the cumulative man hours required to construct GRS Abutment Models #7 and #8. This figure excludes the time required to instrument the structures with WPs and collect data relative to the facing deformations and elevation surveys. With a difference of nearly eight hours, the results are consistent with Doger (2020) as the use of large block facing elements helped expedite the construction process compared to models built with a CMU facing. Though facing type contributed to the resulting construction hours, It is important to note that the uptick in hours related to the construction of GRS Abutment Model #8 were likely heavily influenced by the fact that only one member present had any previous experience constructing GRS abutment models. Table 10 compares the cumulative man hours between GRS Abutment Models #1 through #8.

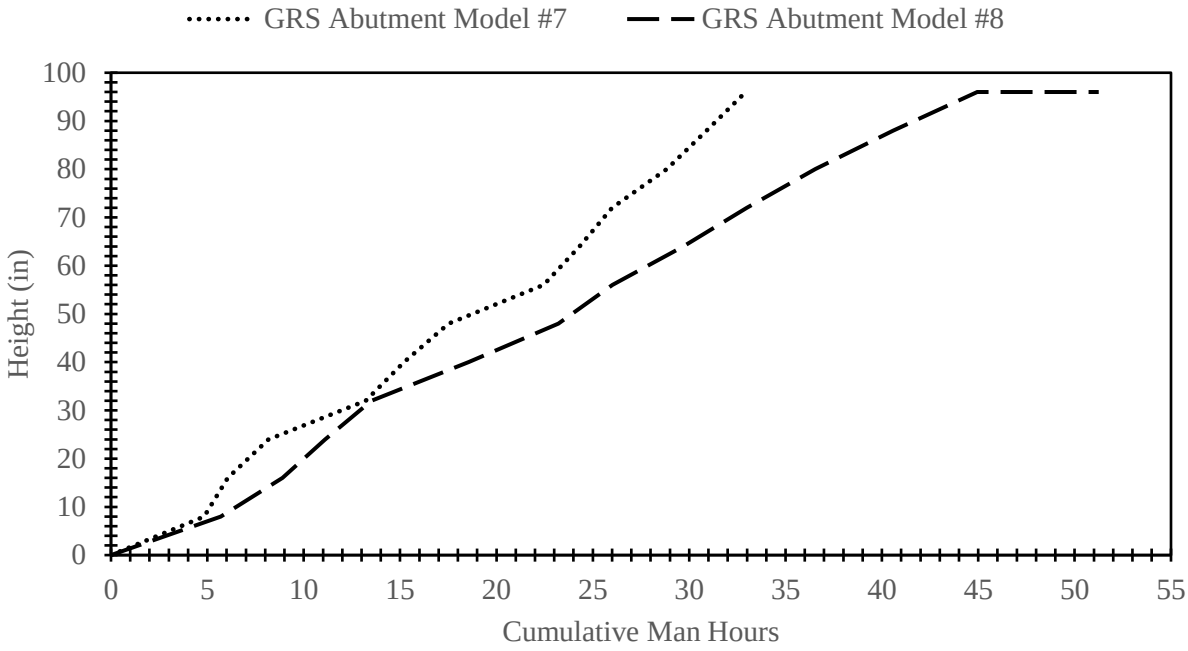

Figure 44 – Cumulative man hours required to construct GRS Abutment Models #7 and #8

Table 10 – Cumulative man hours required to construct GRS Abutment Models #1-8

GRS Abutment Model	1	2	3	4	5	6	7	8
Facing Element	CMU	LB	LB	CMU	CMU	CMU	LB	CMU
Cumulative Man Hours	75	54	34	50	27	27	33	52
Backfill Type	Open	Open	Open	Open	Open	Well	Well	Open

The average cumulative man hours required to construct abutments with large block and CMU facings are 40.3 and 46.2, respectively. These averages do not confirm the 50% reduction in construction time that abutments with large block facing elements provide, as stated by Doger (2020). That does not necessarily mean Doger's finding are incorrect. The difference in average cumulative man hours required can be attributed to the experience of the construction crew. For instance, members present for the construction of GRS Abutment Model #3 had construction experience from GRS Abutment Models #1 and #2, which, along with the implementation of large blocks, may explain the large decrease in construction time throughout these models. The same

principal applies to GRS Abutment Model #6 – most members present for this model had construction experience from GRS Abutment Models #4 and #5; some of those same members had additional experience from GRS Abutment Models #1 through #3, which provides reason why GRS Abutment Models #5 and #6 required the least amount of man hours. Two of the members from GRS Abutment Model #7 had been present for the construction of most of the previous abutment models. Finally, only one member present for the construction of GRS Abutment Model #8 had any previous construction experience, explaining the large difference in construction speed compared to other CMU models.

Though hypothesized, the results do not prove that large block facings can expedite the construction time for abutments built with well-graded aggregate. Figure 45 directly compares the labor required to construct GRS Abutment Models #6 and #7. Though the construction of GRS Abutment Model #6 was quicker than that of GRS Abutment Model #7 by 6 hours, the difference in construction time can be heavily attributed to the exit of experienced members and the introduction of new members. For previous abutment models built with a large block facing, the now retired Fears Structural Laboratory Manager had aided in placement of the blocks. For GRS Abutment Model #7, a crew member was tasked with learning and operating the forklift, which contributed to construction time. The shallower slops of GRS Abutment Model #7 in Figure 45 include the time required to place the large blocks with the forklift. On the same figure, one can see the steeper slopes of GRS Abutment Model #7 is comparable to the slope of GRS Abutment Model #6. There is reason to believe that time taken for a member to operate the forklift contributed heavily to the construction hours. If there was no change in forklift operator, and considering the time taken to pour concrete in the facing of GRS Abutment Model #6, GRS Abutment Model #7 may have actually taken least amount of time to construct of all models. It is important to note that

is merely a speculation as there is no way to solidify this claim. Additionally, comparing only two models built with well-graded aggregate presents a small sample size and additional models may need to be constructed to accurately assess the originally stated hypothesis. Nevertheless, in agreement with Doger (2020), large block facing elements may expedite the construction process in comparison to GRS abutments built with CMUs. More apparently, construction times seem to be strongly dependent on the experience of the crew.

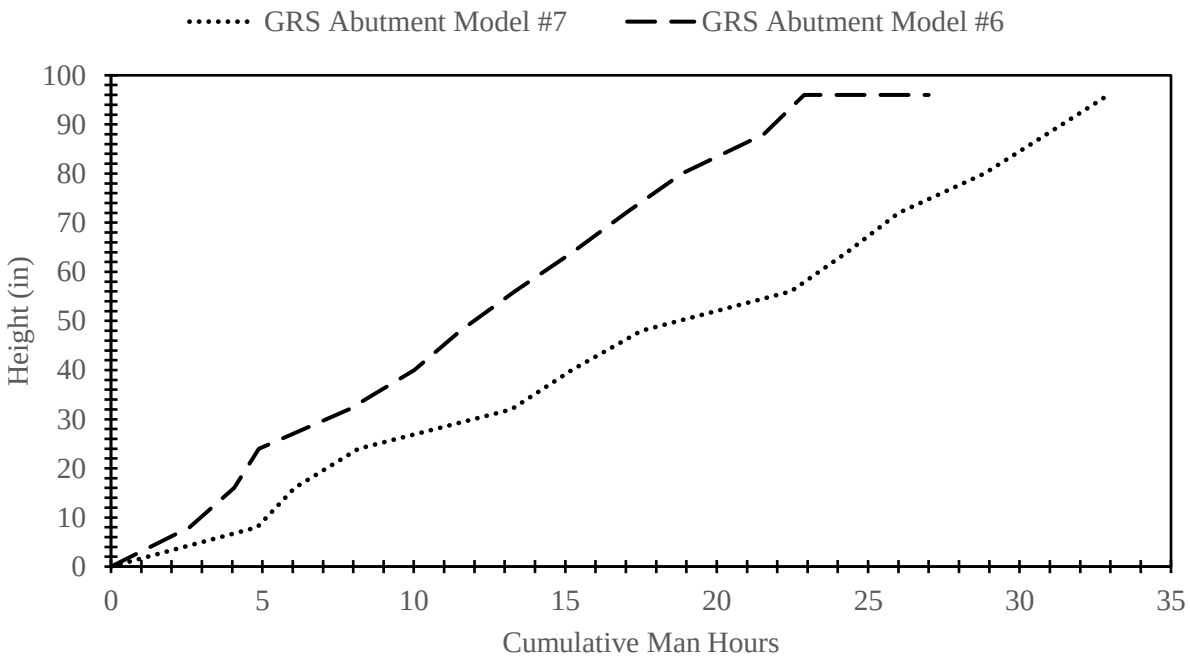

Figure 45 – Cumulative man hours required to construct GRS Abutment Models #6 and #7

Chapter 6 – COMPARISON OF GRS ABUTMENT MODELS

Below, performance results from GRS Abutment Models #7 and #8 will be compared to previous models constructed and tested by Doger (2020) and Boutin (2020).

6.1 GRS Abutment Model #7 Comparisons

In terms of design factors, GRS Abutment Model #7 can be viewed as a hybrid between GRS Abutment Models #2 and #6. GRS Abutment Model #3 was included as an additional comparison. Table 11 displays the similarities in design among the three abutment models.

Table 11 – Models compared to GRS Abutment Model #7

GRS Abutment Model	Facing Type	Aggregate Type	Spacing	Compaction Passes
2	LB	3/8” #2 Cover	8	1
3	LB	3/8” #2 Cover	12	1
6	CMU	ODOT Type A	8	3
7	LB	ODOT Type A	8	3

6.1.1 Facing Deformations

Figure 46 displays the facing deformation comparisons between the abutment models at 20, 100, and 200 kips. GRS Abutment Model #7 began experiencing the largest magnitudes of deformation somewhere between the loading of 20 and 100 kips. Based on the data from Doger (2020) and Boutin (2020), it would be reasonable to assume the combination of well-graded aggregate and large blocks would result in the least amount of facing deformation. According to the data acquired from GRS Abutment Model #7, this does not appear to be the case. Based on the data from Doger (2020), it seems as though facing deformations may be difficult to predict as GRS Abutment Model #3 (12-inch spacing) performed better than GRS Abutment Model #2 (8-inch spacing).

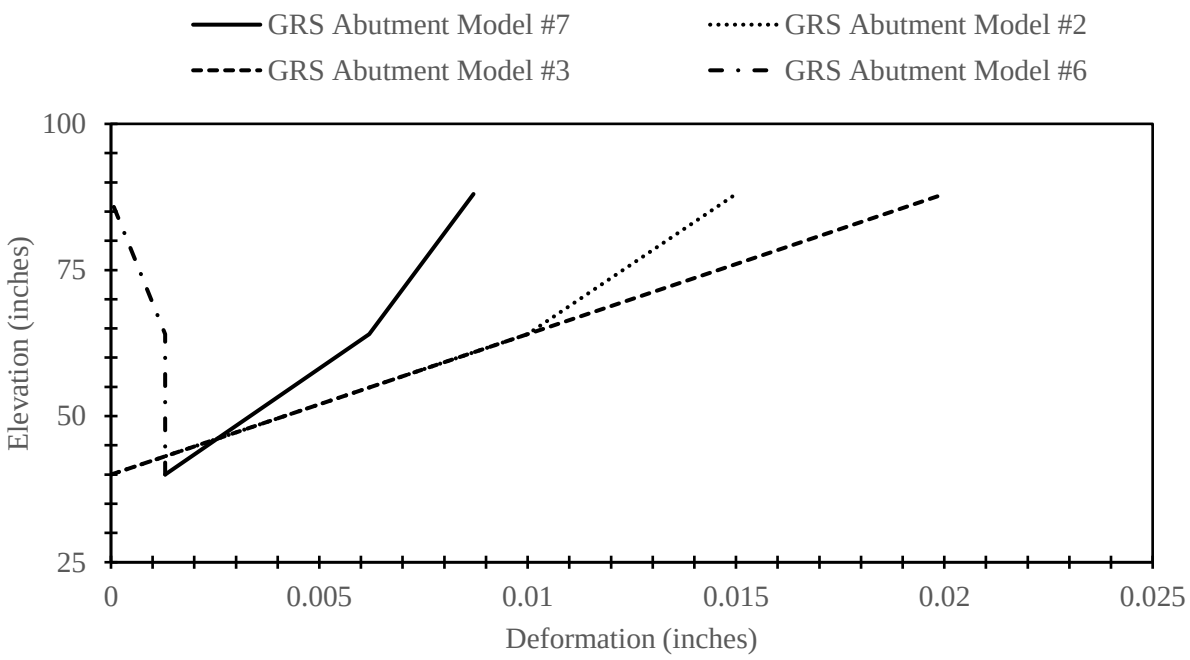
GRS Abutment Model #7
GRS Abutment Model #2
GRS Abutment Model #3
GRS Abutment Model #6
100
75
50
25
Elevation (inches)
0
0.005
0.01
0.015
0.02
0.025
Deformation (inches)

(a)

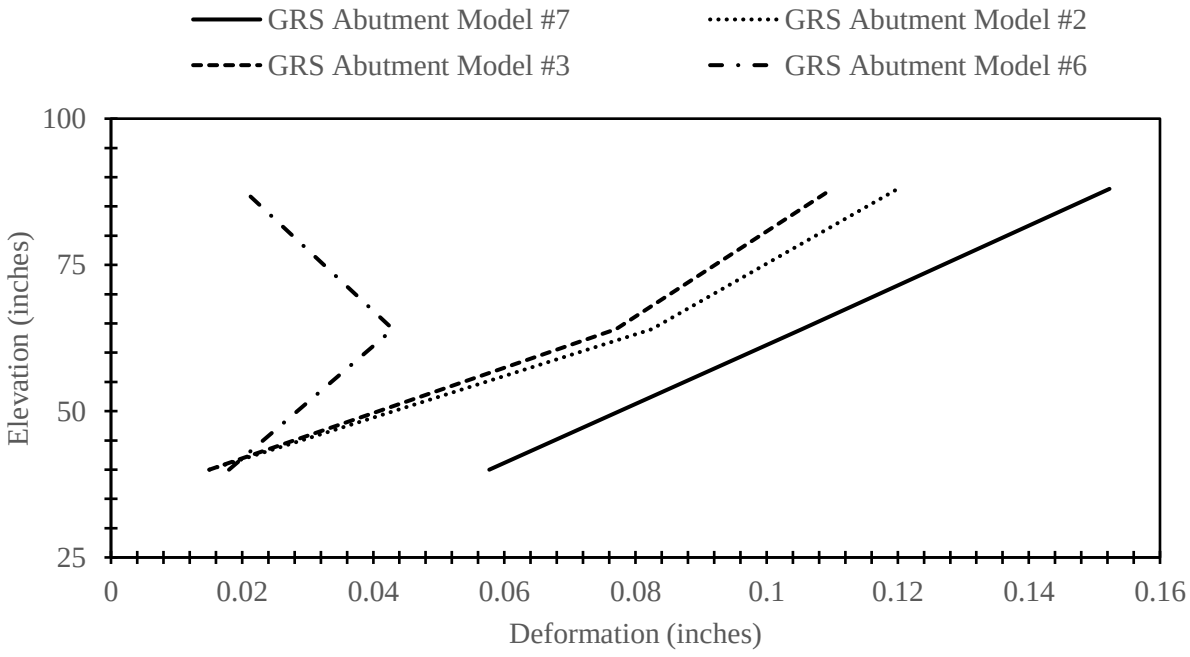
GRS Abutment Model #7
GRS Abutment Model #2
GRS Abutment Model #3
GRS Abutment Model #6
100
75
50
25
Elevation (inches)
0
0.02
0.04
0.06
0.08
0.1
0.12
0.14
0.16
Deformation (inches)

(b)

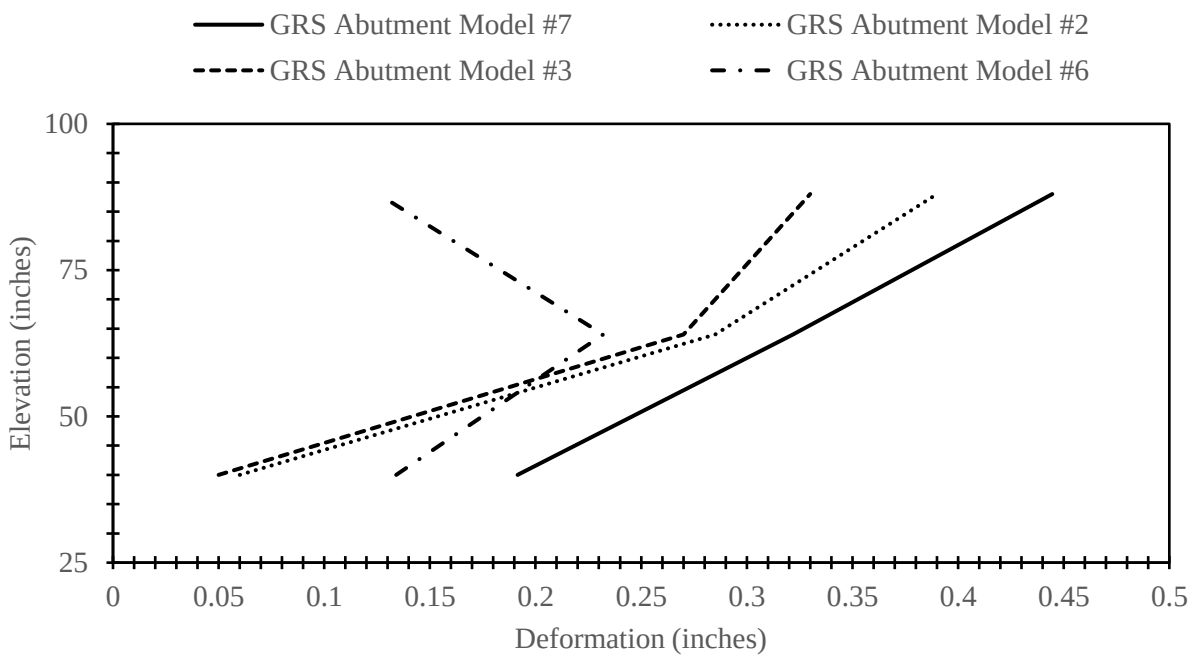

(c)

Figure 46 – Facing deformation comparisons of GRS Abutment Models #2, #3, #6 and #7; (a) at 20 kips, (b) at 100 kips, (c) at 200 kips

6.1.2 Load-Settlement Performances

Figure 47 presents the load-settlement performance data for all four models. The results are perplexing as GRS Abutment Model #7 performed very similarly to other models constructed with large blocks. It appears the dense graded aggregate and increased compaction effort did not contribute much to the performance.

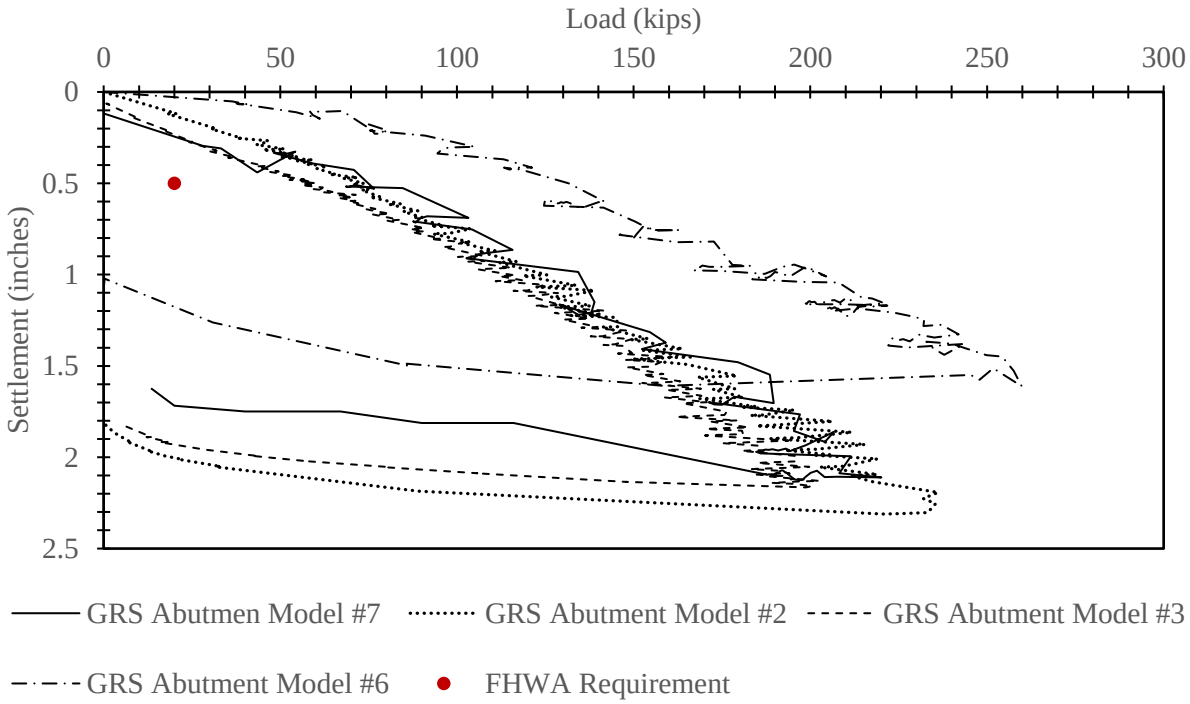

Figure 47 – Load-settlement performances compared to GRS Abutment Model #7

There is not one factor that singlehandedly contributed to the large settlements experienced by GRS Abutment Model #7. As mentioned before, the aggregate was extremely difficult to work with. Upon compaction of the top layer and placement of the beam, the surface was found to be slightly unlevel. To create a level surface for the beam, aggregate was scraped and added as needed below the beam. This disturbance of compacted aggregate may have contributed to some of the settlement experienced early in the loading phase. Nonetheless, it is important to note that every abutment model constructed with large blocks has easily met the FHWA requirements for settlement. It is difficult to make sense of the results from GRS Abutment Model #7. From this study, it can be concluded that: (1) the performance of GRS abutments constructed with large block facings tend to perform similarly regardless of the compaction effort, backfill type, and reinforcement spacing, and (2) practical factors can come into play even in highly controlled environments within degrees of variations.

6.1.3 Unit Weight and Water Content

Figures 48 and 49 compare Sand-Cone Method results from this study with those from GRS Abutment Model #6 conducted by Boutin (2020). Both studies produced unit weight results from different layers. For comparative purposes, Boutin's findings from layers 11, 9, 6, and 3 will be compared to neighboring layers that were investigated in this study (11, 8, 5, 2). Based on the data observed from GRS Abutment Model #6, it does not appear that the Sand-Cone test holes were excavated to the volume required by ASTM D1556. The large difference in unit weights obtained between the studies may be partially attributed to this.

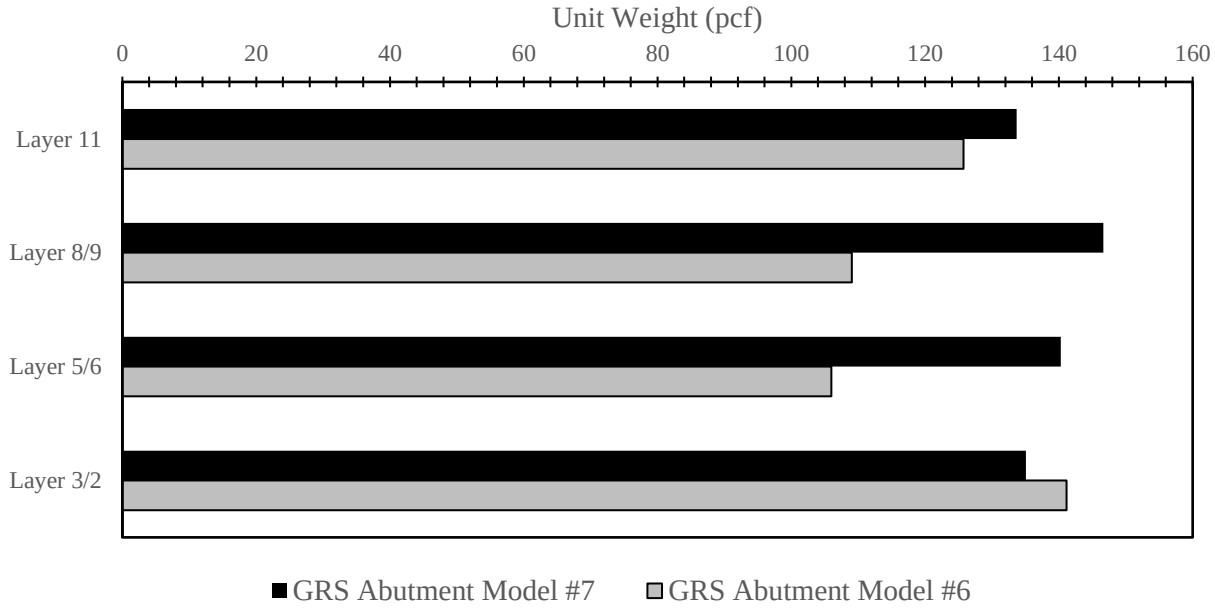

(a)

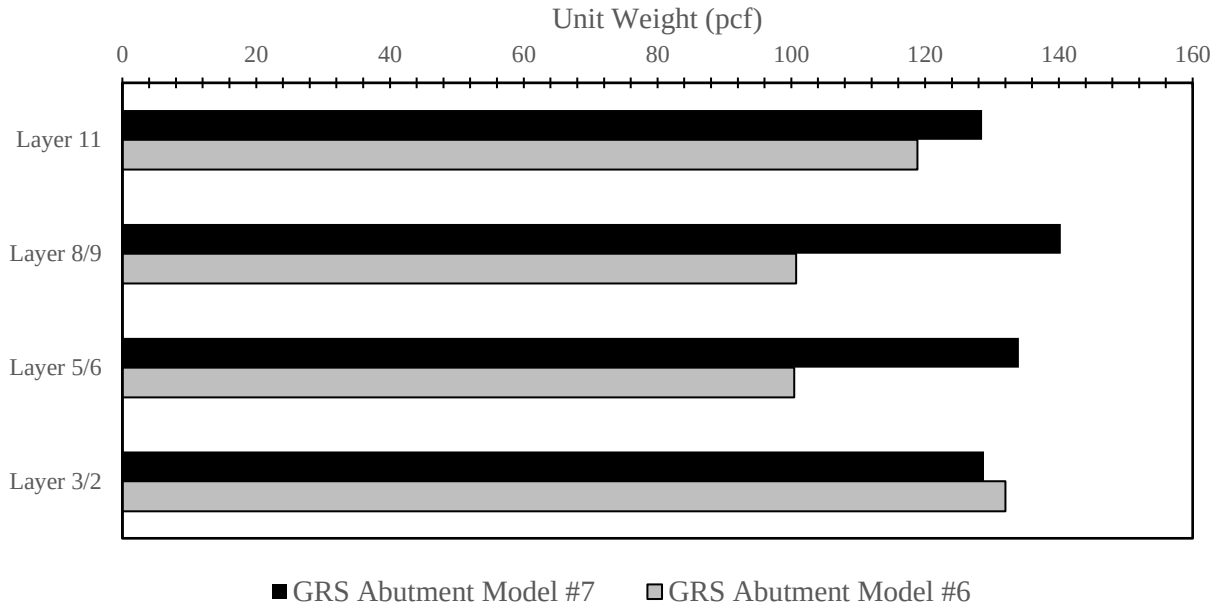

(b)

Figure 48 – Unit weight comparisons for GRS Abutment Models #6 and #7; (a) in-place unit weight, (b) dry unit weight

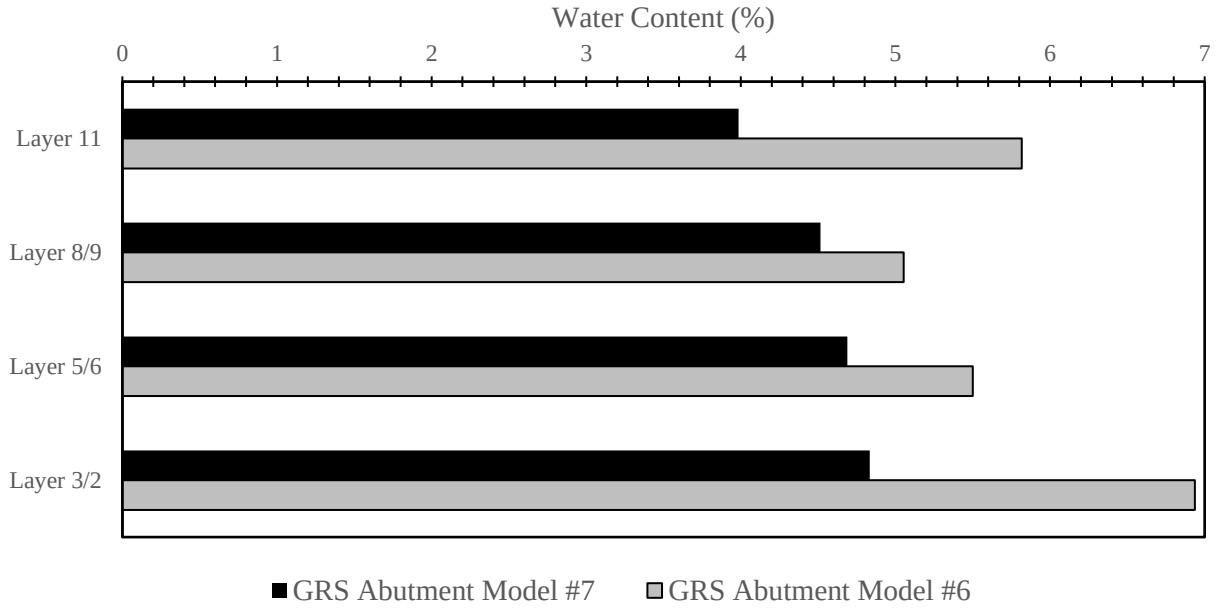

Figure 49 – Water contents of GRS Abutment Model #6 and #7

6.2 GRS Abutment Model #8 Comparisons

Table 12 outlines abutment models built similarly in design. These performance results of these models will be compared throughout this section.

Table 12 – Models compared to GRS Abutment Model #8

GRS Abutment Model	Facing Type	Aggregate Type	Spacing	Compaction Passes	Beam Seat Width (in)
1	CMU	3/8” #2 Cover	8	1	7.625
4	CMU	3/8” #2 Cover	8	3	7.625
8	CMU	3/8” #2 Cover	8	3	24

6.2.1 Facing Deformations

Graphs comparing the facing deformations of GRS Abutment Models #1, #4, and #6 at various loads can be found below in Figures 50 and 51. In relation to performance measured in kips, GRS Abutment Models #4 and #8 experienced less deformation than GRS Abutment Model #1. This confirms that an increased compaction effort can lead to better performance in terms of facing deformation. On the other hand, GRS Abutment Model #4 experienced less deformation than GRS Abutment Model #8. This may be related to the setback distance as Shen et al. (2020) found that decreasing the setback distance can result in a greater additional lateral earth pressure behind the facing. Comparing the performance of these models in terms of pressure, GRS Abutment Model #8 experienced the most lateral deformation. This can be associated with the fact that GRS Abutment Model #8 carried a much larger load for a given pressure due to the increased footprint of the loading beam.

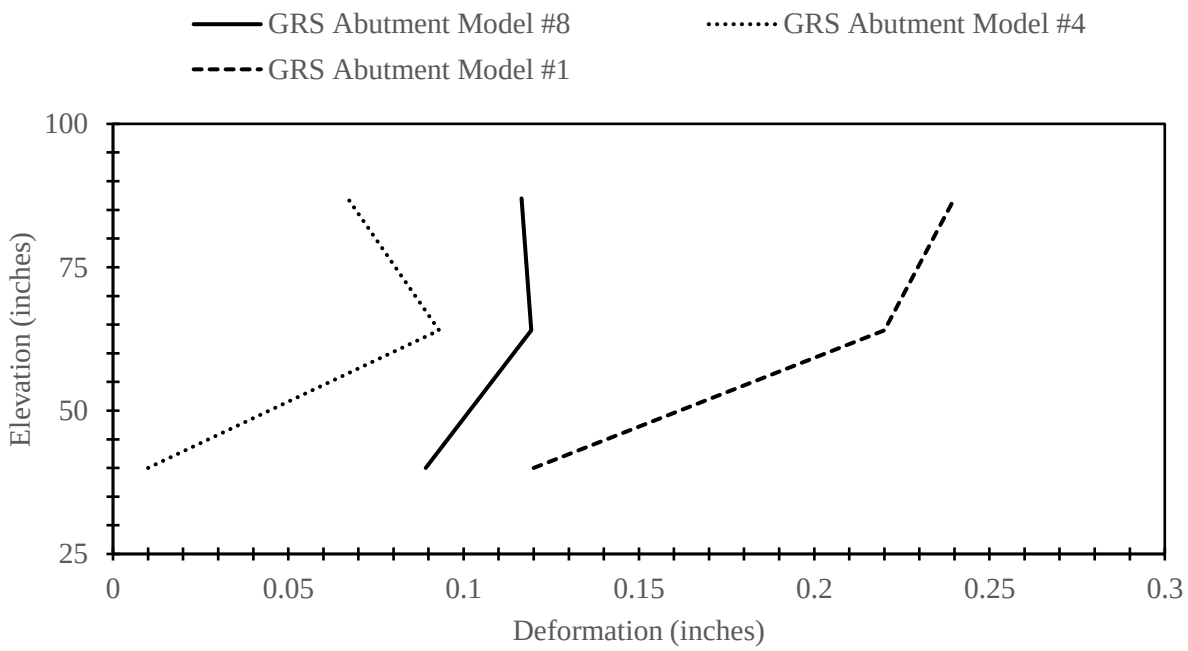

(a)

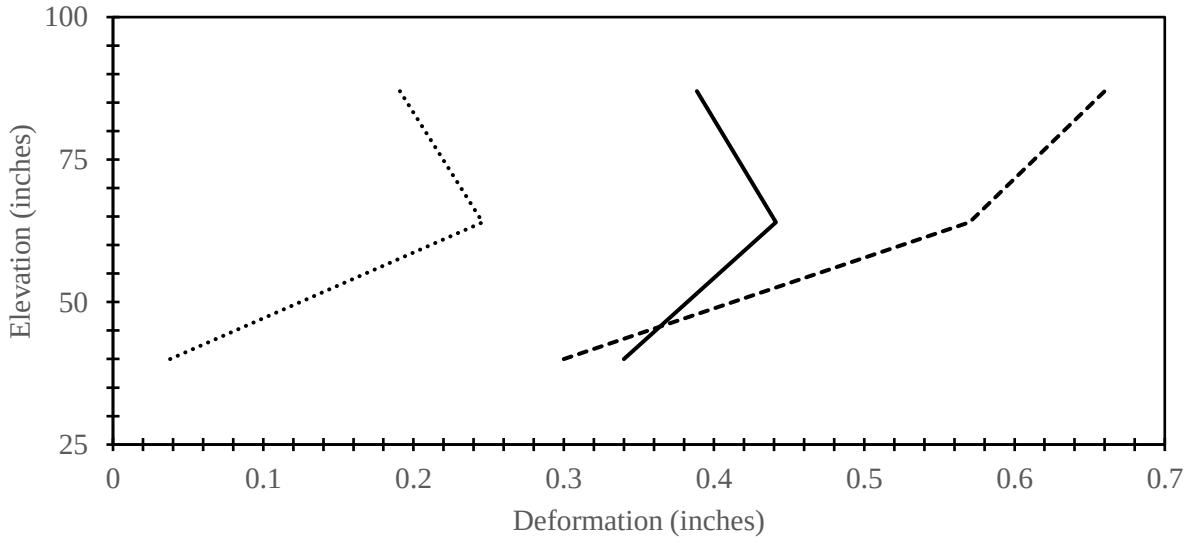

(b)

Figure 50 – Facing deformation comparisons of GRS Abutment Models #4, #6 and #8 (kips); (a) at 100 kips, (b) at 200 kips

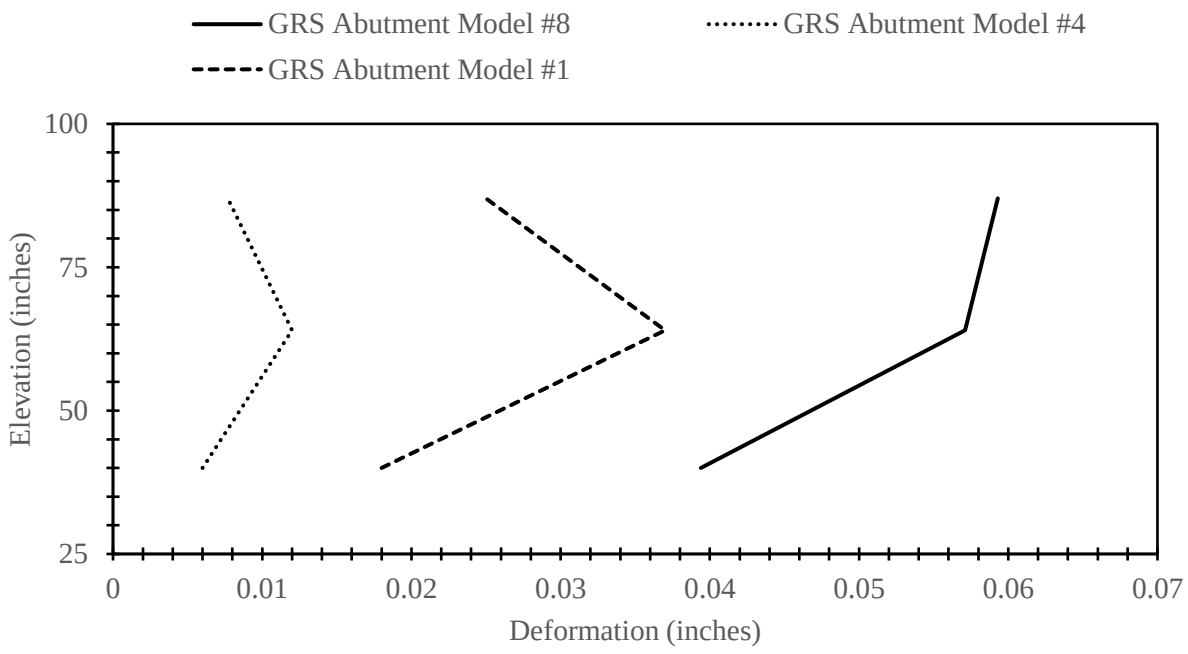

(a)

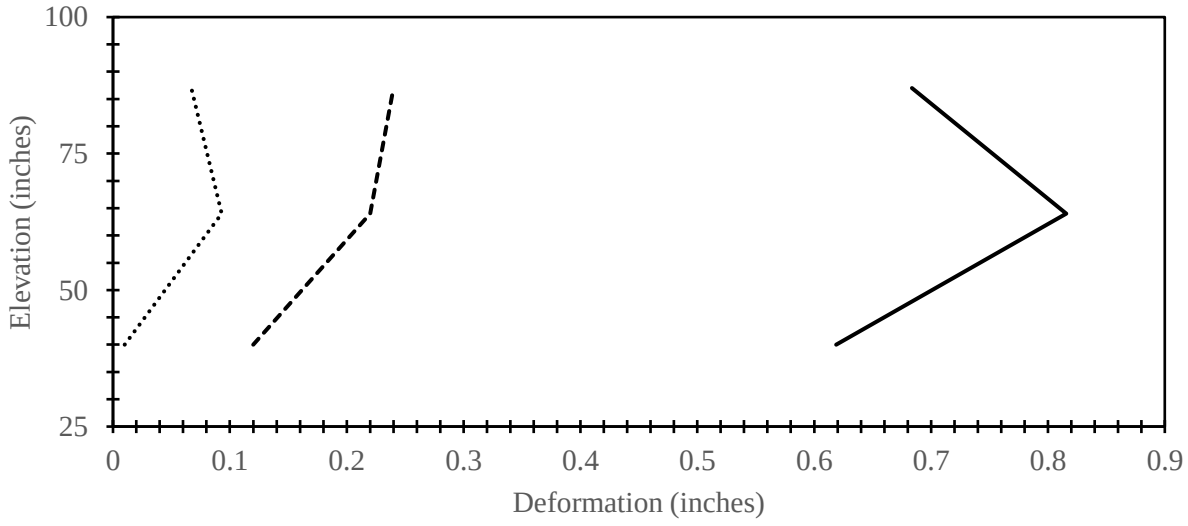

(b)

Figure 51 – Facing deformation comparisons of GRS Abutment Models #4, #6 and #8 (ksf); (a) at 4 ksf, (b) at 20 ksf

6.2.2 Load-Settlement Performances

The load-settlement performances are compared in Figure 52. For a given load, the increased beam seat width permitted less settlement than models implementing a smaller beam seat. This is an expected result as Shen et al. (2020) found that an increased beam seat width results in lower additional vertical stress under the beam. GRS Abutment Model #8 settles more than GRS Abutment Model #4 and less than GRS Abutment Model #1 for the same applied pressure. With a footprint nearly three-times larger, GRS Abutment Model #8 experienced a much greater load than the two other models at a given applied pressure and can be expected to experience a larger magnitude of settlement. It is clear that the influence of an increased compaction effort and increased beam seat footprint can greatly improve the performance of GRS abutments.

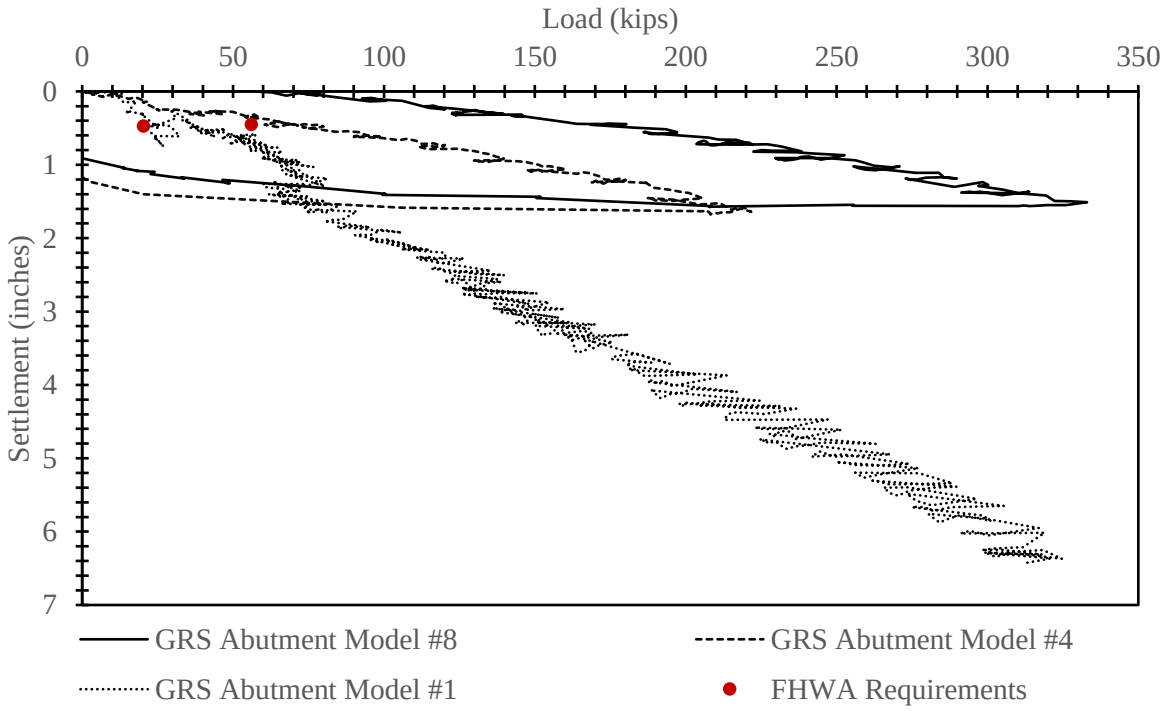

(a)

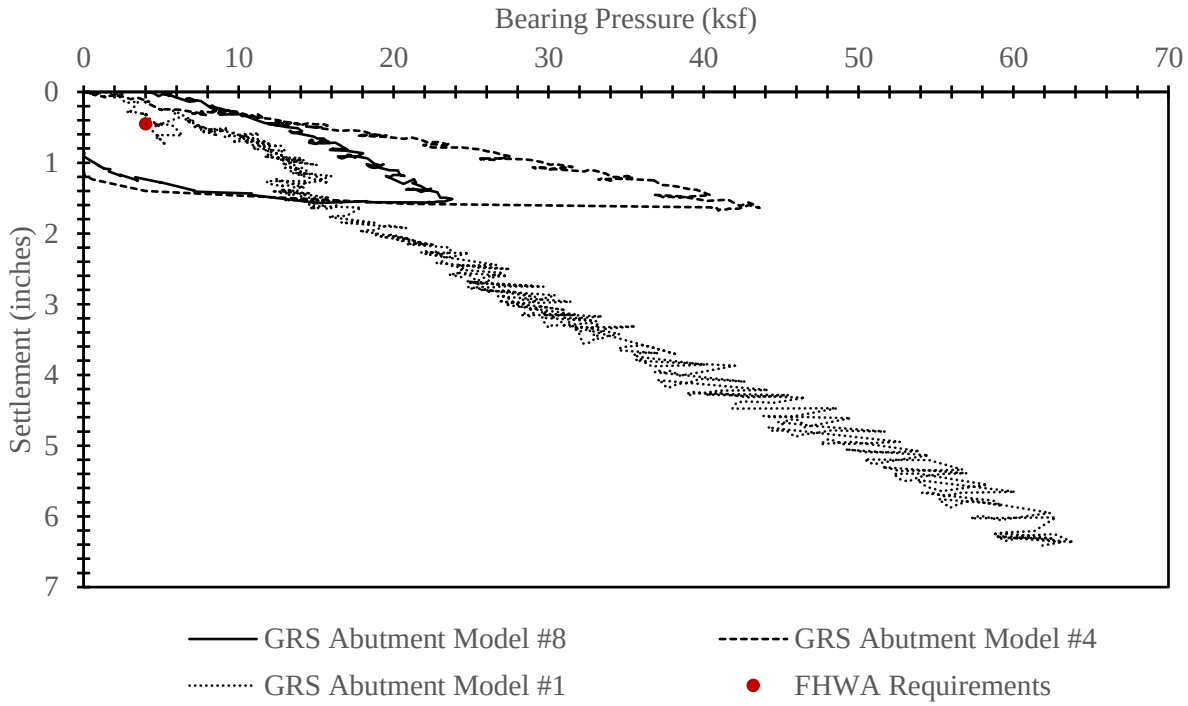

(b)

Figure 52 – Load-settlement performances compared to GRS Abutment Model #8; (a) in kips, (b) in ksf

6.2.3 Reinforcement Strains

The reinforcement strains in Figures 53, 54, and 55 show GRS Abutment Model #8 produced larger strains than those produced by GRS Abutment Models #1 and #6. Looking back at the significantly larger facing deformations of GRS Abutment Model #8 in Figures 46 and 47, it makes sense that the frictionally connected reinforcement would experience larger strains. Shen et al. (2020) found that a larger setback distance and a larger beam seat width resulted in smaller magnitudes of maximum tension in reinforcements. This study incorporated a larger beam seat width with a shorter setback distance relative to previously constructed models. Additional analyses over varying setback distances and beam seat widths would be needed in order to justify the differences in reinforcement strains between the compared models. The reinforcement strains

for all models tend to be larger at elevations of 51 and 75 inches above the foundation slab. Boussinesq's pressure distribution, as expected, shows that larger pressures are located near the footing, with limited range. Near the 51- and 75-inch elevation, pressures are moderately high with larger range, which provides explanation to the larger strains experienced by the reinforcement at these elevations.

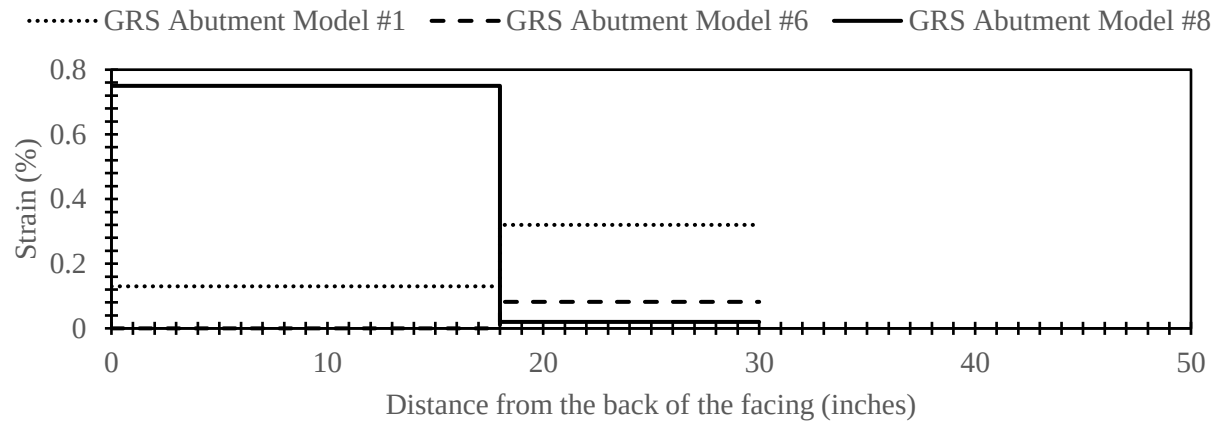

(a)

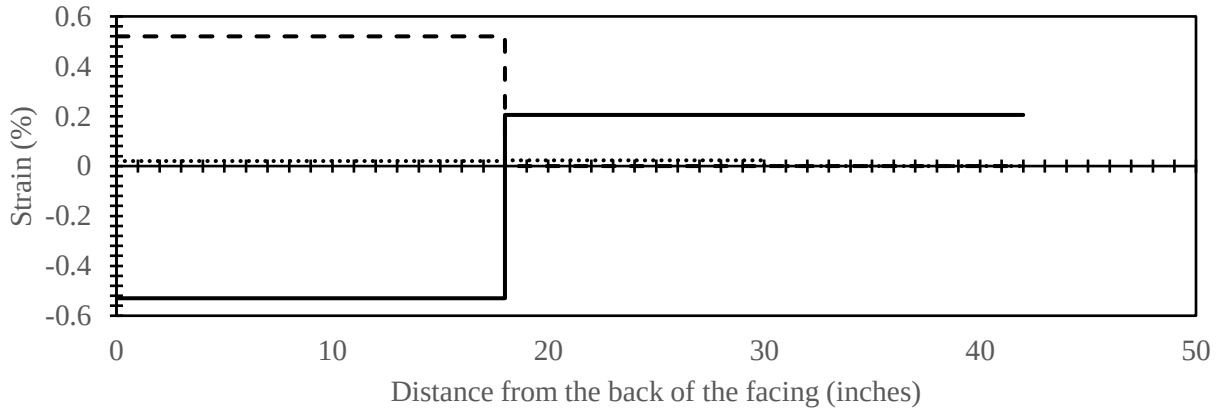

(b)

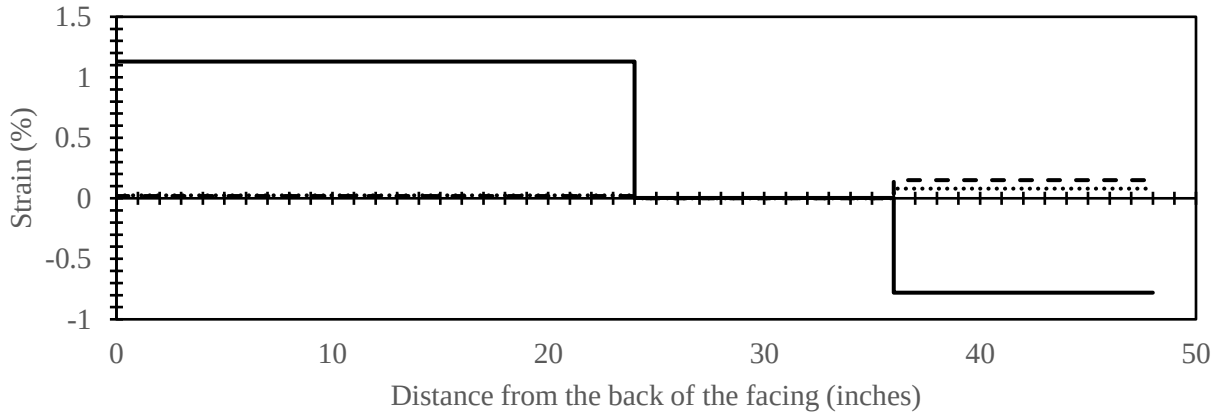

(c)

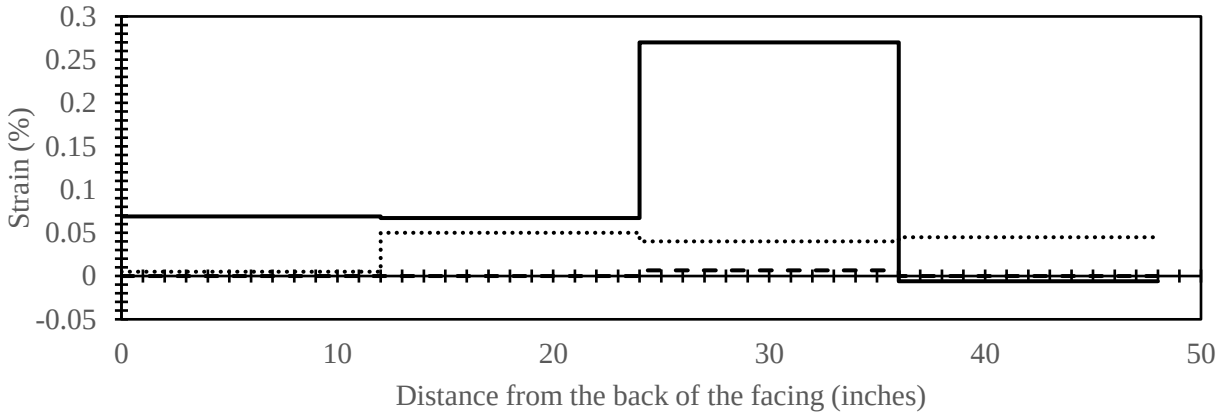

(d)

Figure 53 – Reinforcement strains comparisons at 4 ksf; (a) at 27 inches, (b) at 51 inches, (c) at 75 inches, (d) at 91 inches above foundation slab

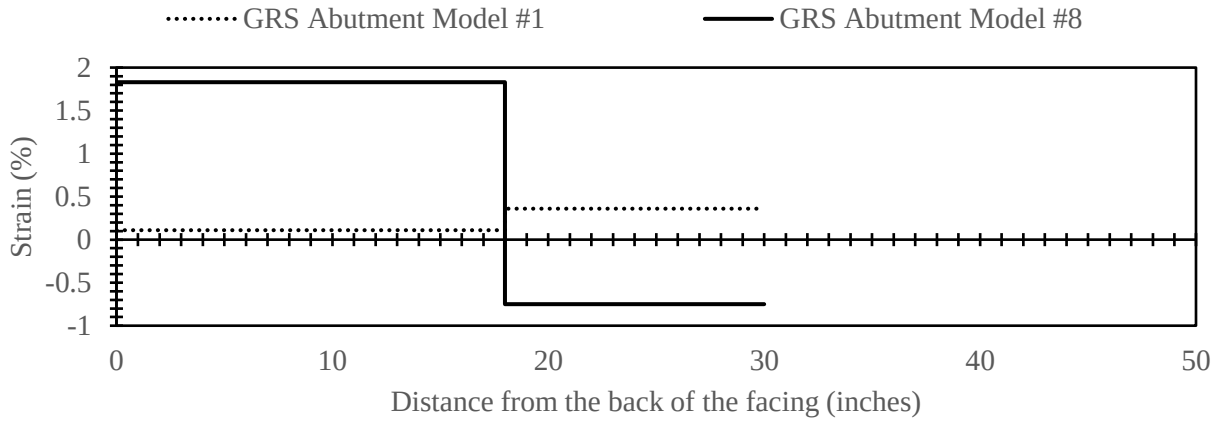

(a)

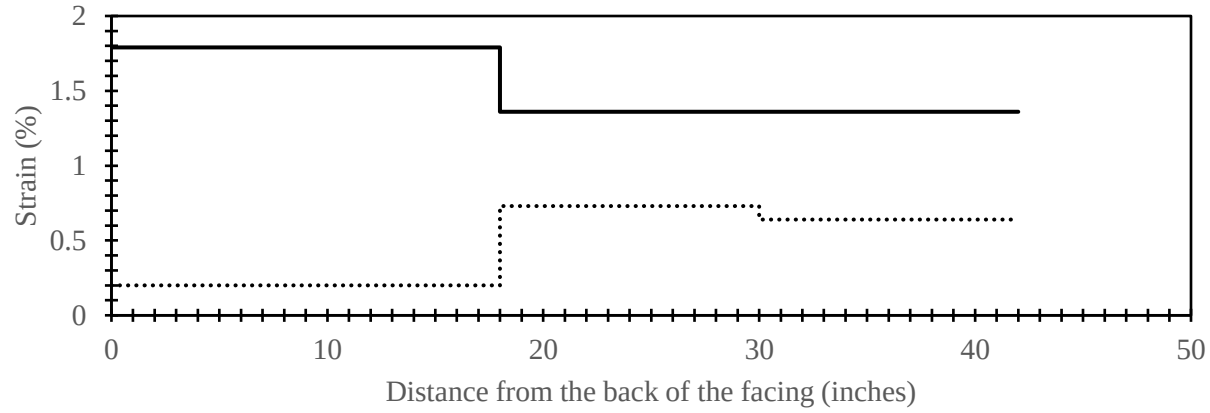

(b)

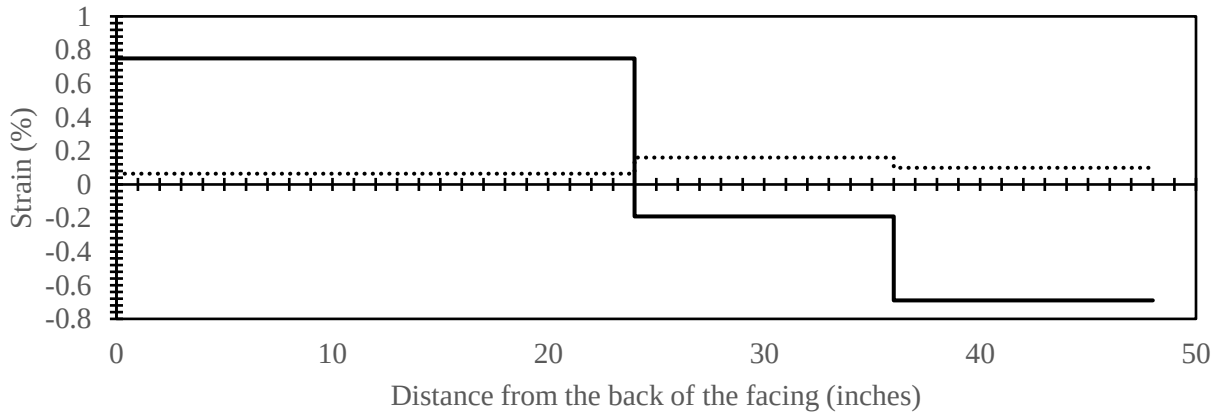

(c)

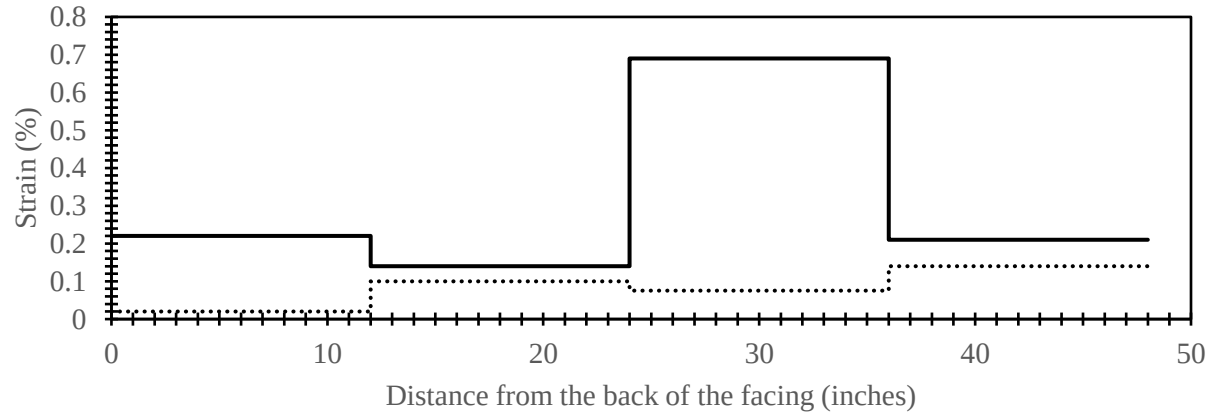

(d)

Figure 54 – Reinforcement strains comparisons at 10 ksf; (a) at 27 inches, (b) at 51 inches, (c) at 75 inches, (d) at 91 inches above foundation slab

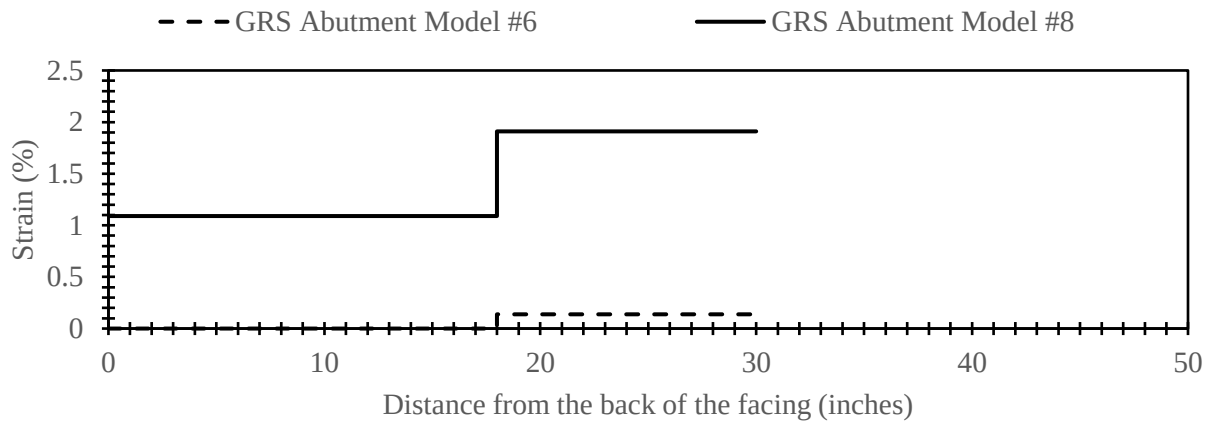
GRS Abutment Model #6
GRS Abutment Model #8
Strain (%)
2.5
2
1.5
1
0.5
0
0
10
20
30
40
50
Distance from the back of the facing (inches)

(a)

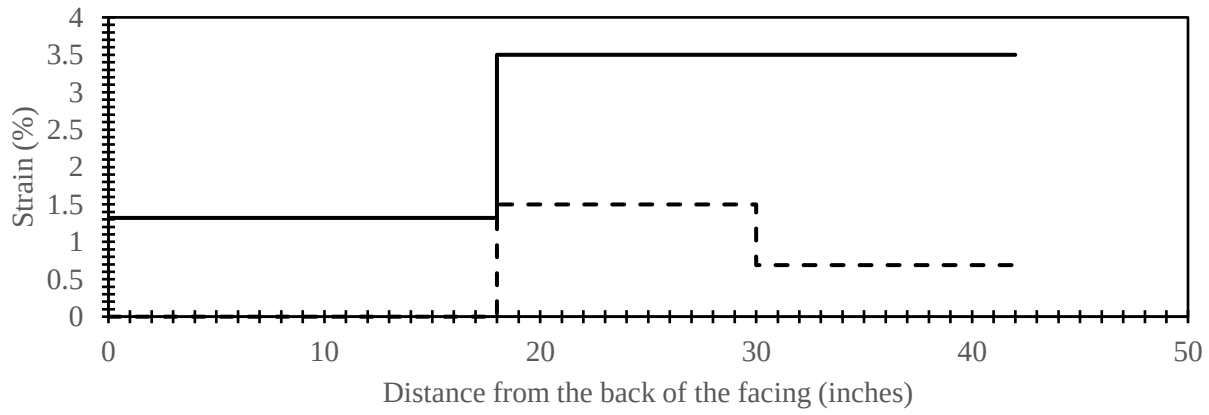
Strain (%)
4
3.5
3
2.5
2
1.5
1
0.5
0
0
10
20
30
40
50
Distance from the back of the facing (inches)

(b)

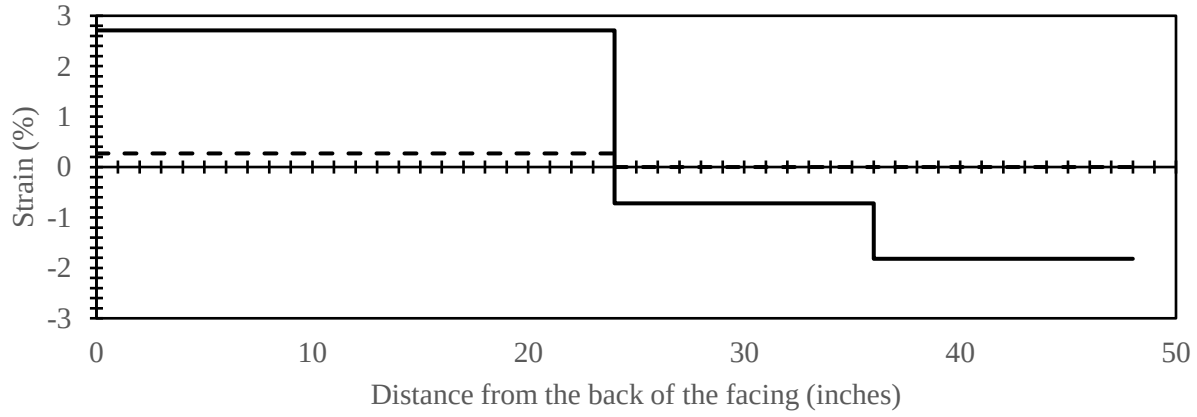
Strain (%)
3
2
1
0
-1
-2
-3
0
10
20
30
40
50
Distance from the back of the facing (inches)

(c)

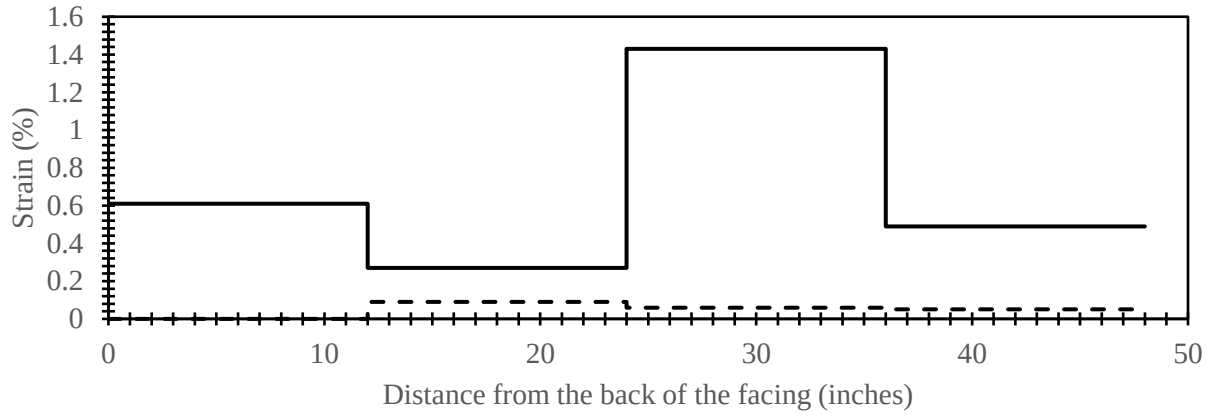

(d)

Figure 55 – Reinforcement strain comparisons at 20 ksf; (a) at 27 inches, (b) at 51 inches, (c) at 75 inches, (d) at 91 inches above foundation slab

Chapter 7 – CONCLUSIONS AND RECOMMENDATIONS FOR FUTURE WORK

7.1 Summary and Conclusions

GRS-IBS is a cost-effective bridge construction alternative to conventional practices. Most suitable to smaller county bridges, GRS-IBS has proven to be serviceable in the field but additional research regarding the performance of these structures is required to better understand their behaviors with the ultimate goals of further implementing this construction technique into practice. GRS Abutment Models #7 and #8 were constructed and testing to analyze its behaviors and compare them to abutment models previously constructed at The University of Oklahoma.

GRS Abutment Model #7 was constructed with large block facing elements, well-graded aggregate, 8-inch spacing, and 3 compaction passes. When compared to a nominally identical model with CMU facing, GRS Abutment Model #7 required more time to construct even with the large block facing. The study does not confirm that the use of large facing blocks can facilitate the construction of GRS abutments constructed with well-graded aggregate. Rather, the experience of the crew is likely the defining factor when comparing labor requirements among various GRS abutment models.

GRS Abutment Model #6 outperformed GRS Abutment Model #7 in terms of load-bearing performance. Though the performance requirements stated by the FHWA were satisfied, GRS Abutment Model #7 experienced additional settlement of nearly one inch when compared to GRS Abutment Model #6 at the same load. When comparing GRS Abutment Model #7 to other previously tested abutment models, one can see that models constructed with large block facing elements tend to behave similarly, regardless of the backfill type, compaction effort, and reinforcement spacing.

The purpose of testing GRS Abutment Model #8 was to investigate the performance of a GRS abutment model using a beam width that is accepted in practice. Results show that GRS Abutment Model #8 experienced the least amount of settlement of all models previously tested. The model also produced some of the largest facing deformations and reinforcement strains experienced by any model, but this may be attributed to the reduced setback distance. Nevertheless, GRS Abutment Model #8 met all criteria required by the FHWA.

7.2 Recommendations for Future Work

There are numerous avenues that this study could explore. The following list represents a few important areas that could be improved and/or investigated in the future.

- For continuity purposes, if the larger loading beam is to be used, the loading frame should be raised. The larger beam presented issues related to space for the LCs between the hydraulic pistons and top of the abutment model. To ensure models are compared accurately, the loading frame should be elevated.
- Various combinations of setback distance and beam seat width should be explored to further understand the relationship between these two factors. Some comparisons can be drawn if the abutment facing is moved outward to permit a setback distance that is comparable to those from GRS Abutment Models #1 through #7.
- EPCs should be repaired. During my experience, the EPCs have often failed once installed in the abutment. The internal pressure should be measured for future models to better understand the internal behavior amongst the various models.
- Though data is only collected from the middle portions of the abutment, there is need to reduce the frictional effects from the sides of the test station. All models have readily met

the minimum performance requirements set by the FHWA. The models may be overly stiff due to frictional influence from the test station.

References

1. ASTM C39, 2021. “Compressive strength of cylindrical concrete specimens.” ASTM International, West Conshohocken, PA.

2. ASTM C136, 2019. “Sieve analysis of fine and coarse aggregate.” ASTM International, West Conshohocken, PA.

3. ASTM D1556, 2015. “Density and unit weight of soil in place by sand-cone method.” ASTM International, West Conshohocken, PA.

4. ASTM D3080, 2011. “Direct Shear Test of Soils Under Consolidated Drained Conditions.” ASTM International, West Conshohocken, PA.

5. Adams, M., Nicks, J., Stabile, T., Wu, J., Schlatter, W., and Hartmann, J., 2011a. “Geosynthetic reinforced soil integrated bridge system interim implementation guide.” *Publication No. FHWA-HRT-11-026*, Federal Highway Administration, McLean, VA.

6. Adams, M., Nicks, J., Stabile, T., Wu, J., Schlatter, W., and Hartmann, J., 2011b. “Geosynthetic reinforced soil integrated bridge system synthesis report.” *Publication No. FHWA-HRT-11-027*, Federal Highway Administration, McLean, VA.

7. Adams, M. and Nicks, J., 2018. “Design and Construction Guidelines for Geosynthetic Reinforced Soil Abutments and Integrated Bridge Systems.” *Publication No. FHWA-HRT-17-080*, Federal Highway Administration, Washington, DC.

8. Akhnoukh, A., 2019. “Accelerated bridge construction projects using high performance concrete.” *Case Studies in Construction Materials*, vol. 12, June 2020.

9. Ardah, A., Abu-Farsakh, M., and Voyiadjis, G., 2020. “Numerical parametric study of geosynthetic reinforced soil integrated bridge system (GRS-IBS).” *Geotextiles and Geomembranes*, vol. 49, Feb. 2021, pp. 289-303.

10. Boutin, J., 2020. *Influence of Compaction and Quality Control on the Performance of GRS-IBS Bridge Abutments*. MS Thesis. University of Oklahoma.

11. Bowles, Joseph E. *Foundation Analysis and Design*. 3rd ed., McGraw-Hill, Inc., 1982.

12. Doger, R., 2020. *Influence of Facing on the Construction and Structural Performance of GRS Bridge Abutments*. PhD Dissertation. University of Oklahoma.

13. Doger, R. and Hatami, K., 2020. “Influence of Facing on the Performance of GRS Bridge Abutments.” *International Journal of Geosynthetics and Ground Engineering*, 6, Article No. 42, September 2020.

14. FHWA, 2012. “Sample Guide Specifications for Construction of Geosynthetic Reinforced Soil-Integrated Bridge System (GRS-IBS).” *Publication No. FHWA-HRT-12-051,* Federal Highway Administration, McLean, VA.

15. Gebremariam, F., Tanyu, B. F., Güler, E., Urgessa, G. S., and Shen, P., 2020. “Numerical Investigation of Reinforced Soil Structures with GRS-IBS Design Features.” *Geosynthetics International*, 28, No. 1, 2021.

16. Hatami, K. and Boutin, J., 2021. “Influence of Backfill Type on the Load-Bearing Performance of GRS Bridge Abutments.” *Geosynthetics International*, in press.

17. Hatami, K. and Doger, R., 2021. “Load-bearing performance of GRS abutments with different facing alternatives.” *Geosynthetics Conference 2021*, Kansas City, MO, February 2021.

18. Hatami, K. and Doger, R., 2021. “Load-Bearing Performance of Model GRS Bridge Abutments with Different Facing and Reinforcement Spacing Configurations.” *Geotextiles and Geomembranes*, vol. 49, issue 5, pg. 1139-1148, October 2021.

19. Hatami, K., Garland, G. S., Simpson, T., Falcon, K., Schnabel, S., and Pena, L., 2019. “Performance Monitoring of GRS Bridges in Oklahoma.” Southern Plains Transportation Center Summer Symposium 2019, National Cowboy & Western Heritage Museum, August 2019. Poster Presentation.

20. Nicks, J.E., Adams, M.T., Ooi, P.S.K, and Stable, T., 2013. “Geosynthetic Reinforced Soil Performance Testing – Axial Load Deformation Relationships.” *Publication No. FHWA-HRT-13-066*, Federal Highway Administration, McLean, VA.

21. ODOT, 2009. “Oklahoma Department of Transportation Standard Specifications.” Oklahoma City, OK.

22. Saghebfar, M., Abu-Farsakh, M., Ardah, A., Chen, Q., and Fernandez, B. A., 2016. “Performance Monitoring of Geosynthetic Reinforced Soil Integrated Bridge System (GRS-IBS) in Louisiana.” *Geotextile and Geomembranes*, vol. 45, issue 2, April 2017.

23. Shen, P., Han, J., Zornberg, J.G., Tanyu, B.F., Christopher, B.R., and Leshchinsky, D, 2020. “Responses of geosynthetic-reinforced soil (GRS) abutments under bridge slab loading: Numerical investigation.” *Computers and Geotechnics*, vol. 123, July 2020.

24. Xiao, M., Qiu, T., Khosrojerdi, M., Basu, P., and Withiam, J. L., 2016. “Synthesis and Evaluation of the Service Limit State of Engineered Fills for Bridge Support.” *Publication No. FHWA-HRT-15-080*, Federal Highway Administration, McLean, VA.

25. Xie, Y., and Leshchinsky, B., 2015. “MSE Walls as Bridge Abutments: Optimal Reinforcement Density.” *Geotextiles and Geomembranes*, vol. 43, issue 2, April 2015.

26. Zheng, Y., Fox, P. J., McCartney, J. S., 2018. “Numerical Study on Maximum Reinforcement Tensile Forces in Geosynthetic Reinforced Soil Bridge Abutments.” *Geotextiles and Geomembranes*, vol. 46, issue 5, October 2018.